1 - INTRODUCTION

A scientifically justifiable Total Maximum Daily Load (TMDL) for a waterbody can only be developed based on a quantitative understanding of the system. In practice, water quality modeling offers a feasible tool to establish this quantitative understanding. A water quality model that is customized for a specific waterbody can simulate the major physical, chemical, and biological processes that occur in the system, and thus provide quantitative relationships between the water quality response and external forcing functions. A customized modeling framework was developed to support determination of nutrient and dissolved oxygen TMDLs for the Christina River Basin. The TMDLs are presented in the report titled *Total Maximum Daily Loads for Nutrients and Dissolved Oxygen in the Christina River Basin, Pennsylvania-Delaware-Maryland* (USEPA, 2005). This report is intended to accompany the TMDL report and provide a more detailed discussion on the models used for the nutrient TMDL analysis, including assumptions, parameters, and references.

The modeling framework used in this study consisted of three major components: (1) a series of watershed loading models (HSPF) developed for each of the four primary subwatersheds in the Christina River Basin (Senior and Koerkle, 2003a, 2003b, 2003c, 2003d), (2) a CSO flow model (XP-SWMM) developed by the City of Wilmington, and (3) a hydrodynamic model developed using the computational framework of the Environmental Fluid Dynamics Code (EFDC) (Hamrick, 1992). A linkage interface was also developed to allow for the transfer of model data results from the HSPF and XP-SWMM model components to the EFDC water quality model.

Under the HSPF model framework, the Christina River Basin was configured into 70 subbasins (see Figure 1-1 and Table 1-1) with each subbasin having 12 land use categories. The XP-SWMM model calculated hourly CSO flow rates from rainfall events. Storm monitoring data were used to determine event mean concentrations to estimate CSO loads for nutrients. The EFDC model framework includes the main channels of Brandywine Creek, East Branch Brandywine Creek, West Branch Brandywine Creek, Buck Run, Red Clay Creek, White Clay Creek, Christina River, Delaware River, and several other smaller tributaries. The EFDC receiving water model was linked to the HSPF and XP-SWMM models to incorporate watershed and CSO loads. The EFDC hydrodynamic and water quality model was used to predict the dissolved oxygen and nutrient concentrations in the main channels of the Christina River, Brandywine Creek, White Clay Creek, and Red Clay Creek watersheds. The water quality constituents were calibrated using monitoring data for the period October 1, 1994 to October 1, 1998 (a period of 4 years). This period included two dry summers (1995 and 1997) as well as a number of high-flow periods, both of which are important to satisfy the TMDL seasonality requirements.

Table 1-1. Subbasins in the HSPF models of Christina River Basin

| Subbasin	Stream Name	Area (mi2)	Subbasin	Stream Name	Area (mi2)
	Brandywine Creek Watershed			*White Clay Creek Watershed*	
B01	Upper Brandywine Creek West Br.	18.39	W01	White Clay Creek West Br.	10.23
B02	Brandywine Creek West Br.	7.38	W02	Upper White Clay Creek Middle Br.	9.51
B03	Brandywine Creek West Br.	6.76	W03	White Clay Creek Middle Br.	6.35
B04	Brandywine Creek West Br.	0.80	W04	Trib. To White Clay Creek East Br.	6.20
B05	Brandywine Creek West Br.	8.82	W05	Trib. To White Clay Creek East Br.	2.65
B06	Brandywine Creek West Br.	8.06	W06	Upper White Clay Creek East Br.	8.57
B07	Brandywine Creek West Br.	13.46	W07	Trout Run	1.37
B08	Brandywine Creek West Br.	3.62	W08	White Clay Creek East Br.	7.47
B09	Upper Brandywine Creek East Br.	14.68	W09	White Clay Creek East Br.	6.85
B10	Brandywine Creek East Br.	18.31	W10	White Clay Creek	3.58
B11	Brandywine Creek East Br.	6.31	W11	White Clay Creek	6.53
B12	Brandywine Creek East Br.	3.70	W12	White Clay Creek	8.76
B13	Brandywine Creek East Br.	7.94	W13	White Clay Creek	2.08
B14	Brandywine Creek East Br.	12.92	W14	White Clay Creek	3.41
B15	Brandywine Creek	10.36	W15	Muddy Run	3.89
B16	Brandywine Creek	14.06	W16	Pike Creek	6.65
B17	Brandywine Creek	7.51	W17	Mill Creek	13.00
B18	Brandywine Creek	10.37		*Red Clay Creek Watershed*	
B19	Brandywine Creek	8.64	R01	Upper Red Clay Creek West Br.	10.08
B20	Upper Buck Run	25.54	R02	Red Clay Creek West Br.	7.39
B21	Upper Doe Run	11.05	R03	Red Clay Creek East Br.	9.90
B22	Lower Doe Run	10.96	R04	Red Clay Creek	5.11
B23	Lower Buck Run	1.95	R05	Red Clay Creek	5.24
B24	Trib. To Broad Run	0.60	R06	Burroughs Run	7.10
B25	Broad Run	5.83	R07	Hoopes Reservoir	2.10
B26	Marsh Creek	2.61	R08	Red Clay Creek	5.38
B27	Marsh Creek	11.54	R09	Red Clay Creek	1.72
B28	Trib. To Valley Creek	2.40		*Christina River Watershed*	
B29	Valley Creek	18.21	C01	Christina River West Br.	6.70
B30	Beaver Creek	18.08	C02	Upper Christina River	9.73
B31	Pocopson Creek	9.19	C03	Christine River	4.47
B32	Birch Run	4.66	C04	Upper Little Mill Creek	5.37
B33	Rock Run	8.03	C05	Little Mill Creek	3.84
B34	Lower Brandywine Creek	6.05	C06	Muddy Run	8.64
B35	Upper Marsh Creek	5.80	C07	Belltown Run	6.37
			C08	Christina River	10.70
			C09	Lower Christina River	21.90
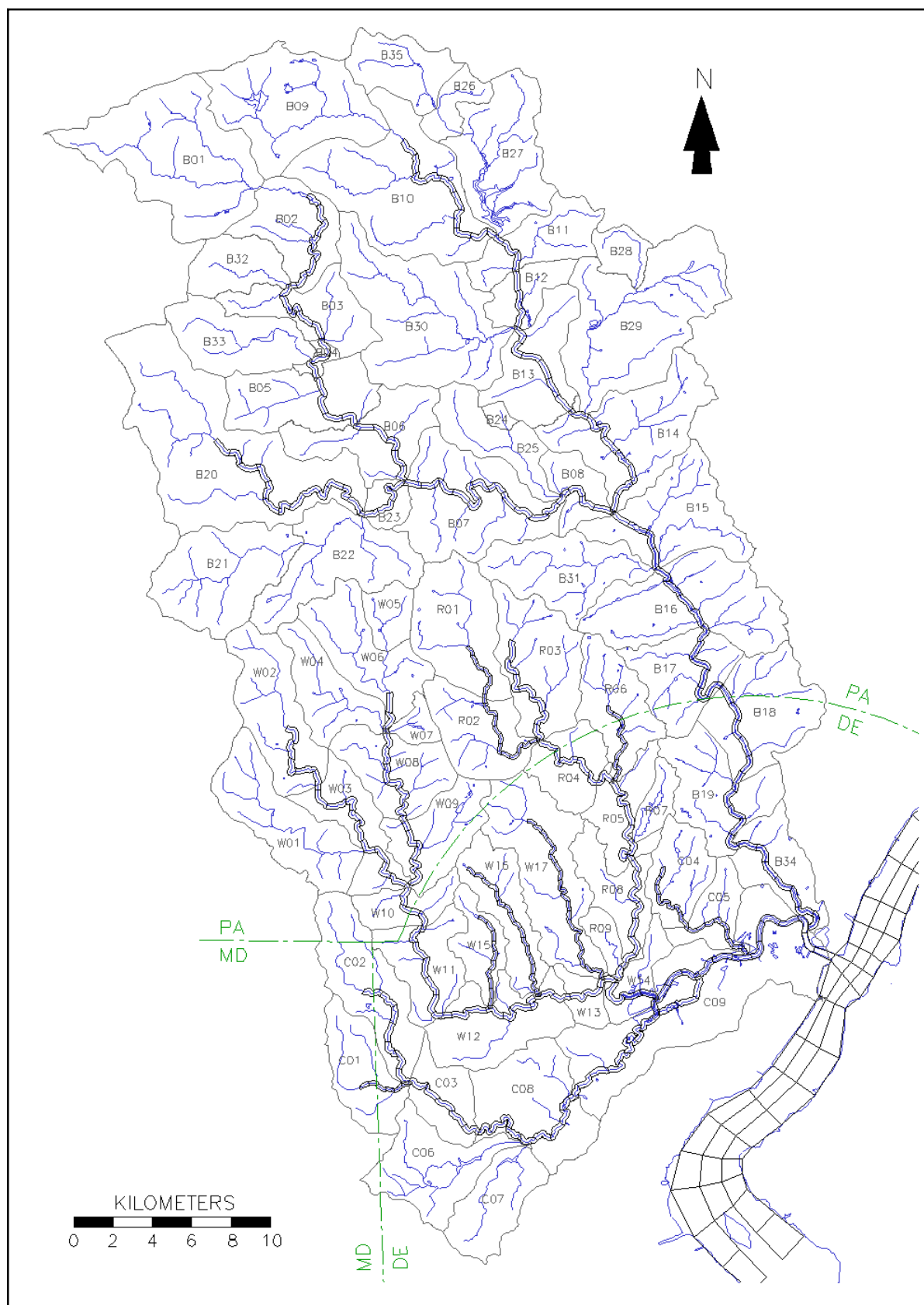
Figure 1-1. Christina River Basin showing HSPF model subbasins and EFDC model grid

2 - WATERSHED LOADING MODELS

A watershed runoff and loading model (HSPF) was developed for the Christina River Basin to estimate the amount of nutrients and oxygen demanding substances introduced to the receiving streams during rainfall-runoff events. In addition, an urban storm water runoff model (XP-SWMM) was developed by the City of Wilmington and was used to estimate combined sewer overflow (CSO) flows and loads to local receiving waters.

2.1   HSPF Model Overview

The Hydrologic Simulation Program—Fortran (HSPF), is a U.S. EPA supported model for simulation of watershed hydrology and water quality for both conventional and toxic organic pollutants. The HSPF model uses information such as the time history of rainfall, temperature and solar radiation; land surface characteristics such as land-use patterns; and land management practices to simulate the processes that occur in a watershed. The result of this simulation is a time history of the quantity and quality of runoff from an urban or agricultural watershed. Flow rate, sediment load, and nutrient and pesticide concentrations are predicted. HSPF includes an internal database management system to process the large amounts of simulation input and output. HSPF includes the source code, executable version, user's guide, and technical support. The HSPF model incorporates the watershed-scale Agricultural Runoff Model (ARM) and Non-Point Source (NPS) models into a basin-scale analysis framework that includes pollutant transport and transformation in stream channels.

The Christina River Basin drains 565 square miles in Pennsylvania, Delaware, and Maryland. Water from the basin is used for recreation, drinking-water supply, and to support aquatic life. The Christina River Basin includes four main watersheds: Brandywine Creek, Red Clay Creek, White Clay Creek, and Christina River. Brandywine Creek is the largest of the watersheds and drains an area of 327 square miles. Water quality in some parts of the Christina River Basin is impaired and does not support designated uses of the streams.

A multi-agency water-quality management strategy included a modeling component to evaluate the effects of point and nonpoint-source contributions of nutrients and suspended sediment on stream water quality. To assist in nonpoint-source evaluation, four independent models, one for each of the four main watersheds of the Christina River Basin, were developed and calibrated using the HSPF modeling framework.

The HSPF models simulate streamflow, suspended sediment, nitrogen, phosphorus, BOD, water temperature, and dissolved oxygen. For the models, the Christina River Basin was subdivided into 70

reaches. Ten different pervious land uses and two impervious land uses were selected for simulation. Land-use areas were determined from 1995 land-use data. The predominant land uses in the basin are forested, agricultural, residential, and urban.

The hydrologic component of the model was run at an hourly time step and calibrated using streamflow data for eight U.S. Geological Survey (USGS) streamflow measurement stations for a period covering four water years from October 1, 1994 to October 1, 1998. Daily precipitation data for three National Oceanic and Atmospheric Administration (NOAA) gages and hourly data for one NOAA gage were used for model input. More detailed descriptions of the HSPF models developed for the Christina River Basin can be found in Senior and Koerkle (2003a, 2003b, 2003c, and 2003d).

2.2   XP-SWMM Model Overview

The City of Wilmington has developed a model (XP-SWMM) to simulate stormwater flows and CSO events in the city's sewer collection system. XP-SWMM is a link-node model that performs hydrology, hydraulics, and water quality analysis of stormwater and wastewater drainage systems including sewage treatment plants, water quality control devices, and best management practices (BMPs). XP-SWMM can be used to model the full hydrologic cycle from stormwater and wastewater flow and pollutant generation to simulation of the hydraulics in any combined system of open and/or closed conduits with any boundary conditions. Typical XP-SWMM applications include predicting combined sewer overflows (CSOs) and sanitary sewer overflows (SSOs), interconnected pond analysis, open and closed conduit flow analysis, major/minor flow analysis, design of new developments, and analysis of existing stormwater and sanitary sewer systems.

XP-SWMM uses a self-modifying dynamic wave solution algorithm. Like all implicit solutions, which solve for the unknown values at a given time simultaneously, XP-SWMM is not Courant-limited. However, XP-SWMM uses the Courant number as a guide, to prevent numerical attenuation that can occur if excessively large time steps are used. This is important in models where pumps are involved or in urban systems where steeply rising hydrographs, requiring responses in seconds or fractions of a second will predominate, or where checks are being made against empirical procedures like the FHWA inlet control scheme for culverts. XP-SWMM will use small time steps when required and larger time steps when appropriate.

XP-SWMM has three computational modules. There is a stormwater module for hydrology and water quality generation, a wastewater module for generation of wastewater flows including Storage/Treatment for BMP and water quality routing, and a hydrodynamic hydraulics module for the hydraulic simulation of open and closed conduit wastewater or stormwater systems.

Hourly flow rates at each of the city's 38 CSO outfalls were calculated by XP-SWMM for the 1994-1998 calibration period based on hourly rainfall measured at New Castle County Airport and Porter Reservoir. Water quality was monitored at three CSO locations (CSO 25, CSO 4b, and the 11th Street Pump Station) for storm events on October 27, 2003, December 17, 2003, and November 4, 2004. Event mean concentrations (EMCs) were estimated for nutrients and oxygen demanding substances (see Tables 2-1a, b, c, and d). The monitoring included 20-day CBOD (CBOD20), 5-day CBOD (CBOD5), dissolved organic carbon (DOC), total organic carbon (TOC), ammonia nitrogen (NH3-N), nitrite+nitrate nitrogen (NOxN), total Kjeldahl nitrogen (TKN), total nitrogen (TN), dissolved orthophosphate (DOrthP), total phosphorus (TP), and total suspended solids (TSS). The EMCs were used in conjunction with the CSO flow rates to estimate daily loads for each CSO outfall. The CSO flows and loads were then input to the EFDC receiving water model to simulate the impact on nutrient and dissolved oxygen concentrations in the tidal Christina River, lower Brandywine Creek, and Little Mill Creek. The annual average baseline and TMDL nutrient loads from each of the CSO discharges for the calibration period are tabulated in Appendix B. The locations of the CSOs are shown in Appendix B, Figure B-1.

Table 2-1a. Storm monitoring at Wilmington CSO 4b

Date	Time	CBOD20 mg/L	CBOD5 mg/L	DOC mg/L	TOC mg/L	NH3-N mg/L	NOxN mg/L	TKN mg/L	TN mg/L	DOrthP mg/L	TP mg/L	TSS mg/L
STORET code –>		80087	80082	00681	00680	00610	00630	00625	****	00671	00665	00530
Storm Event #1												
10/27/2003	11:40	14.62	11.70	6.6	9.1	0.362	0.969	1.400	2.369	0.004	0.238	298
10/27/2003	12:10	13.60	5.82	2.9	3.7	0.137	0.248	0.275	0.523	0.020	0.320	278
10/27/2003	12:40	10.20	5.64	6.1	6.2	0.189	0.502	0.644	1.146	0.100	0.219	195
10/27/2003	13:10	14.48	7.85	5.9	7.1	0.238	0.831	1.080	1.911	0.126	0.270	177
10/27/2003	13:40	13.98	7.65	6.8	8.3	0.244	1.070	1.210	2.280	0.141	0.219	75
10/27/2003	14:10	13.50	10.60	7.3	8.9	0.238	1.290	1.370	2.660	0.159	0.216	32
Storm Event #2												
12/17/2003	09:00	16.20	9.20	4.9	6.8	0.403	0.627	2.650	3.277	0.203	0.388	35
12/17/2003	09:30	16.10	8.65	4.7	6.2	0.480	0.855	2.790	3.645	0.180	0.382	34
12/17/2003	10:00	23.80	12.80	6.8	8.4	4.520	1.210	4.830	6.040	0.222	0.546	25
12/17/2003	10:30	16.20	10.60	5.9	6.1	0.504	1.360	3.060	4.420	0.192	0.416	17
12/17/2003	11:00	12.10	8.18	5.5	6.0	0.486	1.710	2.610	4.320	0.138	0.306	19
12/17/2003	11:30	10.60	6.86	5.0	6.2	0.357	1.970	1.950	3.920	0.112	0.194	19
Storm Event #3												
11/4/2004	13:33	25.10	13.10	22.9	24.4	0.206	0.391	1.250	1.641	0.308	0.489	174
11/4/2004	14:03	28.40	15.20	18.3	20.2	0.154	0.337	0.937	1.274	0.256	0.376	31
11/4/2004	14:33	27.40	15.00	20.6	22.8	0.145	0.540	1.060	1.600	0.268	0.386	14
11/4/2004	15:03	24.50	15.60	22.2	23.5	0.113	0.748	1.080	1.828	0.250	0.314	11
11/4/2004	15:33	23.60	13.60	22.5	29.1	0.197	0.710	1.870	2.580	0.218	0.407	27
Event Mean Concentrations												
	EMC	17.90	10.47	10.29	11.94	0.528	0.904	1.769	2.673	0.170	0.334	86

Table 2-1b. Storm monitoring at Wilmington CSO 25

Date	Time	CBOD20 mg/L	CBOD5 mg/L	DOC mg/L	TOC mg/L	NH3-N mg/L	NOxN mg/L	TKN mg/L	TN mg/L	DOrthP mg/L	TP mg/L	TSS mg/L
STORET code –>		80087	80082	00681	00680	00610	00630	00625	****	00671	00665	00530
Storm Event #1												
10/27/2003	11:00	13.88	13.88	11.8	14.4	0.325	0.516	1.270	1.786	0.234	0.296	32
10/27/2003	11:30	14.76	14.76	10.3	11.6	0.294	0.503	1.050	1.553	0.286	0.397	33
10/27/2003	12:00	7.83	5.36	3.8	4.3	0.136	0.215	0.392	0.607	0.113	0.178	51
10/27/2003	12:30	12.14	12.14	70.5	80.0	0.421	0.634	3.070	3.704	1.870	1.620	39
10/27/2003	13:30	14.10	14.10	10.6	11.6	0.352	0.820	1.900	2.720	0.249	0.450	26
10/27/2003	14:00	14.26	14.26	10.8	12.0	0.455	1.160	2.480	3.640	0.354	0.642	15
Storm Event #2												
12/17/2003	08:45	15.00	9.48	6.3	6.6	0.350	0.547	1.850	2.397	0.202	0.102	27
12/17/2003	09:15	28.30	19.60	9.1	10.2	0.500	0.839	3.140	3.979	0.317	0.296	22
12/17/2003	09:45	28.76	28.76	40.8	44.6	3.720	1.030	5.500	6.530	1.560	1.580	14
Storm Event #3												
11/4/2004	13:20	28.50	14.90	15.4	18.3	0.476	0.272	1.990	2.262	0.277	0.505	42
11/4/2004	13:50	27.74	15.30	14.0	15.2	0.559	0.315	2.220	2.535	1.000	1.100	39
11/4/2004	14:20	28.00	14.10	17.2	19.1	0.606	0.422	2.630	3.052	0.385	0.637	19
11/4/2004	14:50	26.10	15.10	16.4	19.6	0.712	0.513	3.180	3.693	0.436	0.706	16
Event Mean Concentrations												
EMC		19.95	14.75	18.24	20.58	0.685	0.599	2.359	2.958	0.560	0.655	29

Table 2-1c. CSO Storm monitoring at Wilmington 11th Street Pumping Station (CSO 3)

Date	Time	CBOD20 mg/L	CBOD5 mg/L	DOC mg/L	TOC mg/L	NH3-N mg/L	NOxN mg/L	TKN mg/L	TN mg/L	DOrthP mg/L	TP mg/L	TSS mg/L
STORET code –>		80087	80082	00681	00680	00610	00630	00625	****	00671	00665	00530
Storm Event #1												
10/27/2003	11:20	11.76	11.76	23.5	29.6	4.040	0.467	7.250	7.717	0.262	1.470	454
10/27/2003	11:50	10.88	10.88	9.5	11.9	3.070	1.100	3.820	4.920	0.433	0.520	71
10/27/2003	12:10	10.88	10.88	7.7	9.6	1.520	0.545	1.450	1.995	0.202	0.357	166
10/27/2003	12:50	12.98	9.02	4.6	5.8	2.200	0.517	1.400	1.917	0.003	0.366	144
10/27/2003	13:20	11.82	11.82	13.9	15.3	1.720	0.646	0.964	1.610	0.167	0.289	104
10/27/2003	13:50	11.66	11.66	6.8	8.5	2.340	0.753	1.880	2.633	0.311	0.420	106
Storm Event #2												
12/17/2003	08:50	82.32	29.30	8.5	10.4	3.040	0.682	6.790	7.472	0.157	1.160	143
12/17/2003	09:20	26.50	13.80	5.3	6.3	4.520	0.732	4.880	5.612	0.129	0.630	86
12/17/2003	09:50	29.60	15.40	6.0	8.2	1.650	0.820	4.900	5.720	0.004	0.632	91
12/17/2003	10:20	20.80	14.30	6.7	9.1	3.530	0.842	4.670	5.512	0.019	0.645	73
12/17/2003	10:50	42.40	23.70	7.3	11.3	2.940	1.200	5.910	7.110	0.004	0.883	106
12/17/2003	11:20	82.05	82.05	21.4	25.5	1.150	1.140	6.810	7.950	0.341	0.909	64
Storm Event #3												
11/4/2004	13:25	26.82	13.58	20.1	22.6	4.340	0.460	23.200	23.660	0.007	3.400	553
11/4/2004	13:55	30.00	13.70	16.0	23.2	3.080	0.463	12.300	12.763	0.210	1.650	189
11/4/2004	14:25	29.50	12.96	15.6	20.0	2.780	0.506	10.600	11.106	0.182	1.130	181
11/4/2004	14:55	24.36	13.40	14.6	21.5	3.140	0.430	12.600	13.030	0.274	1.470	122
11/4/2004	15:25	20.70	12.40	16.7	21.2	3.050	0.533	11.200	11.733	0.605	1.480	128
11/4/2004	15:55	23.50	12.80	20.9	25.2	2.800	0.630	10.300	10.930	0.644	1.320	104
Event Mean Concentrations												
EMC		28.25	17.97	12.51	15.84	2.828	0.693	7.274	7.966	0.220	1.041	160

Table 2-1d. Event mean concentrations for CSOs other than CSO 3, 4b, and 25

Date	Time	CBOD20 mg/L	CBOD5 mg/L	DOC mg/L	TOC mg/L	NH3-N mg/L	NOxN mg/L	TKN mg/L	TN mg/L	DOrthP mg/L	TP mg/L	TSS mg/L
STORET code –>		80087	80082	00681	00680	00610	00630	00625	****	00671	00665	00530
Event Mean Concentrations												
EMC*		18.79	12.33	13.73	15.68	0.596	0.772	2.025	2.796	0.339	0.473	61

*EMC is calculated as arithmetic mean of combined data from CSO 4b and CSO 25

2.3   Modeling Assumptions

The simulation of streamflow in the Christina River Basin HSPF models considered the following assumptions: (1) inputs of hourly precipitation would be estimated reasonably well by disaggregated 24-hour precipitation data; (2) the average precipitation over a given land segment would be represented adequately by weighted data from a single precipitation gage; and (3) a simplified set of impervious land uses (PERLND) and impervious land uses (IMPLND) would not limit a satisfactory hydrologic calibration (Senior and Koerkle, 2003a).

The simulation of water quality in the HSPF models considered the following assumptions: (1) land-based contributions of sediment and nutrients could be simulated by a simplified set of land-use categories; (2) water quality could be represented by the condition where chemical transformation of nutrients are simulated explicitly in the stream channel but not in land processes; and (3) the contribution of sediment from bank erosion in the stream channel can be estimated by sediment from pervious land areas (Senior and Koerkle, 2003a).

The simulation of CSO nutrient loads assumes that the event mean concentrations (EMCs) are the same no matter what the intensity or duration of the storm event. Nutrient concentrations were monitored only at three locations (CSO 4b, CSO 25, and 11th Street Pumping Station). The EMCs for CSO 3, which is located at the 11th Street Pumping Station, were calculated from the measurements at the 11th Street Pumping Station. The parameter EMCs for the remaining 35 CSO outfalls were assumed to be equivalent to the mean concentration of the combined storm monitoring data at CSO 4b and CSO 25.

2.4   HSPF Model Configuration

2.4.1   HSPF Subbasins

Four separate HSPF models were developed to simulate watershed runoff and nutrient loading in the Christina River Basin. One model was developed for each of the four main watersheds: Brandywine Creek watershed, White Clay Creek watershed, Red Clay Creek watershed, and Christina River watershed. The Christina River Basin was delineated into 70 subbasins (or reaches) for the modeling effort (see Figure 1-1). The size of the subbasins ranged from 0.6 to 25.5 mi^2. The subbasins were delimited based on major tributary inflows, calibration locations (stream gages and water quality monitoring stations), and time-of-travel considerations.

2.4.2   Land Use Classifications

Spatial data input to the HSPF model are used to define the structure fixed characteristics of the model. The principal structural unit of the HSPF model is the hydrologic response units PERLND (pervious land) and IMPLND (impervious land). Fifteen original land-use categories (circa 1995) from several sources were simplified and reclassified into ten pervious and two impervious land-use categories that were expected to have distinct nonpoint-source water-quality characteristics (Table 2-2).

Agricultural land use was divided into three characteristic subtypes for the model. Agricultural-livestock land use identifies relatively small acreage farms with high animals-per-acre densities, limited pasture areas, and rowcrops. Small acreage dairy operations typify this land-use type. Agricultural-rowcrop land use identifies farms with lower animals-per-acre densities (typically beef cattle and horses) and substantial pasture and crop acreage. Agricultural-mushroom land use is the third type of agriculture land use delimited, but mushroom production operations are much more prevalent in the Red Clay Creek and White Clay Creek Basins than in the Brandywine Creek Basin. Residential land use is distributed throughout the basin and is divided into two types: sewered and non-sewered. Sewered residential areas tend to have higher housing densities and are nearer to urban/suburban areas than non-sewered area. Non-sewered residential areas tend to have lower densities and are more rural. Other urban land use is in small boroughs and along major roadways. Forested land is distributed throughout the basin and tends to be along stream channels. The land use delineations for each of the four main watersheds in the Christina River Basin are presented in Tables 2-3 through 2-6.

Table 2-2. Land-use categories used in HSPF models for Christina River Basin

Land-use category for HSPF model		Description
Pervious	Residential-septic	Residential land not within a sewer service area
	Residential-sewer	Residential land within a sewer service area
	Urban	Commercial, industrial, institutional, and transportation uses
	Agricultural-livestock	Predominantly mixed agricultural activities of dairy cows, pasture, and other livestock operations
	Agricultural-rowcrop	Predominantly row crop cultivation (corn, soybean, alfalfa), may include some hay or pasture land
	Agricultural-mushroom	Mushroom-growing activities including compost preparation, mushroom-house operations, spent compost processing
	Open	Recreational and other open land not used for agricultural
	Forested	Predominantly forested land
	Wetlands/water	Wetlands and open water
	Undesignated	Land use not defined
Impervious	Residential	Impervious residential land
	Urban	Impervious commercial, industrial, and other urban land

Table 2-3. Land use characteristics (in percent) for Brandywine Creek Watershed.

Reach	Length (mi)	Area (sq.mi.)	Resident. Septic	Resident. Sewer	Urban	Agriculture livestock	Agriculture row crop	Agriculture mushroom	Forested	Open	Wetland-water	Undesig-nated	Impervious-residential	Impervious-urban
1	6.60	18.39	4.1	1.4	0.6	45.6	22.5	0.0	20.1	2.7	0.5	0.9	1.1	0.7
2	7.60	7.38	17.3	0.6	1.8	9.4	19.0	0.0	46.4	0.5	0.8	0.2	2.2	1.8
3	2.94	6.76	22.3	0.3	1.2	7.5	22.6	0.0	39.8	2.0	0.5	0.0	2.6	1.2
4	1.85	0.80	0.0	7.1	2.1	0.0	14.9	0.0	68.8	0.1	1.7	0.2	3.0	2.1
5	2.91	8.82	1.5	11.0	10.5	0.0	19.1	0.0	34.8	3.6	1.5	2.4	4.9	10.7
6	2.93	8.06	17.1	0.5	1.5	4.0	35.6	0.0	35.4	1.8	0.5	0.0	2.1	1.5
7	7.80	13.46	5.9	0.0	1.5	0.0	49.0	0.0	38.2	1.9	1.2	0.1	0.7	1.5
8	2.19	3.62	9.2	0.0	0.6	0.0	62.6	0.0	24.9	0.0	1.2	0.1	1.0	0.6
9	7.10	14.68	6.1	0.5	0.4	27.0	27.0	0.0	32.6	2.2	2.8	0.2	0.9	0.4
10	12.10	18.31	17.0	0.2	1.2	0.0	36.0	0.0	40.3	1.2	0.6	0.2	2.0	1.2
11	1.79	6.31	4.7	11.6	1.9	0.0	33.1	0.0	35.6	4.7	0.5	0.6	5.5	1.9
12	2.02	3.70	8.4	18.7	4.4	0.0	11.4	0.0	38.9	2.2	1.3	1.3	8.9	4.5
13	3.86	7.94	6.5	10.1	4.3	0.0	14.3	0.0	47.9	3.1	1.4	2.7	5.1	4.6
14	4.86	12.92	8.8	10.8	3.5	0.0	31.9	0.0	30.2	3.2	1.0	1.4	5.6	3.6
15	2.49	10.36	17.6	7.2	1.9	0.0	40.7	0.0	16.8	6.9	1.0	1.0	5.0	1.9
16	2.88	14.06	25.0	0.0	2.4	0.0	25.7	0.0	38.7	1.6	0.9	0.5	2.8	2.4
17	4.15	7.51	12.2	0.0	0.1	0.0	27.0	0.0	48.6	6.1	1.3	0.4	4.1	0.3
18	3.39	10.37	9.2	3.5	1.6	2.1	19.1	0.0	38.2	14.6	1.1	5.8	2.5	2.2
19	2.71	8.64	10.6	10.3	3.4	0.0	4.1	0.0	16.5	40.3	1.0	4.6	5.6	3.6
20	8.66	25.54	7.7	1.8	1.1	5.9	52.9	0.0	25.5	1.3	0.4	0.8	1.6	1.1
21	6.73	11.05	3.5	0.0	0.4	7.6	68.6	0.0	17.3	1.1	0.1	0.5	0.4	0.4
22	3.18	10.96	0.7	0.0	0.9	7.9	71.3	0.0	17.7	0.0	0.3	0.2	0.1	0.9
23	0.87	1.95	0.0	0.0	0.01	4.9	44.4	0.0	49.4	0.0	1.3	0.0	0.0	0.01
24	3.14	0.60	73.2	4.9	0.0	0.0	3.5	0.0	8.2	0.0	0.0	0.0	10.3	0.0
25	3.14	5.83	15.2	3.7	2.3	0.0	40.7	0.0	30.4	1.7	0.1	0.3	3.3	2.3
26	1.60	2.61	8.1	0.0	2.2	6.5	19.6	0.0	59.5	0.3	0.5	0.1	0.9	2.2
27	4.80	11.54	21.5	0.1	0.9	8.9	20.6	0.0	33.9	2.4	7.4	1.1	2.4	0.9
28	2.00	2.40	0.7	37.6	6.5	0.0	3.0	0.0	20.5	5.7	0.0	3.6	16.1	6.7
29	7.20	18.21	4.3	12.9	3.5	0.0	20.9	0.0	35.1	5.0	2.5	3.2	6.0	6.7
30	4.09	18.08	12.2	6.6	4.7	0.0	32.4	0.0	30.0	2.2	0.2	2.7	4.2	5.0
31	4.09	9.19	22.7	0.0	0.8	0.0	48.8	0.0	22.1	1.8	0.3	0.3	2.5	0.8
32	2.00	4.66	11.3	0.0	0.8	15.8	15.8	0.0	52.9	0.9	0.1	0.3	1.3	0.8
33	2.75	8.03	12.2	3.5	1.3	4.2	38.0	0.0	29.8	4.5	2.1	0.4	2.9	1.3
34	4.46	6.05	1.9	2.5	28.0	0.0	1.6	0.0	13.9	12.9	2.6	7.3	1.3	28.2
35	4.00	5.80	6.3	0.0	1.1	12.1	36.3	0.0	34.1	0.3	7.8	0.2	0.7	1.1
Total	144.88	324.59	10.5	3.9	2.7	6.3	32.7	0.0	31.8	3.8	1.2	1.3	2.9	2.8

Table 2-4. Land use characteristics (in percent) for White Clay Creek watershed.

Reach	Length (mi)	Area (sq.mi.)	Resident. Septic	Resident. Sewer	Urban	Agriculture livestock	Agriculture row crop	Agriculture mushroom	Forested	Open	Wetland-water	Undesig-nated	Impervious-residential	Impervious-urban
1	7.33	10.23	15.6	0.0	1.0	10.4	36.2	5.2	26.1	2.1	0.1	0.7	1.8	1.0
2	6.57	9.51	11.3	1.8	0.8	15.9	47.5	0.0	17.7	1.1	0.2	0.9	2.0	0.8
3	7.18	6.35	16.4	0.0	0.0	9.0	33.5	2.2	35.9	0.6	0.5	0.0	1.9	0.0
4	6.02	6.20	6.8	2.6	1.3	11.5	40.2	5.8	23.5	2.4	0.5	2.1	1.9	1.5
5	2.49	2.65	1.5	0.0	0.0	14.7	52.1	7.5	23.0	0.8	0.0	0.4	0.0	0.0
6	6.16	8.57	1.5	0.8	1.3	13.4	47.3	6.8	21.8	2.9	0.2	2.1	0.5	1.3
7	1.75	1.37	5.8	5.1	1.5	0.0	5.8	56.2	17.5	0.0	1.5	2.9	2.9	1.5
8	4.09	7.47	11.6	0.5	0.5	0.0	20.1	30.3	32.4	1.2	0.5	0.8	1.5	0.5
9	4.46	6.85	17.5	7.2	0.7	6.6	22.9	3.2	31.7	2.3	1.6	0.6	5.0	0.7
10	1.67	3.58	11.2	4.5	0.0	5.3	21.8	0.0	53.1	0.3	0.6	0.3	3.1	0.0
11	4.02	6.53	1.2	8.1	4.3	0.0	15.5	0.0	54.8	7.0	0.8	0.3	3.7	4.3
12	5.28	8.76	0.0	24.1	10.2	0.0	9.4	0.0	10.7	9.8	0.9	10.2	10.4	14.4
13	2.21	2.08	0.0	6.7	14.4	0.0	11.1	0.0	11.5	7.2	1.4	27.4	2.9	17.3
14	2.97	3.41	0.0	10.6	11.4	0.0	0.0	0.0	14.1	21.7	14.4	10.6	4.7	12.6
15	4.08	3.89	0.0	14.4	1.8	0.0	29.6	0.0	42.2	3.3	0.0	0.5	6.2	2.1
16	5.85	6.65	0.0	38.9	6.2	0.0	8.4	0.0	12.9	9.2	0.0	1.4	16.7	6.3
17	9.76	13.00	0.5	33.9	6.6	1.1	8.7	1.1	11.7	10.2	0.0	4.1	15.1	7.1
Total	81.89	107.10	6.5	11.1	3.4	5.8	25.3	4.9	24.8	4.9	0.9	2.9	5.5	4.0

Table 2-5. Land use characteristics (in percent) for Red Clay Creek watershed

Reach	Length (mi)	Area (sq.mi.)	Resident. Septic	Resident. Sewer	Urban	Agriculture livestock	Agriculture row crop	Agriculture mushroom	Forested	Open	Wetland-water	Undesig-nated	Impervious-residential	Impervious-urban
1	5.00	10.08	10.4	1.6	2.1	5.9	46.8	5.9	18.4	2.8	0.4	1.6	1.9	2.2
2	4.90	7.39	11.8	0.5	0.7	0.0	40.9	17.5	25.2	0.3	0.2	0.7	1.5	0.7
3	7.20	9.90	14.9	1.9	1.0	0.0	33.1	14.2	22.5	5.8	0.6	2.3	2.5	1.1
4	3.40	5.11	35.5	2.3	1.0	1.8	14.2	1.8	28.4	7.9	0.8	0.6	4.9	1.0
5	5.10	5.24	32.2	2.2	0.2	0.0	14.6	0.0	37.7	6.0	1.2	0.9	4.6	0.2
6	5.00	7.10	23.9	0.0	0.2	0.0	42.4	0.0	25.1	5.1	0.1	0.3	2.7	0.2
7	1.70	2.10	26.1	0.0	0.5	0.0	7.2	0.0	44.4	3.0	14.3	1.1	2.9	0.5
8	4.30	5.38	1.5	35.3	5.3	0.0	1.6	0.0	13.4	13.8	1.4	6.3	15.3	6.0
9	0.84	1.72	0.0	45.5	4.8	0.0	0.0	0.0	10.2	3.8	0.4	9.9	19.5	5.9
Total	37.44	54.02	17.1	6.1	1.6	1.3	29.2	6.3	24.0	5.2	1.2	2.0	4.5	1.7

Table 2-6. Land use characteristics (in percent) for Christina River watershed

Reach	Length (mi)	Area (sq.mi.)	Resident. Septic	Resident. Sewer	Urban	Agriculture livestock	Agriculture row crop	Agriculture mushroom	Forested	Open	Wetland-water	Undesig-nated	Impervious-residential	Impervious-urban
1	1.46	1.87	9.1	0.0	0.4	0.0	58.1	0.0	29.7	1.1	0.0	0.2	1.0	0.4
1	3.33	4.83	7.9	4.0	7.9	0.0	27.1	0.0	23.4	12.5	0.0	6.2	2.6	8.3
2	4.96	7.08	25.5	4.7	0.3	0.0	41.1	0.0	21.7	0.6	0.1	1.0	4.8	0.3
2	3.20	2.65	7.7	25.9	9.6	0.0	4.5	0.0	10.7	13.8	0.0	13.3	12.0	10.2
3	3.24	4.47	4.8	17.5	12.7	0.0	9.2	0.0	18.4	8.0	0.2	9.0	8.0	13.5
4	4.65	5.37	1.5	28.1	12.8	0.0	1.4	0.0	18.3	9.2	0.2	2.6	12.2	13.4
5	2.30	3.84	0.1	20.9	17.6	0.0	0.0	0.0	8.7	15.2	1.1	9.3	8.9	25.6
6	6.73	8.64	6.0	8.8	6.6	0.0	15.5	0.0	38.4	10.6	1.1	1.8	4.5	6.8
7	2.08	6.37	0.6	20.1	6.9	0.0	8.5	0.0	34.3	8.1	0.8	4.7	8.7	7.4
8	6.21	10.70	0.2	19.3	8.4	0.0	10.4	0.0	27.0	7.0	0.5	9.3	8.3	9.2
9	15.09	21.90	0.5	10.3	17.8	0.0	1.8	0.0	12.5	20.0	4.3	9.9	4.5	18.5
Total	53.25	77.70	4.6	13.7	10.8	0.0	11.9	0.0	21.6	11.6	1.6	6.5	6.4	11.4

2.4.3   Nutrient Sources

The HSPF models required large amounts of data to characterize the hydrologic and water quality response of the watershed to precipitation and other inputs. Data used in creating the model structure and parameters were derived primarily from spatial analysis of basin characteristics and other published information. Spatial data analyzed for model construction included land use, land-surface slope, and soil associations. Time-series inputs for streamflow and water-quality simulation included meteorologic, precipitation quality, water-use, and point source quantity and quality data. Nonpoint sources of nutrients were calculated by the model based on build up, storage, and wash off processes inherent in the HSPF model.

2.4.4   Time Step and Simulation Duration

The HSPF models were executed on a 1-hour time step. The duration of the calibration runs was from October 1, 1994 to October 1, 1998, a period that covered four consecutive water years.

2.5   Model Testing and Calibration

Complete descriptions of the calibration of each of the four HSPF models for the Christina River Basin can be found in the USGS Water Resources Investigation Reports (Senior and Koerkle, 2003a, 2003b, 2003c, and 2003d), which are available in Portable Document File (PDF) format at the following website: http://pa.water.usgs.gov/pa_pubs.html

3 - EFDC HYDRODYNAMIC MODEL

Modeling the physics, chemistry, and biology of the receiving waters of streams, lakes, estuaries, or coastal regions requires a model that incorporates all the major processes. Transport processes for this study were simulated using the three-dimensional EFDC hydrodynamic model that includes temperature transport. The EFDC hydrodynamic model was developed by Hamrick (1992a). The model formulation was based on the principles expressed by the equations of motion, conservation of volume, and conservation of mass. Quantities computed by the model included three-dimensional velocities, surface elevation, vertical viscosity and diffusivity, temperature, salinity, and density.

3.1   General

The Environmental Fluid Dynamics Code is a general purpose modeling package for simulating three-dimensional flow, transport, and biogeochemical processes in surface water systems including rivers, lakes, estuaries, reservoirs, wetlands, and coastal regions. The EFDC model was originally developed at the Virginia Institute of Marine Science for estuarine and coastal applications and is considered public domain software. In addition to hydrodynamic and salinity and temperature transport simulation capabilities, EFDC is capable of simulating cohesive and noncohesive sediment transport, near field and far field discharge dilution from multiple sources, eutrophication processes, the transport and fate of toxic contaminants in the water and sediment phases, and the transport and fate of various life stages of finfish and shellfish. Special enhancements to the hydrodynamic portion of the code, including vegetation resistance, drying and wetting, hydraulic structure representation, wave-current boundary layer interaction, and wave-induced currents, allow refined modeling of wetland marsh systems, controlled flow systems, and near-shore wave induced currents and sediment transport. The EFDC model has been extensively tested and documented for more than 20 modeling studies. The model is presently being used by a number of organizations including universities, governmental agencies, and environmental consulting firms.

The structure of the EFDC model includes four major modules: (1) a hydrodynamic model, (2) a water quality model, (3) a sediment transport model, and (4) a toxics model (see Figure 3-1). The EFDC hydrodynamic model itself, which was used for this study, is composed of six transport modules including dynamics, dye, temperature, salinity, near field plume, and drifter (see Figure 3-2). Various products of the dynamics module (i.e., water depth, velocity, and mixing) are directly coupled to the water quality, sediment transport, and toxics models as shown in the following figures. Schematic diagrams for the water quality model, the sediment transport model, and the toxics model are shown in Figures 3-3, 3-4, and 3-5, respectively.

EFDC Model

Hydrodynamics | Water Quality | Sediment Transport | Toxics
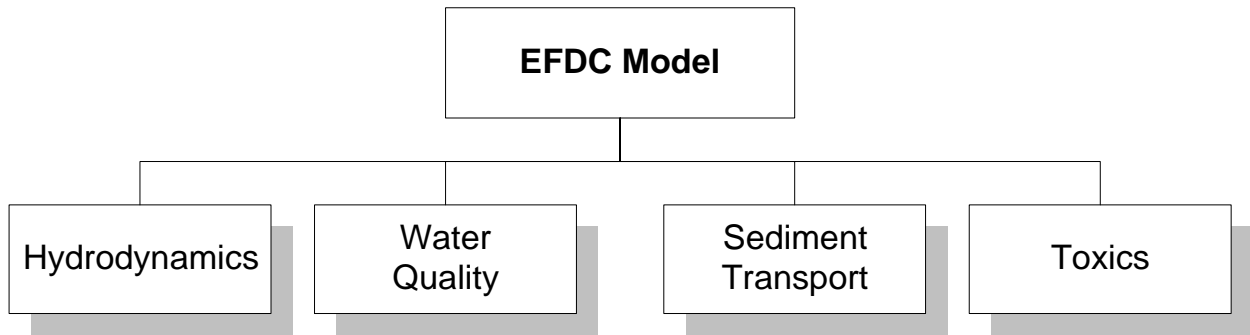
Figure 3-1. Primary modules of the EFDC model

Hydrodynamics

Dynamics (E, u, v, w, mixing) | Dye | Temperature | Salinity | Near Field Plume | Drifter
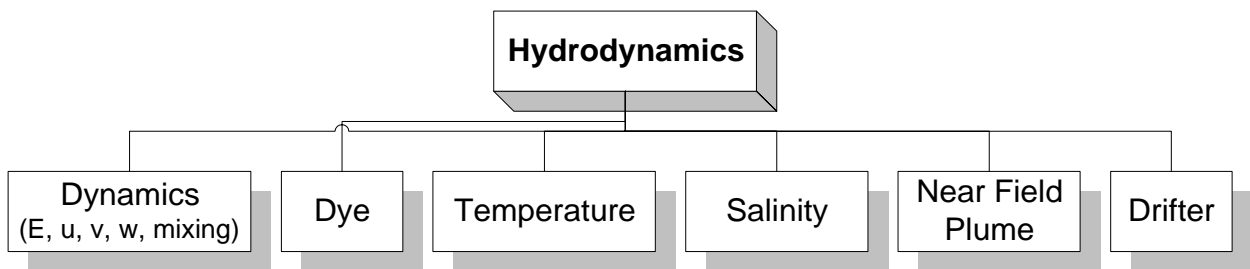
Figure 3-2. Structure of the EFDC hydrodynamic model

Hydrodynamic Model → *Dynamics* → **Water Quality**

Algae | Organic Carbon | Phosphorus | Nitrogen | Silica | DO | COD TAM | FCB | Sediment Diagenesis

Greens
Diatoms
Other

Predicted Flux
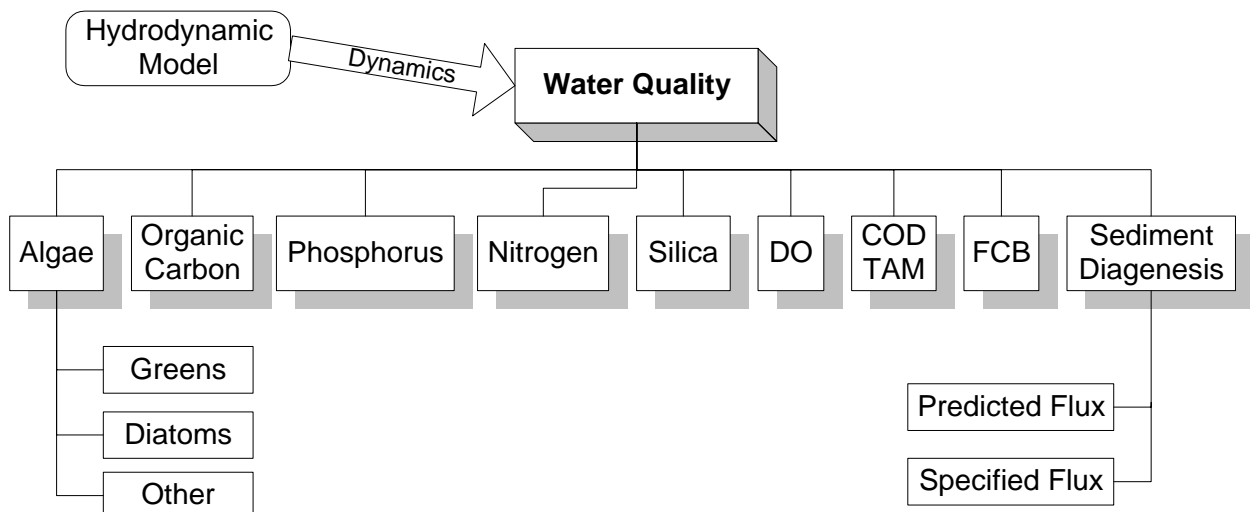Specified Flux

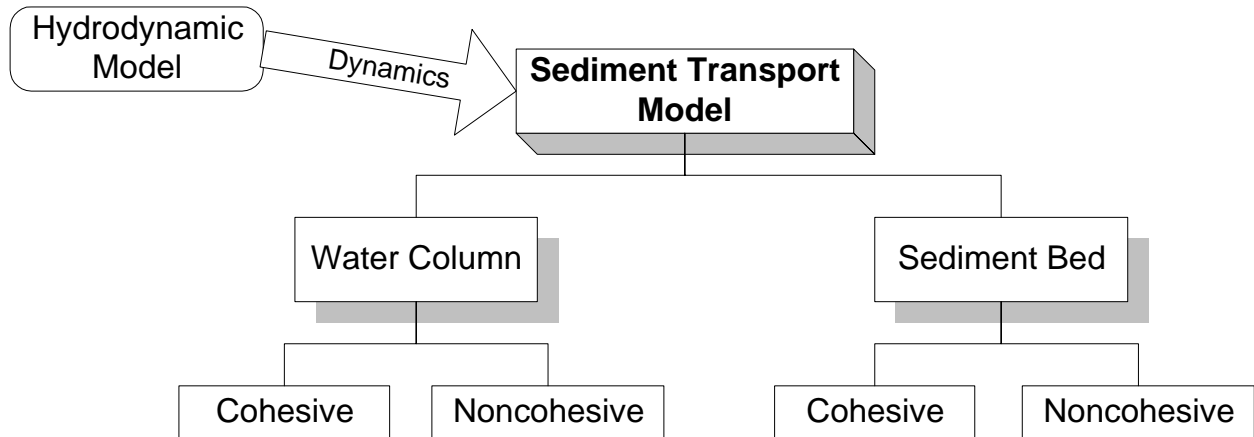**Figure 3-3. Structure of the EFDC water quality model**

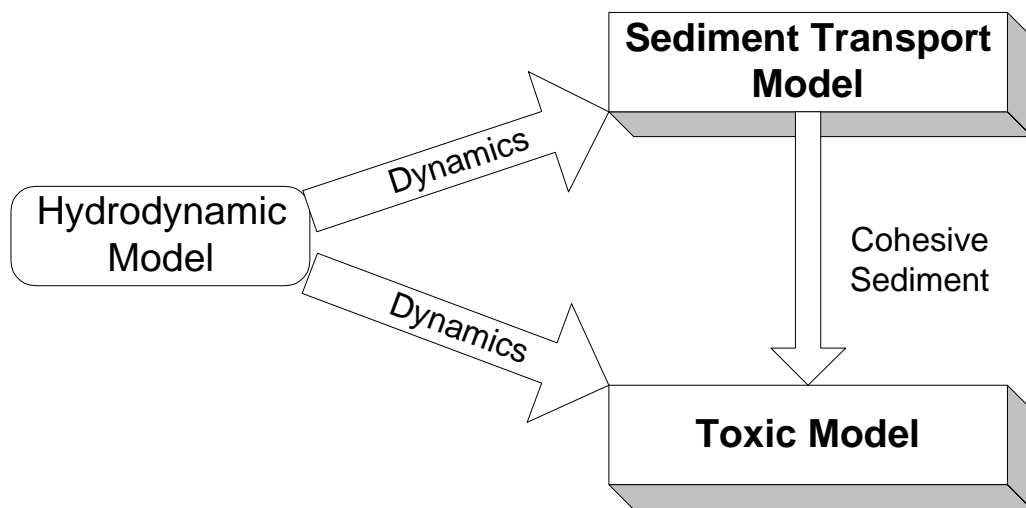**Figure 3-4. Structure of the EFDC sediment transport model**

Figure 3-5. Structure of the EFDC toxics model

3.2 Hydrodynamics and Salinity and Temperature Transport

The physics of the EFDC model and many aspects of the computational scheme are equivalent to the widely used Blumberg-Mellor model (Blumberg and Mellor 1987). The EFDC model solves the three-dimensional, vertically hydrostatic, free surface, turbulent averaged equations of motions for a variable density fluid. Dynamically coupled transport equations for turbulent kinetic energy, turbulent length scale, salinity, and temperature are also solved. The two turbulence parameter transport equations implement the Mellor-Yamada level 2.5 turbulence closure scheme (Mellor and Yamada 1982; Galperin et al. 1988). The EFDC model uses a stretched or sigma vertical coordinate and Cartesian, or curvilinear, orthogonal horizontal coordinates.

The numerical scheme employed in EFDC to solve the equations of motion uses second order accurate spatial finite differencing on a staggered or C grid. The model's time integration employs a second order accurate three-time level, finite difference scheme with an internal-external mode splitting procedure to separate the internal shear or baroclinic mode from the external free surface gravity wave or barotropic mode. The external mode solution is semi-implicit and simultaneously computes the two-dimensional (2-D) surface elevation field by a preconditioned conjugate gradient procedure. The external solution is completed by the calculation of the depth average barotropic velocities using the new surface elevation field. The model's semi-implicit external solution allows large time steps that are constrained only by the stability criteria of the explicit central difference or high order upwind advection scheme (Smolarkiewicz and Margolin 1993) used for the nonlinear accelerations. Horizontal boundary conditions for the external mode solution include options for simultaneously specifying the surface elevation only, the characteristic of an incoming wave (Bennett and McIntosh 1982), free radiation of an outgoing wave (Bennett 1976; Blumberg and Kantha 1985), or the normal volumetric flux on arbitrary portions of the boundary. The EFDC model's internal momentum equation solution, at the same time step as the external solution, is implicit with respect to vertical diffusion. The internal solution of the momentum equations is in terms of the vertical profile of shear stress and velocity shear, which results in the simplest and most accurate form of the baroclinic pressure gradients and eliminates the over determined character of alternate internal mode formulations. Time splitting inherent in the three-time-level scheme is controlled by periodic insertion of a second order accurate two-time-level trapezoidal step. EFDC is also readily configured as a 2-D model in either the horizontal or vertical planes.

The EFDC model implements a second order accurate in space and time, mass conservation fractional step solution scheme for the Eulerian transport equations for salinity, temperature, suspended sediment, water quality constituents, and toxic contaminants. The transport equations are temporally integrated at the same time step or twice the time step of the momentum equation solution (Smolarkiewicz and Margolin 1993). The advective step of the transport solution uses either the central difference scheme used in the Blumberg-Mellor model or a hierarchy of positive definite upwind difference schemes. The

highest accuracy upwind scheme, second order accurate in space and time, is based on a flux-corrected transport version Smolarkiewicz's multidimensional positive-definite advection transport algorithm (Smolarkiewicz and Clark, 1986; Smolarkiewicz and Grabowski 1990), which is monotonic and minimizes numerical diffusion. The horizontal diffusion step, if required, is explicit in time, whereas the vertical diffusion step is implicit. Horizontal boundary conditions include time variable material inflow concentrations, upwind outflow, and a damping relaxation specification of climatological boundary concentration. The NOAA Geophysical Fluid Dynamics Laboratory's atmospheric heat exchange model (Rosati and Miyakoda 1988) is implemented for the temperature transport equation.

3.3   Sediment Transport

The EFDC code is capable of simulating the transport and fate of multiple size classes of cohesive and noncohesive suspended sediment including bed deposition and resuspension. Water column transport is based on the same high order advection-diffusion scheme used for salinity and temperature. A number of options are included for the specification of settling velocities. For the transport of multiple size classes of cohesive sediment, an optional flocculation model (Burban et al. 1989, 1990) can be activated. Sediment mass conservative deposited bed formulations are included for both cohesive and noncohesive sediment. The deposited bed may be represented by a single layer or multiple layers. The multiple bed layer option provides a time since deposition versus vertical position in the bed relationship to be established. Water column/sediment bed interface elevation changes can be optionally incorporated into the hydrodynamic continuity equation. An optional one-dimensional (1-D) in the vertical, bed consolidation calculation can be performed for cohesive beds.

3.4   Water Quality and Eutrophication Simulation

The EFDC code includes two internal eutrophication submodels for water quality simulation (Park et al. 1995). The simple or reduced eutrophication model is functionally equivalent to the WASP5 EUTRO model (Ambrose et al. 1993). The complex or full eutrophication model is functionally equivalent to the CE-QUAL-ICM or Chesapeake Bay Water Quality model (Cerco and Cole 1993). Both water column eutrophication models are coupled to a functionally equivalent implementation of the CE-QUAL-ICM sediment diagenesis or biogeochemical processes model (DiToro and Fitzpatrick 1993). The eutrophication models can be executed simultaneously with the hydrodynamic component of EFDC, or EFDC simulated hydrodynamic transport fields can be saved, allowing the EFDC code to be executed in a water quality only simulation mode.

The computational scheme used in the internal eutrophication models employs a fractional step extension of the same advective and diffusive algorithms used for salinity and temperature, which guarantee positive constituent concentrations. A novel ordering of the reaction sequence in the reactive source and sink fractional step allows the linearized reactions to be solved implicitly, further guaranteeing positive

concentrations. The eutrophication models accept an arbitrary number of point and nonpoint source loadings as well as atmospheric and ground water loadings.

In addition to the internal eutrophication models, the EFDC model can be externally linked to the WASP5 model. In the external linking mode, the EFDC model generates WASP5 input files describing cell geometry and connectivity as well as advective and diffusive transport fields. For estuary simulation, the transport fields may be intratidally time averaged or intertidally time averaged using the averaging procedure described by Hamrick (1994).

3.5   Toxic Contaminant Transport and Fate

The EFDC code includes two internal submodels for simulating the transport and fate of toxic contaminants. A simple, single contaminant submodel can be activated from the master input file. The simple model accounts for water and suspended sediment phase transport with equilibrium partitioning and a lumped first order reaction. Contaminant mass per unit area in the sediment bed is also simulated. The second, more complex, submodel simulates the transport and fate of an arbitrary number of reacting contaminants in the water and sediment phases of both the water column and sediment bed. In this mode, the contaminant transport and fate simulation is functionally similar to the WASP5 TOXIC model (Ambrose et al. 1993), with the added flexibility of simulating an arbitrary number of contaminants, and the improved accuracy of utilizing more complex three-dimensional physical transport fields in a highly accurate numerical transport scheme. Water-sediment phases interaction may be represented by equilibrium or nonlinear sorption processes. In this mode, the multilayer sediment bed formulation is active, with sediment bed water volume and dissolved contaminant mass balances activated to allow contaminants to reenter the water column by sediment resuspension, pore water expulsion due to consolidation, and diffusion from the pore water into the water column. The complex contaminant model activates a subroutine describing reaction processes with appropriate reaction parameters provided by the toxic reaction processes input file.

3.6   Finfish and Shellfish Transport

The EFDC code includes the capability of simulating the transport and fate of various life stages of finfish and shellfish. In addition to advection and diffusion by the ambient flow, mortality, predation, toxicity, and swimming behavior are simulated. Organism age and ambient environment queued vertical and horizontal swimming and settling is simulated. Environmental queues include light intensity, temperature, salinity, and tidal phases.

3.7   Near-Field Discharge Dilution and Mixing Zone Analysis

In addition to the far-field transport and fate simulation capability incorporated into the EFDC code's water quality and toxic contaminant modules, the code includes a near-field discharge dilution and mixing

zone module. The near field model is based on a Lagrangian buoyant jet and plume model (Frick 1984; Lee and Cheung 1990) and allows representation of submerged single and multiple port diffusers and buoyant surface jets. The near field model provides analysis capabilities similar to CORMIX (Jirka and Doneker 1991; Jirka and Akar 1991) while offering two distinct advantages. The first advantage is that a more realistic representation of ambient current and stratification conditions, provided directly by the EFDC hydrodynamic module, is incorporated into the analysis. The second advantage is that multiple discharges and multiple near field analysis times may be specified to account for varying ambient current and stratification conditions. For example, the analysis of 10 discharges under six ambient conditions each would require 60 executions of CORMIX, while the entire analysis of the 60 situations would be produced in a single EFDC simulation. The near-field simulation may be executed in two modes. The first provides virtual source information for representing the discharges in a standard EFDC far-field transport and fate simulation. In the second mode the near-field and far-field transport are directly coupled, using a virtual source formulation, to provide simultaneous near and far field transport and fate simulation.

3.8   Spill Trajectory and Search and Rescue Simulation

In addition to the Eulerian transport equation formulation used for far field analysis and the Lagrangian jet and plume module used for near field analysis, the EFDC code incorporates a number of Lagrangian particle transport formulations based on an implicit trilinear interpolation scheme (Bennett and Clites 1987). The first formulation allows release of neutrally buoyant or buoyant drifters at user specified locations and times. This formulation is useful in simulating spill trajectories, search and rescue operations, and oceanographic instrument drifters. The second formulation releases drifters in each three-dimensional model cell at a specified sequence of times and calculates the generalized Lagrangian mean velocity field (Andrews and McIntyre 1978) relative to a user-specified averaging interval.

3.9   Wetland, Marsh, and Tidal Flat Simulation Extension

The EFDC model provides a number of enhancements for the simulation of flow and transport in wetlands, marshes, and tidal flats. The code allows for drying and wetting in shallow areas by a mass conservative scheme. The drying and wetting formulation is coupled to the mass transport equations in a manner that prevents negative concentrations of dissolved and suspended materials. A number of alternatives are in place in the model to simulate general discharge control structures such as weirs, spillways, culverts, and water surface elevation activated pumps. The effect of submerged and emergent plants is incorporated into the turbulence closure model and flow resistance formulation. Plant density and geometric characteristics of individual and composite plants are required as input for the vegetation resistance formulation. A simple soil moisture model, allowing rainfall infiltration and soil water loss due to evapotranspiration under dry conditions, is implemented. To represent narrow channels and canals in wetland, marsh and tidal flat systems, a subgrid scale channel model is implemented. The subgrid

channel model allows a 1-D network in the horizontal channels to be dynamically coupled to the two-dimensional horizontal grid representing the wetland, marsh, or tidal flat system. Volume and mass exchanges between 2-D wetland cells and the 1-D channels are accounted for. The channels may continue to flow when the 2-D wetland cells become dry.

3.10   Nearshore Wave-Induced Currents and Sediment Transport Extensions

The EFDC code includes a number of extensions for simulation of nearshore wave-induced currents and noncohesive sediment transport. The extensions include a wave-current boundary layer formulation similar to that of Grant and Madsen (1986); modifications of the hydrodynamic model's momentum equations to represent wave period averaged Eulerian mean quantities; the inclusion of the three-dimensional wave-induced radiation or Reynold's stresses in the momentum equations; and modifications of the velocity fields in the transport equations to include advective transport by the wave-induced Stoke's drift. High frequency surface wave fields are provide by an external wave refraction-diffraction model or by an internal mild slope equation submodel similar to that of Madsen and Larsen (1987). The internal refraction-diffraction computation is executed on a refined horizontal grid coincident with the main model's horizontal grid.

3.11   User Interface

The EFDC modeling package's user interface is based on text input file templates. This choice was selected in the interest of maintaining model portability across a range of computing platforms and readily allows the model user to modify input files using most text editing software. The text interface also allows modification of model files on remote computing systems and in hetrogeneous network environments. All input files have standard templates available with the EFDC code and in the digital version of the user's manual. The file templates include extensive built-in documentation and an explanation of numerical input data quantities. Actual numerical input data are inserted into the text template in a flexible free format as internally specified in the file templates. Extensive checking of input files is implemented in the code and diagnostic on screen messages indicate the location and nature of input file errors. All input files involving dimensional data have unit conversion specifications for the Meters-Kilograms-Seconds (MKS) international system of units used internally in the model.

3.12   Preprocessing Software

The EFDC modeling package includes a grid generating preprocessor code, GEFDC, which is used to construct the horizontal model grid, and interpolate bathymetry and initial fields such as water surface elevation, salinity, to the grid cells. EFDC inputs files specifying the grid geometry and initial fields are generated by the preprocessor. The preprocessor is capable of generating Cartesian and curvilinear-orthogonal grids using a number of grid generation schemes (Mobley and Stewart 1980; Ryskin and Leal 1983; Kang and Leal 1992).

3.13   Program Configuration

The EFDC code exists in only one generic version. A model application is specified entirely by information in the input files. To minimize memory requirements for specific applications, an executable file is created by adjusting the appropriate variable array size in the model's parameter file and compiling the source code. The EFDC model can be configured to execute all or a portion of a model application in reduced spatial dimension mode including 2-D depth or width averaged and 1-D cross section averaged. The number of layers used in the 3-D mode or 2-D width averaged mode is readily changed by one line of model input. Model grid sections specified as 2-D width averaged are allowed to have depth varying widths to provide representations equivalent to those of 2-D width averaged estuarine and reservoir models such as CE-QUAL-W2 (Cole and Buchak 1994).

3.14   Run-Time Diagnostics

The EFDC modeling package includes extensive built-in run-time diagnostics that may be activated in the master input file by the model user. Representative diagnostics include records of maximum CFL numbers, times and locations of negative depths, a variety of volume and mass balance checks, and global mass and energy balances. An on screen print of model variables in a specified cell can be activated during modeling execution. The model generates a number of log files that allow additional diagnostics of any run-time problems encountered during the set-up of a new application.

3.15   Model Output Options

A wide variety of output options are available for the EFDC model, including (1) specification of output files for horizontal plane and vertical plane transect plotting of vector and scalar field at a specified time; (2) the generation of time series of model variables at selected locations and time intervals; (3) grab sample simulation at specified times and locations; and (4) the specification of least squares analysis of selected model variables at a defined location over a specified interval. A general three-dimensional output option allows saving of all major model variables in a compressed-file format at specified times. A restart file is generated at user-specified intervals during model execution.

3.16   Postprocessing, Graphics, and Visualization

The generic model output files can be readily processed by a number of third party graphics and visualization software packages, often without the need for intermediate processing (Rennie and Hamrick 1992). The availability of the source code to the user allows the code to be modified for specific output options. Graphics and visualization software successfully used with EFDC output include: APE, AVS, IDL, Mathematica, MatLab, NCAR Graphics, PV-Wave, Techplot, SiteView, Spyglass Transform and Slicer, Voxelview, and GrADS. The model developer currently uses Spyglass and Voxelview and a number of postprocessor applications are available for special image enhancement for these products.

3.17   Documentation

Extensive documentation of the EFDC model is available. Theoretical and computational aspects of the model are described by Hamrick (1992a). The model user's manual (Hamrick 1996) provides details on use of the GEFDC preprocessor and set-up of the EFDC input files. Input file templates are also included. A number of papers describe model applications and capabilities (Hamrick 1992b; Hamrick 1994; Moustafa and Hamrick 1994; Hamrick and Wu 1996; and Wu et al. 1996).

3.18   Computer Requirements

The EFDC modeling system is written in FORTRAN 77. The few nonstandard VAX FORTRAN language extensions in the code are supported by a wide variety of ANSI standard FORTRAN 77 compilers. The generic or universal source code has been compiled and executed on most UNIX workstations (DEC Alpha, Hewlett-Packard, IBM RISC6000, Silicon Graphics, Sun and Sparc compatibles) Cray and Convex supercomputers, and PC compatible and Macintosh personal computers. Absoft, Lahey, and Microsoft compilers are supported on PC compatibles, while Absoft, Language Systems, and Motorola compilers are supported on Macintosh and compatible systems.

4 - EFDC WATER QUALITY MODEL

4.1 Introduction

The central issues in the water quality model are primary production of carbon by algae and concentration of dissolved oxygen. Primary production provides the energy required by the ecosystem to function. However, excessive primary production is detrimental since its decomposition in the water and sediments consumes oxygen. Dissolved oxygen is necessary to support the life functions of higher organisms and is considered an indicator of the health of estuarine systems. To predict primary production and dissolved oxygen, a large suite of model state variables is necessary (Table 4-1). The nitrate state variable in the model represents the sum of nitrate and nitrite nitrogen. The three variables (salinity, water temperature, and total suspended solids) needed for computation of the above 21 state variables are provided by the EFDC hydrodynamic model. The interactions among the state variables is illustrated in Figure 4-1. The kinetic processes included in the EFDC water quality model are mostly from the Chesapeake Bay three-dimensional water quality model, CE-QUAL-ICM (Cerco and Cole 1994). The kinetic sources and sinks, as well as the external loads for each state variable, are described in Sections 4.3 to 4.11. The kinetic processes include the exchange of fluxes at the sediment-water interface, including sediment oxygen demand, which are explained in Section 5 (EFDC Sediment Process Model) of this report. The description of the EFDC water column water quality model in this section is from Park et al. (1995).

Table 4-1. EFDC model water quality state variables

(1) cyanobacteria	(12) labile particulate organic nitrogen
(2) diatom algae	(13) dissolved organic nitrogen
(3) green algae	(14) ammonia nitrogen
(4) refractory particulate organic carbon	(15) nitrate nitrogen
(5) labile particulate organic carbon	(16) particulate biogenic silica
(6) dissolved organic carbon	(17) dissolved available silica
(7) refractory particulate organic phosphorus	(18) chemical oxygen demand
(8) labile particulate organic phosphorus	(19) dissolved oxygen
(9) dissolved organic phosphorus	(20) total active metal
(10) total phosphate	(21) fecal coliform bacteria
(11) refractory particulate organic nitrogen	(22) macroalgae
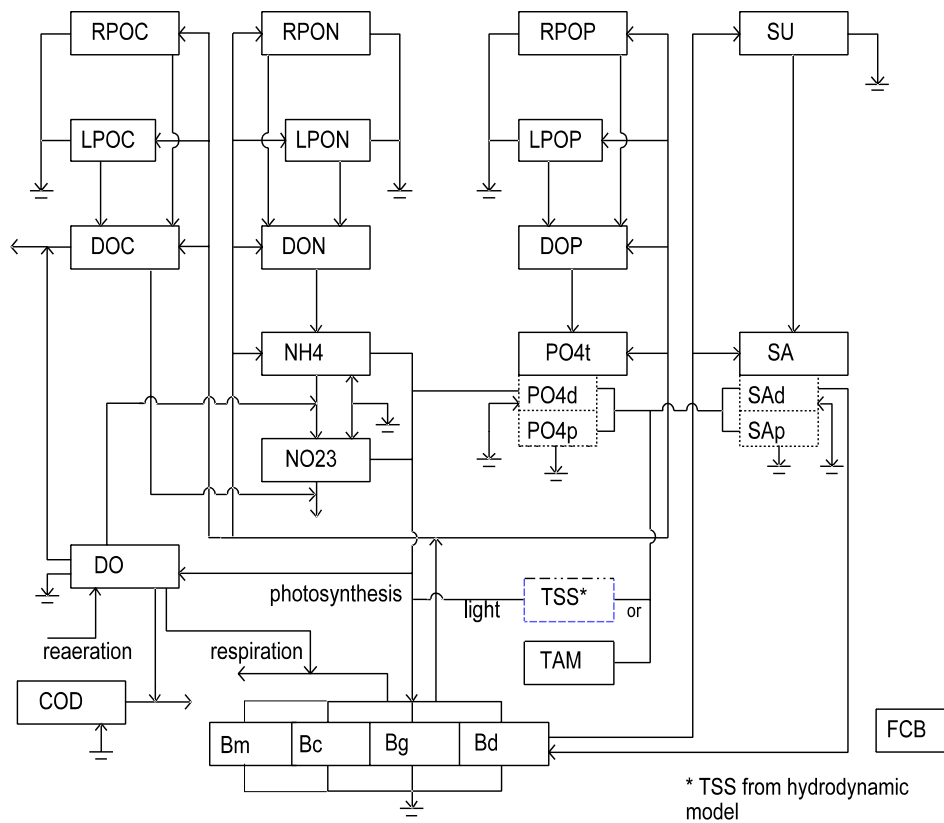
Figure 4-1. Schematic diagram for the EFDC water column water quality model

4.1.1 Algae

Algae are grouped into four model classes: cyanobacteria, diatoms, greens, and macroalgae. The grouping is based upon the distinctive characteristics of each class and upon the significant role the characteristics play in the ecosystem. Cyanobacteria, commonly called blue-green algae, are characterized by their abundance (as picoplankton) in saline water and by their bloom-forming characteristics in fresh water. Cyanobacteria are unique in that some species fix atmospheric nitrogen, although nitrogen fixers are not believed to be predominant in many river systems. Diatoms are distinguished by their requirement of silica as a nutrient to form cell walls. Diatoms are large algae characterized by high settling velocities. Settling of spring diatom blooms to the sediments may be a significant source of carbon for sediment oxygen demand. Algae that do not fall into the preceding two groups are lumped into the heading of green algae. Green algae settle at a rate intermediate between cyanobacteria and diatoms and are subject to greater grazing pressure than cyanobacteria. Macroalgae are

almost always attached to a stable substrate and are therefore most abundant in the areas of harbors and near shore. The waters in many stream systems are characterized by various rooted macrophytes and periphyton. All species of macroalgae in this study have been lumped into a single class of macroalgae. Because of their attachment to the substrate, they are limited to growing in the bottom water-column layer and are not subject to physical transport.

4.1.2   Organic Carbon

Three organic carbon state variables are considered: dissolved, labile particulate, and refractory particulate. Labile and refractory distinctions are based upon the time scale of decomposition. Labile organic carbon decomposes on a time scale of days to weeks whereas refractory organic carbon requires more time. Labile organic carbon decomposes rapidly in the water column or the sediments. Refractory organic carbon decomposes slowly, primarily in the sediments, and may contribute to sediment oxygen demand years after deposition.

4.1.3   Nitrogen

Nitrogen is first divided into organic and mineral fractions. Organic nitrogen state variables are dissolved organic nitrogen, labile particulate organic nitrogen, and refractory particulate organic nitrogen. Two mineral nitrogen forms are considered: ammonium and nitrate. Both are utilized to satisfy algal nutrient requirements, although ammonium is preferred from thermodynamic considerations. The primary reason for distinguishing the two is that ammonium is oxidized by nitrifying bacteria into nitrate. This oxidation can be a significant sink of oxygen in the water column and sediments. An intermediate in the complete oxidation of ammonium, nitrite, also exists. Nitrite concentrations are usually much less than nitrate, and for modeling purposes, nitrite is combined with nitrate. Hence the nitrate state variable actually represents the sum of nitrate plus nitrite.

4.1.4   Phosphorus

As with carbon and nitrogen, organic phosphorus is considered in three states: dissolved, labile particulate, and refractory particulate. Only a single mineral form, total phosphate, is considered. Total phosphate exists as several states within the model ecosystem: dissolved phosphate, phosphate sorbed to inorganic solids, and phosphate incorporated in algal cells. Equilibrium partition coefficients are used to distribute the total among the three states.

4.1.5   Silica

Silica is divided into two state variables: available silica and particulate biogenic silica. Available silica is primarily dissolved and can be utilized by diatoms. Particulate biogenic silica cannot be utilized. In the model, particulate biogenic silica is produced through diatom mortality. Particulate biogenic silica undergoes dissolution to available silica or else settles to the bottom sediments.

4.1.6   Chemical Oxygen Demand

In the context of this study, chemical oxygen demand is the concentration of reduced substances that are oxidizable by inorganic means. The primary component of chemical oxygen demand is sulfide released from sediments. Oxidation of sulfide to sulfate may remove substantial quantities of dissolved oxygen from the water column.

4.1.7   Dissolved Oxygen

Dissolved oxygen is required for the existence of higher life forms. Oxygen availability determines the distribution of organisms and the flows of energy and nutrients in an ecosystem. Dissolved oxygen is a central component of the water quality model.

4.1.8   Total Active Metal

Both phosphate and dissolved silica sorb to inorganic solids, primarily iron and manganese. Sorption and subsequent settling is one pathway for removal of phosphate and silica from the water column. Consequently, the concentration and transport of iron and manganese are represented in the model. Limited data do not allow a complete treatment of iron and manganese chemistry, however. Rather, a single-state variable, total active metal, is defined as the total concentration of metals that are active in phosphate and silica transport. Total active metal is partitioned between particulate and dissolved phases by an oxygen-dependent partition coefficient.

4.1.9   Salinity

Salinity is a conservative tracer that provides verification of the transport component of the model and facilitates examination of conservation of mass. Salinity also influences the dissolved oxygen saturation concentration and is used in the determination of kinetics constants that differ in saline and fresh water.

4.1.10   Temperature

Temperature is a primary determinant of the rate of biochemical reactions. Reaction rates increase as a function of temperature, although extreme temperatures result in the mortality of organisms.

4.2   Conservation of Mass Equation

The governing mass-balance equation for each of the water quality state variables may be expressed as:

$$\frac{\partial C}{\partial t} + \frac{\partial(uC)}{\partial x} + \frac{\partial(vC)}{\partial y} + \frac{\partial(wC)}{\partial z} =$$

$$\frac{\partial}{\partial x}\left(K_x\frac{\partial C}{\partial x}\right) \; + \; \frac{\partial}{\partial y}\left(K_y\frac{\partial C}{\partial y}\right) \; + \; \frac{\partial}{\partial z}\left(K_z\frac{\partial C}{\partial z}\right) \; + \; S_C \tag{4-1}$$

C	= concentration of a water quality state variable
u, v, w	= velocity components in the x-, y-, and z-directions, respectively
K_x, K_y, K_z	= turbulent diffusivities in the x-, y-, and z-directions, respectively
S_C	= internal and external sources and sinks per unit volume.

The last three terms on the left-hand side (LHS) of Eq. 4-1 account for the advective transport, and the first three terms on the right-hand side (RHS) of Eq. 4-1 account for the diffusive transport. These six terms for physical transport are analogous to, and thus the numerical method of solution is the same as, those in the mass-balance equation for salinity in the hydrodynamic model (Hamrick 1992a). The last term in Eq. 4-1 represents the kinetic processes and external loads for each of the state variables. The present model solves Eq. 4-1 after decoupling the kinetic terms from the physical transport terms. The solution scheme for both the physical transport (Hamrick 1992a) and the kinetic equations is second-order accurate.

The governing mass-balance equation for water quality state variables (Eq. 4-1) consists of physical transport, advective and diffusive, and kinetic processes. When solving Eq. 4-1, the kinetic terms are decoupled from the physical transport terms. The mass-balance equation for physical transport only, which takes the same form as the salt-balance equation, is:

$$\frac{\partial C}{\partial t} \; + \; \frac{\partial(uC)}{\partial x} \; + \; \frac{\partial(vC)}{\partial y} \; + \; \frac{\partial(wC)}{\partial z} \; = \; \frac{\partial}{\partial x}\left(K_x\frac{\partial C}{\partial x}\right) \; + \; \frac{\partial}{\partial y}\left(K_y\frac{\partial C}{\partial y}\right) \; + \; \frac{\partial}{\partial z}\left(K_z\frac{\partial C}{\partial z}\right) \tag{4-2}$$

The equation for kinetic processes only, which will be referred to as the kinetic equation, is:

$$\frac{\partial C}{\partial t} \; = \; S_C \tag{4-3}$$

which may be expressed as:

$$\frac{\partial C}{\partial t} \; = \; K \cdot C \; + \; R \tag{4-4}$$

where K is kinetic rate (time^{-1}) and R is source/sink term (mass volume^{-1} time^{-1}). Equation 4-4 is obtained by linearizing some terms in the kinetic equations, mostly Monod type expressions. Hence, K and R are known values in Eq. 4-4. Equation 4-2 is identical to, and thus its numerical method of solution is the same as, the mass-balance equation for salinity (Hamrick 1992a).

The remainder of this chapter details the kinetics portion of the mass-conservation equation for each state variable. Parameters are defined where they first appear. All parameters are listed, in alphabetical order, in an appendix. For consistency with reported rate coefficients, kinetics are detailed using a temporal dimension of days. Within the CE-QUAL-ICM computer code, kinetics sources and sinks are converted to a dimension of seconds before employment in the mass-conservation equation.

4.3   Algae

Algae, which occupies a central role in the model (Figure 4-1), are grouped into three model state variables: cyanobacteria (blue-green algae), diatoms, and green algae. The subscript, **x**, is used to denote four algal groups: **c** for cyanobacteria, **d** for diatoms, **g** for green algae, and **m** for macroalgae. Sources and sinks included in the model are

- growth (production)
- basal metabolism
- predation
- settling
- external loads

Equations describing these processes are largely the same for the four algal groups with differences in the values of parameters in the equations. The kinetic equation describing these processes is:

$$\frac{\partial B_x}{\partial t} = (P_x - BM_x - PR_x)B_x + \frac{\partial}{\partial z}(WS_x \cdot B_x) + \frac{WB_x}{V} \tag{4-5}$$

B_x = algal biomass of algal group x (g C m^{-3})

t   = time (day)

P_x = production rate of algal group x (day^{-1})

BM_x = basal metabolism rate of algal group x (day^{-1})

PR_x = predation rate of algal group x (day^{-1})

WS_x = settling velocity of algal group x (m day^{-1})

WB_x = external loads of algal group x (g C day^{-1})

V   = cell volume (m^3).

The model simulates the total biomass of the macroalgae rather than the size of the macroalgae; therefore, they can be treated as other groups of algae. Since macroalgae attach to the bottom, they are limited to growing in the bottom layer only and are not be transported through water movement.

4.3.1   Production (Algal Growth)

Algal growth depends on nutrient availability, ambient light, and temperature. The effects of these processes are considered to be multiplicative:

$$P_x = PM_x \cdot f_1(N) \cdot f_2(I) \cdot f_3(T) \qquad (4\text{-}6)$$

PM$_x$ = maximum growth rate under optimal conditions for algal group x (day^{-1})
$f_1(N)$ = effect of suboptimal nutrient concentration ($0 \le f_1 \le 1$)
$f_2(I)$ = effect of suboptimal light intensity ($0 \le f_2 \le 1$)
$f_3(T)$ = effect of suboptimal temperature ($0 \le f_3 \le 1$).

The freshwater cyanobacteria may undergo rapid mortality in salt water, e.g., freshwater organisms in the Potomac River (Thomann et al. 1985). For the freshwater organisms, the increased mortality may be included in the model by retaining the salinity toxicity term in the growth equation for cyanobacteria:

$$P_c = PM_c \cdot f_1(N) \cdot f_2(I) \cdot f_3(T) \cdot f_4(S) \qquad (4\text{-}7)$$

$f_4(S)$ = effect of salinity on cyanobacteria growth ($0 \le f_4 \le 1$).

Activation of the salinity toxicity term, $f_4(S)$, is an option in the source code.

4.3.2   Effect of Nutrients on Algal Growth

Using Liebig's "law of the minimum" (Odum 1971) that growth is determined by the nutrient in least supply, the nutrient limitation for growth of cyanobacteria and green algae is expressed as:

$$f_1(N) = minimum \left(\frac{NH4 + NO3}{KHN_x + NH4 + NO3}, \frac{PO4d}{KHP_x + PO4d} \right) \qquad (4\text{-}8)$$

NH4 = ammonium nitrogen concentration (g N m^{-3})
NO3 = nitrate nitrogen concentration (g N m^{-3})
KHN$_x$ = half-saturation constant for nitrogen uptake for algal group x (g N m^{-3})
PO4d = dissolved phosphate phosphorus concentration (g P m^{-3})
KHP$_x$ = half-saturation constant for phosphorus uptake for algal group x (g P m^{-3}).

Some cyanobacteria, e.g., *Anabaena*, can fix nitrogen from atmosphere and thus are not limited by nitrogen. Hence, Eq. 4-8 is not applicable to the growth of nitrogen fixers.

Since diatoms require silica as well as nitrogen and phosphorus for growth, the nutrient limitation for diatoms is expressed as:

$$f_1(N) = minimum \left(\frac{NH4 + NO3}{KHN_d + NH4 + NO3}, \frac{PO4d}{KHP_d + PO4d}, \frac{SAd}{KHS + SAd} \right) \qquad (4\text{-}9)$$

SAd   = concentration of dissolved available silica (g Si m^{-3})

KHS   = half-saturation constant for silica uptake for diatoms (g Si m^{-3}).

4.3.3   Effect of Light on Algal Growth

The daily and vertically integrated form of Steele's equation is:

$$f_2(I) = \frac{2.718 \cdot FD}{Kess \cdot \Delta z}(e^{-\alpha_B} - e^{-\alpha_T}) \tag{4-10}$$

$$\alpha_B = \frac{I_o}{FD \cdot (I_s)_x} \cdot \exp(-Kess[H_T + \Delta z]) \tag{4-11}$$

$$\alpha_T = \frac{I_o}{FD \cdot (I_s)_x} \cdot \exp(-Kess \cdot H_T) \tag{4-12}$$

FD   = fractional daylength ($0 \leq FD \leq 1$)

Kess   = total light extinction coefficient (m^{-1})

Δz = layer thickness (m)

I_o = daily total light intensity at water surface (langleys day^{-1})

$(I_s)_x$ = optimal light intensity for algal group x (langleys day^{-1})

H_T = depth from the free surface to the top of the layer (m).

Light extinction in the water column consists of three fractions in the model: a background value dependent on water color, extinction due to suspended particles, and extinction due to light absorption by ambient chlorophyll:

$$Kess = Ke_b + Ke_{TSS} \cdot TSS + Ke_{Chl} \cdot \sum_{x=c,d,g}\left(\frac{B_x}{CChl_x}\right) \tag{4-13}$$

Ke_b = background light extinction (m^{-1})

Ke_{TSS} = light extinction coefficient for total suspended solid (m^{-1} per g m^{-3})

TSS   = total suspended solid concentration (g m^{-3}) provided from the hydrodynamic model

Ke_{Chl} = light extinction coefficient for chlorophyll 'a' (m^{-1} per mg Chl m^{-3})

$CChl_x$ = carbon-to-chlorophyll ratio in algal group x (g C per mg Chl).

Since macroalgae only attach to the bottom, they are not included in computation of the light extinction Self shading is not considered for macroalgae for the present model. For a model application that does not simulate TSS, the Ke_{TSS} term may be set to zero and Ke_b may be estimated to include light extinction due to suspended solid.

Optimal light intensity (I_s) for photosynthesis depends on algal taxonomy, duration of exposure, temperature, nutritional status, and previous acclimation. Variations in I_s are largely due to adaptations by algae intended to maximize production in a variable environment. Steel (1962) noted the result of adaptations is that optimal intensity is a consistent fraction (approximately 50%) of daily intensity. Kremer and Nixon (1981) reported an analogous finding that maximum algal growth occurs at a constant depth (approximately 1 m) in the water column. Their approach is adopted so that optimal intensity is expressed as:

$$(I_s)_x = maximum\ \{(I_o)_{avg} \cdot e^{-Kess \cdot (D_{opt})_x}\ ,\ (I_s)_{min}\} \tag{4-14}$$

$(D_{opt})_x$ = depth of maximum algal growth for algal group x (m)
$(I_o)_{avg}$ = adjusted surface light intensity (langleys day^{-1}).

A minimum, $(I_s)_{min}$, in Eq. 4-14 is specified so that algae do not thrive at extremely low light levels. The time required for algae to adapt to changes in light intensity is recognized by estimating $(I_s)_x$ based on a time-weighted average of daily light intensity:

$$(I_o)_{avg} = CI_a \cdot I_o + CI_b \cdot I_1 + CI_c \cdot I_2 \tag{4-15}$$

I_1 = daily light intensity 1 day preceding model day (langleys day^{-1})
I_2 = daily light intensity 2 days preceding model day (langleys day^{-1})
CI_a, CI_b, CI_c = weighting factors for I_0, I_1 and I_2, respectively: $CI_a + CI_b + CI_c = 1$.

4.3.4 Effect of Temperature on Algal Growth

A Gaussian probability curve is used to represent temperature dependency of algal growth:

$$\begin{aligned} f_3(T) &= \exp(-KTG1_x[T - TM_x]^2) & if \quad T \le TM_x \\ &= \exp(-KTG2_x[TM_x - T]^2) & if \quad T > TM_x \end{aligned} \tag{4-16}$$

T = temperature (°C) provided from the hydrodynamic model
TM_x = optimal temperature for algal growth for algal group x (°C)
$KTG1_x$ = effect of temperature below TM_x on growth for algal group x (°C^{-2})
$KTG2_x$ = effect of temperature above TM_x on growth for algal group x (°C^{-2}).

4.3.5 Effect of Salinity on Growth of Freshwater Cyanobacteria

The growth of freshwater cyanobacteria in salt water is limited by:

$$f_4(S) = \frac{STOX^2}{STOX^2 + S^2} \tag{4-17}$$

STOX = salinity at which Microcystis growth is halved (ppt)

S   = salinity in water column (ppt) provided from the hydrodynamic model.

4.3.6   Algal Basal Metabolism

Algal biomass in the present model decreases through basal metabolism (respiration and excretion) and predation. Basal metabolism in the present model is the sum of all internal processes that decrease algal biomass and consists of two parts; respiration and excretion. In basal metabolism, algal matter (carbon, nitrogen, phosphorus, and silica) is returned to organic and inorganic pools in the environment, mainly to dissolved organic and inorganic matter. Respiration, which may be viewed as a reversal of production, consumes dissolved oxygen. Basal metabolism is considered to be an exponentially increasing function of temperature:

$$BM_x = BMR_x \cdot \exp(KTB_x[T - TR_x]) \tag{4-18}$$

BMR_x = basal metabolism rate at TR_x for algal group x (day^{-1})

KTB_x = effect of temperature on metabolism for algal group x (°C^{-1})

TR_x = reference temperature for basal metabolism for algal group x (°C).

4.3.7   Algal Predation

The present model does not include zooplankton. Instead, a constant rate is specified for algal predation, which implicitly assumes zooplankton biomass is a constant fraction of algal biomass. An equation similar to that for basal metabolism (Eq. 4-18) is used for predation:

$$PR_x = PRR_x \cdot \exp(KTB_x[T - TR_x]) \tag{4-19}$$

PRR_x = predation rate at TR_x for algal group x (day^{-1}).

The difference between predation and basal metabolism lies in the distribution of the end products of the two processes. In predation, algal matter (carbon, nitrogen, phosphorus, and silica) is returned to organic and inorganic pools in the environment, mainly to particulate organic matter. The predation for macroalgae is a lumped parameter that includes losses due to grazing, frond breakage, and other losses. This implicitly assumes that the losses are a fraction of the biomass.

4.3.8   Algal Settling

Settling velocities for four algal groups, WS_c, WS_d , WS_g, and WS_m, are specified as an input. Seasonal variations in settling velocity of diatoms can be accounted for by specifying time-varying WS_d.

4.4   Organic Carbon

The present model has three state variables for organic carbon: refractory particulate, labile particulate, and dissolved.

4.4.1 Particulate Organic Carbon

Labile and refractory distinctions are based on the time scale of decomposition. Labile particulate organic carbon with a decomposition time scale of days to weeks decomposes rapidly in the water column or in the sediments. Refractory particulate organic carbon with a longer-than-weeks decomposition time scale decomposes slowly, primarily in the sediments, and may contribute to sediment oxygen demand years after decomposition. For labile and refractory particulate organic carbon, sources and sinks included in the model are (Fig. 4-1):

- algal predation
- dissolution to dissolved organic carbon
- settling
- external loads.

The governing equations for refractory and labile particulate organic carbons are:

$$\frac{\partial RPOC}{\partial t} = \sum_{x=c,d,g,m} FCRP \cdot PR_x \cdot B_x - K_{RPOC} \cdot RPOC + \frac{\partial}{\partial z}(WS_{RP} \cdot RPOC) + \frac{WRPOC}{V} \quad (4\text{-}20)$$

$$\frac{\partial LPOC}{\partial t} = \sum_{x=c,d,g,m} FCLP \cdot PR_x \cdot B_x - K_{LPOC} \cdot LPOC + \frac{\partial}{\partial z}(WS_{LP} \cdot LPOC) + \frac{WLPOC}{V} \quad (4\text{-}21)$$

RPOC = concentration of refractory particulate organic carbon (g C m^{-3})

LPOC = concentration of labile particulate organic carbon (g C m^{-3})

FCRP = fraction of predated carbon produced as refractory particulate organic carbon

FCLP = fraction of predated carbon produced as labile particulate organic carbon

K_{RPOC} = dissolution rate of refractory particulate organic carbon (day^{-1})

K_{LPOC} = dissolution rate of labile particulate organic carbon (day^{-1})

WS_{RP} = settling velocity of refractory particulate organic matter (m day^{-1})

WS_{LP} = settling velocity of labile particulate organic matter (m day^{-1})

WRPOC = external loads of refractory particulate organic carbon (g C day^{-1})

WLPOC = external loads of labile particulate organic carbon (g C day^{-1}).

4.4.2 Dissolved Organic Carbon

Sources and sinks for dissolved organic carbon included in the model are (Fig. 4-1):

- algal excretion (exudation) and predation
- dissolution from refractory and labile particulate organic carbon
- heterotrophic respiration of dissolved organic carbon (decomposition)
- denitrification

- external loads

The kinetic equation describing these processes is:

$$\frac{\partial DOC}{\partial t} = \sum_{x=c,d,g,m} \left(\left[FCD_x + (1 - FCD_x)\frac{KHR_x}{KHR_x + DO} \right] BM_x + FCDP \cdot PR_x \right) \cdot B_x$$

$$+ K_{RPOC} \cdot RPOC + K_{LPOC} \cdot LPOC - K_{HR} \cdot DOC - Denit \cdot DOC + \frac{WDOC}{V} \quad (4\text{-}22)$$

DOC   = concentration of dissolved organic carbon (g C m^{-3})

FCD$_x$ = fraction of basal metabolism exuded as dissolved organic carbon at infinite dissolved oxygen concentration for algal group x

KHR$_x$ = half-saturation constant of dissolved oxygen for algal dissolved organic carbon excretion for group x (g O$_2$ m^{-3})

DO   = dissolved oxygen concentration (g O$_2$ m^{-3})

FCDP   = fraction of predated carbon produced as dissolved organic carbon

K$_{HR}$ = heterotrophic respiration rate of dissolved organic carbon (day^{-1})

Denit   = denitrification rate (day^{-1}) given in Eq. 4-34

WDOC = external loads of dissolved organic carbon (g C day^{-1}).

The remainder of this section explains each term in Equations 4-20 to 4-22.

4.4.3   Effect of Algae on Organic Carbon

The terms within summation ($\sum$) in Equations 4-20 to 4-22 account for the effects of algae on organic carbon through basal metabolism and predation.

4.4.3.1 Basal metabolism. Basal metabolism, consisting of respiration and excretion, returns algal matter (carbon, nitrogen, phosphorus, and silica) back to the environment. Loss of algal biomass through basal metabolism is (Eq. 4-18):

$$\frac{\partial B_x}{\partial t} = -BM_x \cdot B_x \qquad (4\text{-}23)$$

which indicates that the total loss of algal biomass due to basal metabolism is independent of ambient dissolved oxygen concentration. In this model, it is assumed that the distribution of total loss between respiration and excretion is constant as long as there is sufficient dissolved oxygen for algae to respire. Under that condition, the losses by respiration and excretion may be written as:

$$(1 - FCD_x) \cdot BM_x \cdot B_x \qquad \text{due to respiration} \qquad (4\text{-}24)$$

$$FCD_x \cdot BM_x \cdot B_x \qquad \text{due to excretion} \qquad (4\text{-}25)$$

where FCD_x is a constant of value between 0 and 1. Algae cannot respire in the absence of oxygen, however. Although the total loss of algal biomass due to basal metabolism is oxygen-independent (Eq. 4-23), the distribution of total loss between respiration and excretion is oxygen-dependent. When oxygen level is high, respiration is a large fraction of the total. As dissolved oxygen becomes scarce, excretion becomes dominant. Thus, Eq. 4-24 represents the loss by respiration only at high oxygen levels. In general, Eq. 4-24 can be decomposed into two fractions as a function of dissolved oxygen availability:

$$(1 - FCD_x)\frac{DO}{KHR_x + DO}BM_x{\cdot}B_x \qquad\qquad \text{due to respiration} \qquad\qquad (4\text{-}26)$$

$$(1 - FCD_x)\frac{KHR_x}{KHR_x + DO}BM_x{\cdot}B_x \qquad\qquad \text{due to excretion} \qquad\qquad (4\text{-}27)$$

Equation 4-26 represents the loss of algal biomass by respiration, and Eq. 4-27 represents additional excretion due to insufficient dissolved oxygen concentration. The parameter KHR_x, which is defined as the half-saturation constant of dissolved oxygen for algal dissolved organic carbon excretion in Eq. 4-22, can also be defined as the half-saturation constant of dissolved oxygen for algal respiration in Eq. 4-26.

Combining Equations 4-25 and 4-27, the total loss due to excretion is:

$$\left(FCD_x + (1 - FCD_x)\frac{KHR_x}{KHR_x + DO} \right) BM_x{\cdot}B_x \qquad\qquad (4\text{-}28)$$

Equations 4-26 and 4-28 combine to give the total loss of algal biomass due to basal metabolism, $BM_x{\cdot}B_x$ (Eq. 4-23). The definition of FCD_x in Eq. 4-22 becomes apparent in Eq. 4-28; i.e., fraction of basal metabolism exuded as dissolved organic carbon at infinite dissolved oxygen concentration. At zero oxygen level, 100% of total loss due to basal metabolism is by excretion regardless of FCD_x. The end carbon product of respiration is primarily carbon dioxide, an inorganic form not considered in the present model, while the end carbon product of excretion is primarily dissolved organic carbon. Therefore, Eq. 4-28, that appears in Eq. 4-22, represents the contribution of excretion to dissolved organic carbon, and there is no source term for particulate organic carbon from algal basal metabolism in Equations 4-20 and 4-21.

4.4.3.2 Predation. Algae produce organic carbon through the effects of predation. Zooplankton take up and redistribute algal carbon through grazing, assimilation, respiration, and excretion. Since zooplankton are not included in the model, routing of algal carbon through zooplankton predation is simulated by

empirical distribution coefficients in Equations 4-20 to 4-22; FCRP, FCLP, and FCDP. The sum of these three predation fractions should be unity.

4.4.4   Heterotrophic Respiration and Dissolution

The second term on the RHS of Equations 4-20 and 4-21 represents dissolution of particulate to dissolved organic carbon and the third term in the second line of Eq. 4-22 represents heterotrophic respiration of dissolved organic carbon. The oxic heterotrophic respiration is a function of dissolved oxygen: the lower the dissolved oxygen, the smaller the respiration term becomes. Heterotrophic respiration rate, therefore, is expressed using a Monod function of dissolved oxygen:

$$K_{HR} = \frac{DO}{KHOR_{DO} + DO} K_{DOC} \tag{4-29}$$

$KHOR_{DO}$ = oxic respiration half-saturation constant for dissolved oxygen (g O_2 m^{-3})

K_{DOC} = heterotrophic respiration rate of dissolved organic carbon at infinite dissolved oxygen concentration (day^{-1}).

Dissolution and heterotrophic respiration rates depend on the availability of carbonaceous substrate and on heterotrophic activity. Algae produce labile carbon that fuels heterotrophic activity: dissolution and heterotrophic respiration do not require the presence of algae though, and may be fueled entirely by external carbon inputs. In the model, algal biomass, as a surrogate for heterotrophic activity, is incorporated into formulations of dissolution and heterotrophic respiration rates. Formulations of these rates require specification of algal-dependent and algal-independent rates:

$$K_{RPOC} = (K_{RC} + K_{RCalg} \sum_{x=c,d,g} B_x) \cdot \exp(KT_{HDR}[T - TR_{HDR}]) \tag{4-30}$$

$$K_{LPOC} = (K_{LC} + K_{LCalg} \sum_{x=c,d,g} B_x) \cdot \exp(KT_{HDR}[T - TR_{HDR}]) \tag{4-31}$$

$$K_{DOC} = (K_{DC} + K_{DCalg} \sum_{x=c,d,g} B_x) \cdot \exp(KT_{MNL}[T - TR_{MNL}]) \tag{4-32}$$

K_{RC} = minimum dissolution rate of refractory particulate organic carbon (day^{-1})

K_{LC} = minimum dissolution rate of labile particulate organic carbon (day^{-1})

K_{DC} = minimum respiration rate of dissolved organic carbon (day^{-1})

K_{RCalg}, K_{LCalg} = constants that relate dissolution of refractory and labile particulate organic carbon, respectively, to algal biomass (day^{-1} per g C m^{-3})

K_{DCalg} = constant that relates respiration to algal biomass (day^{-1} per g C m^{-3})

KT_{HDR} = effect of temperature on hydrolysis of particulate organic matter (°C^{-1})

TR_{HDR} = reference temperature for hydrolysis of particulate organic matter (°C)

KT_{MNL} = effect of temperature on mineralization of dissolved organic matter (°C^{-1})

TR_{MNL} = reference temperature for mineralization of dissolved organic matter (°C).

Equations 4-30 to 4-32 have exponential functions that relate rates to temperature.

In the present model, the term "hydrolysis" is defined as the process by which particulate organic matter is converted to dissolved organic form, and thus includes both dissolution of particulate carbon and hydrolysis of particulate phosphorus and nitrogen. Therefore, the parameters, KT_{HDR} and TR_{HDR}, are also used for the temperature effects on hydrolysis of particulate phosphorus (Equations 4-28 and 4-29) and nitrogen (Equations 4-54 and 4-55). The term "mineralization" is defined as the process by which dissolved organic matter is converted to dissolved inorganic form, and thus includes both heterotrophic respiration of dissolved organic carbon and mineralization of dissolved organic phosphorus and nitrogen. Therefore, the parameters, KT_{MNL} and TR_{MNL}, are also used for the temperature effects on mineralization of dissolved phosphorus (Eq. 4-46) and nitrogen (Eq. 4-56).

4.4.5   Effect of Denitrification on Dissolved Organic Carbon

As oxygen is depleted from natural systems, organic matter is oxidized by the reduction of alternate electron acceptors. Thermodynamically, the first alternate acceptor reduced in the absence of oxygen is nitrate. The reduction of nitrate by a large number of heterotrophic anaerobes is referred to as denitrification, and the stoichiometry of this reaction is (Stumm and Morgan 1981):

$$4NO_3^- + 4H^+ + 5CH_2O \rightarrow 2N_2 + 7H_2O + 5CO_2 \tag{4-33}$$
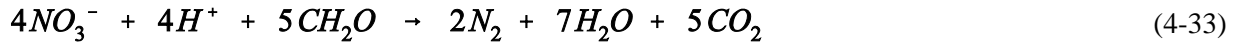
The last term in Eq. 4-22 accounts for the effect of denitrification on dissolved organic carbon. The kinetics of denitrification in the model are first-order:

$$Denit = \frac{KHOR_{DO}}{KHOR_{DO} + DO} \frac{NO3}{KHDN_N + NO3} AANOX \cdot K_{DOC} \tag{4-34}$$

$KHDN_N$ = denitrification half-saturation constant for nitrate (g N m^{-3})

$AANOX$ = ratio of denitrification rate to oxic dissolved organic carbon respiration rate.

In Eq. 4-34, the dissolved organic carbon respiration rate, K_{DOC}, is modified so that significant decomposition via denitrification occurs only when nitrate is freely available and dissolved oxygen is depleted. The ratio, AANOX, makes the anoxic respiration slower than oxic respiration. Note that K_{DOC}, defined in Eq. 4-32, includes the temperature effect on denitrification.

4.5   Phosphorus

The present model has four state variables for phosphorus: three organic forms (refractory particulate, labile particulate, and dissolved) and one inorganic form (total phosphate).

4.5.1   Particulate Organic Phosphorus

For refractory and labile particulate organic phosphorus, sources and sinks included in the model are (Fig. 4-1):

- algal basal metabolism and predation
- dissolution to dissolved organic phosphorus
- settling
- external loads.

The kinetic equations for refractory and labile particulate organic phosphorus are:

$$\frac{\partial RPOP}{\partial t} = \sum_{x=c,d,g,m} (FPR_x \cdot BM_x + FPRP \cdot PR_x) APC \cdot B_x - K_{RPOP} \cdot RPOP$$

$$+ \frac{\partial}{\partial z}(WS_{RP} \cdot RPOP) + \frac{WRPOP}{V} \tag{4-35}$$

$$\frac{\partial LPOP}{\partial t} = \sum_{x=c,d,g,m} (FPL_x \cdot BM_x + FPLP \cdot PR_x) APC \cdot B_x - K_{LPOP} \cdot LPOP$$

$$+ \frac{\partial}{\partial z}(WS_{LP} \cdot LPOP) + \frac{WLPOP}{V} \tag{4-36}$$

RPOP   = concentration of refractory particulate organic phosphorus (g P m^{-3})

LPOP   = concentration of labile particulate organic phosphorus (g P m^{-3})

FPR_x = fraction of metabolized phosphorus by algal group x produced as refractory particulate organic phosphorus

FPL_x = fraction of metabolized phosphorus by algal group x produced as labile particulate organic phosphorus

FPRP   = fraction of predated phosphorus produced as refractory particulate organic phosphorus

FPLP   = fraction of predated phosphorus produced as labile particulate organic phosphorus

APC   = mean algal phosphorus-to-carbon ratio for all algal groups (g P per g C)

K_{RPOP} = hydrolysis rate of refractory particulate organic phosphorus (day^{-1})

K_{LPOP} = hydrolysis rate of labile particulate organic phosphorus (day^{-1})

WRPOP = external loads of refractory particulate organic phosphorus (g P day^{-1})

WLPOP = external loads of labile particulate organic phosphorus (g P day^{-1}).

4.5.2   Dissolved Organic Phosphorus

Sources and sinks for dissolved organic phosphorus included in the model are (Fig. 4-1):

- algal basal metabolism and predation
- dissolution from refractory and labile particulate organic phosphorus
- mineralization to phosphate phosphorus

- external loads.

The kinetic equation describing these processes is:

$$\frac{\partial DOP}{\partial t} = \sum_{x=c,d,g,m}(FPD_x{\cdot}BM_x + FPDP{\cdot}PR_x)APC{\cdot}B_x$$

$$+ K_{RPOP}{\cdot}RPOP + K_{LPOP}{\cdot}LPOP - K_{DOP}{\cdot}DOP + \frac{WDOP}{V} \tag{4-37}$$

DOP   = concentration of dissolved organic phosphorus (g P m^{-3})

FPD$_x$ = fraction of metabolized phosphorus by algal group x produced as dissolved organic phosphorus

FPDP   = fraction of predated phosphorus produced as dissolved organic phosphorus

K$_{DOP}$ = mineralization rate of dissolved organic phosphorus (day^{-1})

WDOP = external loads of dissolved organic phosphorus (g P day^{-1}).

4.5.3   Total Phosphate

For total phosphate that includes both dissolved and sorbed phosphate (Section 4.5.4), sources and sinks included in the model are (Fig. 4-1):

- algal basal metabolism, predation, and uptake
- mineralization from dissolved organic phosphorus
- settling of sorbed phosphate
- sediment-water exchange of dissolved phosphate for the bottom layer only
- external loads.

The kinetic equation describing these processes is:

$$\frac{\partial PO4t}{\partial t} = \sum_{x=c,d,g,m}(FPI_x{\cdot}BM_x + FPIP{\cdot}PR_x - P_x)APC{\cdot}B_x + K_{DOP}{\cdot}DOP$$

$$+ \frac{\partial}{\partial z}(WS_{TSS}{\cdot}PO4p) + \frac{BFPO4d}{\Delta z} + \frac{WPO4t}{V} \tag{4-38}$$

PO4t   = total phosphate (g P m^{-3}) = PO4d + PO4p   (4-39)

PO4d   = dissolved phosphate (g P m^{-3})

PO4p   = particulate (sorbed) phosphate (g P m^{-3})

FPI$_x$ = fraction of metabolized phosphorus by algal group x produced as inorganic phosphorus

FPIP   = fraction of predated phosphorus produced as inorganic phosphorus

WS$_{TSS}$ = settling velocity of suspended solid (m day^{-1}), provided by the hydrodynamic model

BFPO4d = sediment-water exchange flux of phosphate (g P m^{-2} day^{-1}), applied to the bottom layer only

WPO4t = external loads of total phosphate (g P day^{-1}).

In Eq. 4-38, if total active metal is chosen as a measure of sorption site, the settling velocity of total suspended solid, WS_{TSS}, is replaced by that of particulate metal, WS_s (Sections 4.5.4 and 4.10). The remainder of this section explains each term in Equations 4-35 to 4-38, except BFPO4d (benthic flux of dissolved orthophosphate), which is described in Chapter 5.

4.5.4   Total Phosphate System

Suspended and bottom sediment particles (clay, silt, and metal hydroxides) adsorb and desorb phosphate in river and estuarine waters. This adsorption-desorption process has been suggested to buffer phosphate concentration in water column and to enhance the transport of phosphate away from its external sources (Carritt and Goodgal 1954; Froelich 1988; Lebo 1991). To ease the computational complication due to the adsorption-desorption of phosphate, dissolved and sorbed phosphate are treated and transported as a single state variable. Therefore, the model phosphate state variable, total phosphate, is defined as the sum of dissolved and sorbed phosphate (Eq. 4-39), and the concentrations for each fraction are determined by equilibrium partitioning of their sum.

In CE-QUAL-ICM, sorption of phosphate to particulate species of metals including iron and manganese was considered based on a phenomenon observed in the monitoring data from the mainstem of the Chesapeake Bay: phosphate was rapidly depleted from anoxic bottom waters during the autumn reaeration event (Cerco and Cole 1993). Their hypothesis was that reaeration of bottom waters caused dissolved iron and manganese to precipitate, and phosphate sorbed to newly formed metal particles and rapidly settled to the bottom. One state variable, total active metal, in CE-QUAL-ICM was defined as the sum of all metals that act as sorption sites, and the total active metal was partitioned into particulate and dissolved fractions via an equilibrium partitioning coefficient (Section 4.10). Then phosphate was assumed to sorb to only the particulate fraction of the total active metal.

In the treatment of phosphate sorption in CE-QUAL-ICM, the particulate fraction of metal hydroxides was emphasized as a sorption site in bottom waters under anoxic conditions. Phosphorus is a highly particle-reactive element, and phosphate in solution reacts quickly with a wide variety of surfaces, being taken up by and released from particles (Froelich 1988). The present model has two options, total suspended solid and total active metal, as a measure of a sorption site for phosphate, and dissolved and sorbed fractions are determined by equilibrium partitioning of their sum as a function of total suspended solid or total active metal concentration:

$$PO4p = \frac{K_{PO4p} \cdot TSS}{1 + K_{PO4p} \cdot TSS} PO4t \quad \text{or} \quad PO4p = \frac{K_{PO4p} \cdot TAMp}{1 + K_{PO4p} \cdot TAMp} PO4t \qquad (4\text{-}40)$$

$$PO4d = \frac{1}{1 + K_{PO4p} \cdot TSS} PO4t \quad \text{or} \quad PO4d = \frac{1}{1 + K_{PO4p} \cdot TAMp} PO4t$$

$$= \ PO4t \ - \ PO4p \tag{4-41}$$

K_{PO4p} = empirical coefficient relating phosphate sorption to total suspended solid (per g m^{-3}) or

particulate total active metal (per mol m^{-3}) concentration

TAMp = particulate total active metal (mol m^{-3}).

Dividing Eq. 4-40 by Eq. 4-41 gives:

$$K_{PO4p} \ = \ \frac{PO4p}{PO4d}\frac{1}{TSS} \qquad \text{or} \qquad K_{PO4p} \ = \ \frac{PO4p}{PO4d}\frac{1}{TAMp} \tag{4-42}$$

where the meaning of K_{PO4p} becomes apparent, i.e., the ratio of sorbed to dissolved phosphate per unit concentration of total suspended solid or particulate total active metal (i.e., per unit sorption site available).

4.5.5   Algal Phosphorus-to-Carbon Ratio (APC)

Algal biomass is quantified in units of carbon per volume of water. In order to express the effects of algal biomass on phosphorus and nitrogen, the ratios of phosphorus-to-carbon and nitrogen-to-carbon in algal biomass must be specified. Although global mean values of these ratios are well known (Redfield et al. 1963), algal composition varies especially as a function of nutrient availability. As phosphorus and nitrogen become scarce, algae adjust their composition so that smaller quantities of these vital nutrients are required to produce carbonaceous biomass (DiToro 1980; Parsons et al. 1984). Examining the field data from the surface of upper Chesapeake Bay, Cerco and Cole (1993) showed that the variation of nitrogen-to-carbon stoichiometry was small and thus used a constant algal nitrogen-to-carbon ratio, ANC_x. Large variations, however, were observed for algal phosphorus-to-carbon ratio indicating the adaptation of algae to ambient phosphorus concentration (Cerco and Cole 1993): algal phosphorus content is high when ambient phosphorus is abundant and is low when ambient phosphorus is scarce. Thus, a variable algal phosphorus-to-carbon ratio, APC, is used in model formulation. A mean ratio for all algal groups, APC, is described by an empirical approximation to the trend observed in field data (Cerco & Cole 1994):

$$APC \ = \ \left(CP_{prm1} \ + \ CP_{prm2}\cdot\exp\left[- \ CP_{prm3}\cdot PO4d\right]\right)^{-1} \tag{4-43}$$

CP_{prm1} = minimum carbon-to-phosphorus ratio (g C per g P)
CP_{prm2} = difference between minimum and maximum carbon-to-phosphorus ratio (g C per g P)
CP_{prm3} = effect of dissolved phosphate concentration on carbon-to-phosphorus ratio (per g P m^{-3}).

4.5.6   Effect of Algae on Phosphorus

The terms within summation ($\sum$) in Equations 4-35 to 4-38 account for the effects of algae on phosphorus. Both basal metabolism (respiration and excretion) and predation are considered, and thus formulated, to contribute to organic and phosphate phosphorus. That is, the total loss by basal metabolism ($BM_x \cdot B_x$ in Eq. 4-5) is distributed using distribution coefficients; FPR_x, FPL_x, FPD_x, and FPI_x. The total loss by predation ($PR_x \cdot B_x$ in Eq. 4-5), is also distributed using distribution coefficients; FPRP, FPLP, FPDP, and FPIP. The sum of four distribution coefficients for basal metabolism should be unity, and so is that for predation. Algae take up dissolved phosphate for growth, and algae uptake of phosphate is represented by ($- \sum P_x \cdot APC \cdot B_x$) in Eq. 4-38.

4.5.7 Mineralization and Hydrolysis

The third term on the RHS of Equations 4-35 and 4-36 represents hydrolysis of particulate organic phosphorus, and the last term in Eq. 3-7 represents mineralization of dissolved organic phosphorus. Mineralization of organic phosphorus is mediated by the release of nucleotidase and phosphatase enzymes by bacteria (Chróst and Overbek 1987) and algae (Boni et al. 1989). Since the algae themselves release the enzymes and bacterial abundance is related to algal biomass, the rate of organic phosphorus mineralization is related to algal biomass in model formulation. Another mechanism included in model formulation is that algae stimulate production of an enzyme that mineralizes organic phosphorus to phosphate when phosphate is scarce (Chróst and Overbek 1987; Boni et al. 1989). The formulations for hydrolysis and mineralization rates including these processes are:

$$K_{RPOP} = (K_{RP} + \frac{KHP}{KHP + PO4d} K_{RPalg} \sum_{x=c,d,g} B_x) \cdot \exp(KT_{HDR}[T - TR_{HDR}]) \tag{4-44}$$

$$K_{LPOP} = (K_{LP} + \frac{KHP}{KHP + PO4d} K_{LPalg} \sum_{x=c,d,g} B_x) \cdot \exp(KT_{HDR}[T - TR_{HDR}]) \tag{4-45}$$

$$K_{DOP} = (K_{DP} + \frac{KHP}{KHP + PO4d} K_{DPalg} \sum_{x=c,d,g} B_x) \cdot \exp(KT_{MNL}[T - TR_{MNL}]) \tag{4-46}$$

K_{RP} = minimum hydrolysis rate of refractory particulate organic phosphorus (day^{-1})

K_{LP} = minimum hydrolysis rate of labile particulate organic phosphorus (day^{-1})

K_{DP} = minimum mineralization rate of dissolved organic phosphorus (day^{-1})

K_{RPalg}, K_{LPalg} = constants that relate hydrolysis of refractory and labile particulate organic phosphorus, respectively, to algal biomass (day^{-1} per g C m^{-3})

K_{DPalg} = constant that relates mineralization to algal biomass (day^{-1} per g C m^{-3})

KHP = mean half-saturation constant for algal phosphorus uptake (g P m^{-3}).

$$= \frac{1}{3} \sum_{x=c,d,g} KHP_x \tag{4-47}$$

When phosphate is abundant relative to KHP, the rates become close to the minimum values with little influence from algal biomass. When phosphate becomes scarce relative to KHP, the rates increase with the magnitude of increase depending on algal biomass. Equations 4-44 to 4-46 have exponential functions that relate rates to temperature.

4.6 Nitrogen

The present model has five state variables for nitrogen: three organic forms (refractory particulate, labile particulate, and dissolved) and two inorganic forms (ammonium and nitrate). The nitrate state variable in the model represents the sum of nitrate and nitrite.

4.6.1 Particulate Organic Nitrogen

For refractory and labile particulate organic nitrogen, sources and sinks included in the model are (Figure 4-1):

- algal basal metabolism and predation
- dissolution to dissolved organic nitrogen
- settling
- external loads.

The kinetic equations for refractory and labile particulate organic nitrogen are:

$$\frac{\partial RPON}{\partial t} = \sum_{x=c,d,g,m} (FNR_x \cdot BM_x + FNRP \cdot PR_x) ANC_x \cdot B_x - K_{RPON} \cdot RPON$$

$$+ \frac{\partial}{\partial z}(WS_{RP} \cdot RPON) + \frac{WRPON}{V} \tag{4-48}$$

$$\frac{\partial LPON}{\partial t} = \sum_{x=c,d,g,m} (FNL_x \cdot BM_x + FNLP \cdot PR_x) ANC_x \cdot B_x - K_{LPON} \cdot LPON$$

$$+ \frac{\partial}{\partial z}(WS_{LP} \cdot LPON) + \frac{WLPON}{V} \tag{4-49}$$

RPON = concentration of refractory particulate organic nitrogen (g N m^{-3})

LPON = concentration of labile particulate organic nitrogen (g N m^{-3})

FNR$_x$ = fraction metabolized nitrogen by algal group x as refractory particulate organic nitrogen

FNL$_x$ = fraction of metabolized nitrogen by algal group x produced as labile particulate organic nitrogen

FNRP = fraction of predated nitrogen produced as refractory particulate organic nitrogen

FNLP = fraction of predated nitrogen produced as labile particulate organic nitrogen

ANC_x = nitrogen-to-carbon ratio in algal group x (g N per g C)

K_{RPON} = hydrolysis rate of refractory particulate organic nitrogen (day^{-1})

K_{LPON} = hydrolysis rate of labile particulate organic nitrogen (day^{-1})

WRPON = external loads of refractory particulate organic nitrogen (g N day^{-1})

WLPON = external loads of labile particulate organic nitrogen (g N day^{-1}).

4.6.2   Dissolved Organic Nitrogen

Sources and sinks for dissolved organic nitrogen included in the model are (Fig. 4-1):

- algal basal metabolism and predation
- dissolution from refractory and labile particulate organic nitrogen
- mineralization to ammonium
- external loads.

The kinetic equation describing these processes is:

$$\frac{\partial DON}{\partial t} = \sum_{x=c,d,g,m} (FND_x \cdot BM_x + FNDP \cdot PR_x) ANC_x \cdot B_x$$

$$+ \ K_{RPON} \cdot RPON + K_{LPON} \cdot LPON - K_{DON} \cdot DON + \frac{WDON}{V} \qquad (4\text{-}50)$$

DON   = concentration of dissolved organic nitrogen (g N m^{-3})

FND_x = fraction of metabolized nitrogen by algal group x produced as dissolved organic nitrogen

FNDP = fraction of predated nitrogen produced as dissolved organic nitrogen

K_{DON} = mineralization rate of dissolved organic nitrogen (day^{-1})

WDON = external loads of dissolved organic nitrogen (g N day^{-1}).

4.6.3   Ammonium Nitrogen

Sources and sinks for ammonia nitrogen included in the model are (Fig. 4-1):

- algal basal metabolism, predation, and uptake
- mineralization from dissolved organic nitrogen
- nitrification to nitrate
- sediment-water exchange for the bottom layer only
- external loads.

The kinetic equation describing these processes is:

$$\frac{\partial NH4}{\partial t} = \sum_{x=c,d,g,m} (FNI_x \cdot BM_x + FNIP \cdot PR_x - PN_x \cdot P_x) ANC_x \cdot B_x + K_{DON} \cdot DON$$

$$- \ Nit \cdot NH4 + \frac{BFNH4}{\Delta z} + \frac{WNH4}{V} \qquad (4\text{-}51)$$

FNI_x = fraction of metabolized nitrogen by algal group x produced as inorganic nitrogen

FNIP = fraction of predated nitrogen produced as inorganic nitrogen

PN_x = preference for ammonium uptake by algal group x ($0 \le PN_x \le 1$)

Nit = nitrification rate (day^{-1}) given in Eq. 4-59

BFNH4 = sediment-water exchange flux of ammonium (g N m^{-2} day^{-1}), applied to the bottom layer only

WNH4 = external loads of ammonium (g N day^{-1}).

4.6.4   Nitrate Nitrogen

Sources and sinks for nitrate nitrogen included in the model are (Fig. 4-1):

- algal uptake
- nitrification from ammonium
- denitrification to nitrogen gas
- sediment-water exchange for the bottom layer only
- external loads.

The kinetic equation describing these processes is:

$$\frac{\partial NO3}{\partial t} = -\sum_{x=c,d,g,m} (1 - PN_x)P_x \cdot ANC_x \cdot B_x + Nit \cdot NH4 - ANDC \cdot Denit \cdot DOC$$

$$+ \frac{BFNO3}{\Delta z} + \frac{WNO3}{V} \qquad (4\text{-}52)$$

ANDC = mass of nitrate nitrogen reduced per mass of dissolved organic carbon oxidized (0.933 g N per g C from Eq. 4-33)

BFNO3 = sediment-water exchange flux of nitrate (g N m^{-2} day^{-1}), applied to the bottom layer only

WNO3 = external loads of nitrate (g N day^{-1}).

The remainder of this section explains each term in Equations 4-48 to 4-52, except BFNH4 and BFNO3 which are described in Chapter 5.

4.6.5   Effect of Algae on Nitrogen

The terms within summation ($\sum$) in Equations 4-48 to 4-52 account for the effects of algae on nitrogen. As in phosphorus, both basal metabolism (respiration and excretion) and predation are considered, and thus formulated, to contribute to organic and ammonium nitrogen. That is, algal nitrogen released by both basal metabolism and predation are represented by distribution coefficients; FNR_x, FNL_x, FND_x, FNI_x, FNRP, FNLP, FNDP, and FNIP. The sum of four distribution coefficients for basal metabolism should be unity; the sum of the predation distribution coefficients should also be unity.

Algae take up ammonium and nitrate for growth, and ammonium is preferred from thermodynamic considerations. The preference of algae for ammonium is expressed as:

$$PN_x = NH4\frac{NO3}{(KHN_x + NH4)(KHN_x + NO3)} + NH4\frac{KHN_x}{(NH4 + NO3)(KHN_x + NO3)} \qquad (4\text{-}53)$$

This equation forces the preference for ammonium to be unity when nitrate is absent, and to be zero when ammonium is absent.

4.6.6   Mineralization and Hydrolysis

The third term on the RHS of Equations 4-48 and 4-49 represents hydrolysis of particulate organic nitrogen and the last term in Eq. 4-50 represents mineralization of dissolved organic nitrogen. Including a mechanism for accelerated hydrolysis and mineralization during nutrient-limited conditions (Section 4.5.7), the formulations for these processes are:

$$K_{RPON} = (K_{RN} + \frac{KHN}{KHN + NH4 + NO3}K_{RNalg}\sum_{x=c,d,g}B_x)\cdot\exp(KT_{HDR}[T - TR_{HDR}]) \qquad (4\text{-}54)$$

$$K_{LPON} = (K_{LN} + \frac{KHN}{KHN + NH4 + NO3}K_{LNalg}\sum_{x=c,d,g}B_x)\cdot\exp(KT_{HDR}[T - TR_{HDR}]) \qquad (4\text{-}55)$$

$$K_{DON} = (K_{DN} + \frac{KHN}{KHN + NH4 + NO3}K_{DNalg}\sum_{x=c,d,g}B_x)\cdot\exp(KT_{MNL}[T - TR_{MNL}]) \qquad (4\text{-}56)$$

K_{RN} = minimum hydrolysis rate of refractory particulate organic nitrogen (day^{-1})

K_{LN} = minimum hydrolysis rate of labile particulate organic nitrogen (day^{-1})

K_{DN} = minimum mineralization rate of dissolved organic nitrogen (day^{-1})

K_{RNalg}, K_{LNalg} = constants that relate hydrolysis of refractory and labile particulate organic nitrogen, respectively, to algal biomass (day^{-1} per g C m^{-3})

K_{DNalg} = constant that relates mineralization to algal biomass (day^{-1} per g C m^{-3})

KHN   = mean half-saturation constant for algal nitrogen uptake (g N m^{-3}).

$$= \frac{1}{3}\sum_{x=c,d,g}KHN_x \qquad (4\text{-}57)$$

Equations 4-54 to 4-56 have exponential functions that relate rates to temperature.

4.6.7   Nitrification

Nitrification is a process mediated by autotrophic nitrifying bacteria that obtain energy through the oxidation of ammonium to nitrite and of nitrite to nitrate. The stoichiometry of complete reaction is (Bowie et al. 1985):

$$NH_4^+ + 2O_2 \rightarrow NO_3^- + H_2O + 2H^+ \tag{4-58}$$

The first term in the second line of Eq. 4-51 and its corresponding term in Eq. 4-52 represent the effect of nitrification on ammonium and nitrate, respectively. The kinetics of complete nitrification process are formulated as a function of available ammonium, dissolved oxygen and temperature:

$$Nit = \frac{DO}{KHNit_{DO} + DO} \frac{NH4}{KHNit_N + NH4} Nit_m \cdot f_{Nit}(T) \tag{4-59}$$

$$
\begin{aligned}
f_{Nit}(T) &= \exp(-KNit1[T - TNit]^2) \qquad &if \quad T \le TNit \\
&= \exp(-KNit2[TNit - T]^2) \qquad &if \quad T > TNit
\end{aligned}
\tag{4-60}
$$

$KHNit_{DO}$ = nitrification half-saturation constant for dissolved oxygen (g O_2 m^{-3})

$KHNit_N$ = nitrification half-saturation constant for ammonium (g N m^{-3})

Nit_m = maximum nitrification rate at TNit (g N m^{-3} day^{-1})

$TNit$ = optimum temperature for nitrification (°C)

$KNit1$ = effect of temperature below TNit on nitrification rate (°C^{-2})

$KNit2$ = effect of temperature above TNit on nitrification rate (°C^{-2}).

The Monod function of dissolved oxygen in Eq. 4-59 indicates the inhibition of nitrification at low oxygen level. The Monod function of ammonium indicates that when ammonium is abundant, the nitrification rate is limited by the availability of nitrifying bacteria. The effect of suboptimal temperature is represented using Gaussian form.

4.6.8   Denitrification

The effect of denitrification on dissolved organic carbon was described in Section 4.4.5. Denitrification removes nitrate from the system in stoichiometric proportion to carbon removal as determined by Eq. 4-33. The last term in the first line of Eq. 4-52 represents this removal of nitrate.

4.7   Silica

The present model has two state variables for silica: particulate biogenic silica and available silica.

4.7.1   Particulate Biogenic Silica

Sources and sinks for particulate biogenic silica included in the model are (Fig. 4-1):

- diatom basal metabolism and predation
- dissolution to available silica
- settling
- external loads

The kinetic equation describing these processes is:

$$\frac{\partial SU}{\partial t} = (FSP_d{\cdot}BM_d + FSPP{\cdot}PR_d)ASC_d{\cdot}B_d - K_{SUA}{\cdot}SU + \frac{\partial}{\partial z}(WS_d{\cdot}SU) + \frac{WSU}{V} \qquad (4\text{-}61)$$

SU = concentration of particulate biogenic silica (g Si m^{-3})

FSP$_d$ = fraction of metabolized silica by diatoms produced as particulate biogenic silica

FSPP = fraction of predated diatom silica produced as particulate biogenic silica

ASC$_d$ = silica-to-carbon ratio of diatoms (g Si per g C)

K$_{SUA}$ = dissolution rate of particulate biogenic silica (day^{-1})

WSU = external loads of particulate biogenic silica (g Si day^{-1}).

4.7.2 Available Silica

Sources and sinks for available silica included in the model are (Fig. 4-1):

- diatom basal metabolism, predation, and uptake
- settling of sorbed (particulate) available silica
- dissolution from particulate biogenic silica
- sediment-water exchange of dissolved silica for the bottom layer only
- external loads.

The kinetic equation describing these processes is:

$$\frac{\partial SA}{\partial t} = (FSI_d{\cdot}BM_d + FSIP{\cdot}PR_d - P_d)ASC_d{\cdot}B_d + K_{SUA}{\cdot}SU + \frac{\partial}{\partial z}(WS_{TSS}{\cdot}SAp)$$

$$+ \; \frac{BFSAd}{\Delta z} + \frac{WSA}{V} \qquad\qquad\qquad (4\text{-}62)$$

SA = concentration of available silica (g Si m^{-3}) = SAd + SAp   (4-63)

SAd = dissolved available silica (g Si m^{-3})

SAp = particulate (sorbed) available silica (g Si m^{-3})

FSI$_d$ = fraction of metabolized silica by diatoms produced as available silica

FSIP = fraction of predated diatom silica produced as available silica

BFSAd = sediment-water exchange flux of available silica (g Si m^{-2} day^{-1}), applied to bottom layer only

WSA = external loads of available silica (g Si day^{-1}).

In Eq. 4-62, if total active metal is chosen as a measure of sorption site, the settling velocity of total suspended solid, WS$_{TSS}$, is replaced by that of particulate metal, WS$_s$ (Sections 4.7.3 and 4.10).

4.7.3 Available Silica System

Analysis of Chesapeake Bay monitoring data indicates that silica shows similar behavior as phosphate in the adsorption-desorption process (Cerco and Cole 1993). As in phosphate, therefore, available silica is defined to include both dissolved and sorbed fractions (Eq. 4-63). Treatment of available silica is the same as total phosphate, and the same method to partition dissolved and sorbed phosphate is used to partition dissolved and sorbed available silica:

$$SAp = \frac{K_{SAp} \cdot TSS}{1 + K_{SAp} \cdot TSS} SA \quad \text{or} \qquad SAp = \frac{K_{SAp} \cdot TAMp}{1 + K_{SAp} \cdot TAMp} SA \qquad (4\text{-}64)$$

$$SAd = \frac{1}{1 + K_{SAp} \cdot TSS} SA \quad \text{or} \qquad SAd = \frac{1}{1 + K_{SAp} \cdot TAMp} SA$$

$$= SA - SAp \qquad (4\text{-}65)$$

K_{SAp} = empirical coefficient relating available silica sorption to total suspended solid (per g m^{-3}) or particulate total active metal (per mol m^{-3}) concentration.

As in K_{PO4p} in Section 4.5.4, K_{SAp} is the ratio of sorbed to dissolved available silica per unit sorption site available.

4.7.4   Effect of Diatoms on Silica

In Equations 4-62 and 4-63, those terms expressed as a function of diatom biomass (B_d) account for the effects of diatoms on silica. As in phosphorus and nitrogen, both basal metabolism (respiration and excretion) and predation are considered, and thus formulated, to contribute to particulate biogenic and available silica. That is, diatom silica released by both basal metabolism and predation are represented by distribution coefficients; FSP_d, FSI_d, FSPP, and FSIP. The sum of two distribution coefficients for basal metabolism should be unity and so is that for predation. Diatoms require silica as well as phosphorus and nitrogen, and diatom uptake of available silica is represented by ($- P_d \cdot ASC_d \cdot B_d$) in Eq. 4-63.

4.7.5   Dissolution

The term ($- K_{SUA} \cdot SU$) in Eq. 4-62 and its corresponding term in Eq. 4-63 represent dissolution of particulate biogenic silica to available silica. The dissolution rate is expressed as an exponential function of temperature:

$$K_{SUA} = K_{SU} \cdot \exp(KT_{SUA}[T - TR_{SUA}]) \qquad (4\text{-}66)$$

K_{SU} = dissolution rate of particulate biogenic silica at TR_{SUA} (day^{-1})
KT_{SUA} = effect of temperature on dissolution of particulate biogenic silica (°C^{-1})
TR_{SUA} = reference temperature for dissolution of particulate biogenic silica (°C).

4.8   Chemical Oxygen Demand

In the present model, chemical oxygen demand is the concentration of reduced substances that are oxidizable through inorganic means. The source of chemical oxygen demand in saline water is sulfide released from sediments. A cycle occurs in which sulfate is reduced to sulfide in the sediments and reoxidized to sulfate in the water column. In fresh water, methane is released to the water column by the sediment process model. Both sulfide and methane are quantified in units of oxygen demand and are treated with the same kinetic formulation. The kinetic equation, including external loads, if any, is:

$$\frac{\partial COD}{\partial t} = -\frac{DO}{KH_{COD} + DO}KCOD{\cdot}COD + \frac{BFCOD}{\Delta z} + \frac{WCOD}{V}$$ (4-67)

COD   = concentration of chemical oxygen demand (g O_2-equivalents m^{-3})

KH_{COD} = half-saturation constant of dissolved oxygen required for oxidation of chemical oxygen demand

(g O_2 m^{-3})

KCOD = oxidation rate of chemical oxygen demand (day^{-1})

BFCOD = sediment flux of chemical oxygen demand (g O_2-equivalents m^{-2} day^{-1}), applied to bottom

layer only

WCOD = external loads of chemical oxygen demand (g O_2-equivalents day^{-1}).

An exponential function is used to describe the temperature effect on the oxidation rate of chemical oxygen demand:

$$KCOD = K_{CD}{\cdot}\exp(KT_{COD}[T - TR_{COD}])$$ (4-68)

K_{CD} = oxidation rate of chemical oxygen demand at TR_{COD} (day^{-1})

KT_{COD} = effect of temperature on oxidation of chemical oxygen demand (°C^{-1})

TR_{COD} = reference temperature for oxidation of chemical oxygen demand (°C).

4.9   Dissolved Oxygen

Sources and sinks of dissolved oxygen in the water column included in the model are (Fig. 4-1):

- algal photosynthesis and respiration
- nitrification
- heterotrophic respiration of dissolved organic carbon
- oxidation of chemical oxygen demand
- surface reaeration for the surface layer only
- sediment oxygen demand for the bottom layer only
- external loads.

The kinetic equation describing these processes is:

$$\frac{\partial DO}{\partial t} = \sum_{x=c,d,g,m} \left((1.3 - 0.3 \cdot PN_x) P_x - (1 - FCD_x) \frac{DO}{KHR_x + DO} BM_x \right) AOCR \cdot B_x$$

$$- AONT \cdot Nit \cdot NH4 - AOCR \cdot K_{HR} \cdot DOC - \frac{DO}{KH_{COD} + DO} KCOD \cdot COD$$

$$+ K_r (DO_s - DO) + \frac{SOD}{\Delta z} + \frac{WDO}{V} \tag{4-69}$$

AONT = mass of dissolved oxygen consumed per unit mass of ammonium nitrogen nitrified (4.33 g O_2 per g N; see Section 4.9.2)

AOCR = dissolved oxygen-to-carbon ratio in respiration (2.67 g O_2 per g C; see Section 4.9.1)

K_r = reaeration coefficient (day^{-1}): the reaeration term is applied to the surface layer only

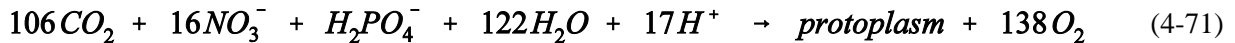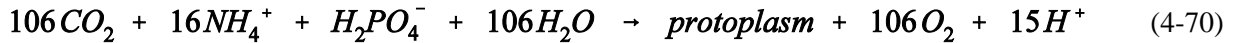DO_s = saturated concentration of dissolved oxygen (g O_2 m^{-3})

SOD = sediment oxygen demand (g O_2 m^{-2} day^{-1}), applied to the bottom layer only; positive is to the water column

WDO = external loads of dissolved oxygen (g O_2 day^{-1}).

The two sink terms in Eq. 4-69, heterotrophic respiration and chemical oxygen demand, are explained in Section 4.4.4 (Eq. 4-29) and Section 4.8 (Eq. 4-67), respectively. The remainder of this section explains the effects of algae, nitrification, and surface reaeration.

4.9.1   Effect of Algae on Dissolved Oxygen

The first line on the RHS of Eq. 4-69 accounts for the effects of algae on dissolved oxygen. Algae produce oxygen through photosynthesis and consume oxygen through respiration. The quantity produced depends on the form of nitrogen utilized for growth. Equations describing production of dissolved oxygen are (Morel 1983):

$$106 CO_2 + 16 NH_4^+ + H_2 PO_4^- + 106 H_2 O \rightarrow protoplasm + 106 O_2 + 15 H^+ \tag{4-70}$$

$$106 CO_2 + 16 NO_3^- + H_2 PO_4^- + 122 H_2 O + 17 H^+ \rightarrow protoplasm + 138 O_2 \tag{4-71}$$

When ammonium is the nitrogen source, one mole of oxygen is produced per mole of carbon dioxide fixed. When nitrate is the nitrogen source, 1.3 moles of oxygen are produced per mole of carbon dioxide fixed. The quantity, (1.3 - 0.3·PN$_x$), in the first term of Eq. 4-69 is the photosynthesis ratio and represents the molar quantity of oxygen produced per mole of carbon dioxide fixed. It approaches unity as the algal preference for ammonium approaches unity.

The last term in the first line of Eq. 4-69 accounts for the oxygen consumption due to algal respiration (Eq. 4-26). A simple representation of respiration process is:

$$CH_2O \ + \ O_2 \ = \ CO_2 \ + \ H_2O \tag{4-72}$$

from which, AOCR = 2.67 g O_2 per g C.

4.9.2   Effect of Nitrification on Dissolved Oxygen

The stoichiometry of nitrification reaction (Eq. 4-58) indicates that two moles of oxygen are required to nitrify one mole of ammonium into nitrate. However, cell synthesis by nitrifying bacteria is accomplished by the fixation of carbon dioxide so that less than two moles of oxygen are consumed per mole ammonium utilized (Wezernak and Gannon 1968), i.e., AONT = 4.33 g O_2 per g N.

4.9.3   Effect of Surface Reaeration on Dissolved Oxygen

The reaeration rate of dissolved oxygen at the air-water interface is proportional to the oxygen gradient across the interface, (DO_s - DO), when assuming the air is saturated with oxygen. The saturated concentration of dissolved oxygen, which decreases as temperature and salinity increase, is specified using an empirical formula (Genet et al. 1974):

$$DO_s \ = \ 14.5532 \ - \ 0.38217 \cdot T \ + \ 5.4258 \times 10^{-3} \cdot T^2$$
$$- \ CL \cdot (1.665 \times 10^{-4} \ - \ 5.866 \times 10^{-6} \cdot T \ + \ 9.796 \times 10^{-8} \cdot T^2) \tag{4-73}$$

CL   = chloride concentration (mg/L) = S/1.80655.

The reaeration coefficient includes the effect of turbulence generated by bottom friction (O'Connor and Dobbins 1958) and that by surface wind stress (Banks and Herrera 1977):

$$K_r \ = \ \left(K_{ro} \sqrt{\frac{u_{eq}}{h_{eq}}} \ + \ W_{rea} \right) \frac{1}{\Delta z} \cdot KT_r^{T \ - \ 20} \tag{4-74}$$

K_{ro} = proportionality constant = 3.933 in MKS unit
u_{eq} = weighted velocity over cross-section (m sec^{-1}) = $\sum(u_k V_k)/\sum(V_k)$
h_{eq} = weighted depth over cross-section (m) = $\sum(V_k)/B_\eta$
B_η = width at the free surface (m)
W_{rea} = wind-induced reaeration (m day^{-1})

$$= \ 0.728 \, U_w^{\frac{1}{2}} \ - \ 0.317 \, U_w \ + \ 0.0372 \, U_w^{\,2} \tag{4-75}$$

U_w = wind speed (m sec^{-1}) at the height of 10 m above surface
KT_r = constant for temperature adjustment of DO reaeration rate.

4.10   Total Active Metal

The present model requires simulation of total active metal for adsorption of phosphate and silica if that option is chosen (Fig. 4-1). The total active metal state variable is the sum of iron and manganese concentrations, both particulate and dissolved. In the model, the origin of total active metal is benthic sediments. Since sediment release of metal is not explicit in the sediment model (see Chapter 5), release is specified in the kinetic portion of the water column model. The only other term included is settling of the particulate fraction. Then the kinetic equation for total active metal, including external loads, if any, may be written as:

$$\frac{\partial TAM}{\partial t} = \frac{KHbmf}{KHbmf + DO}\frac{BFTAM}{\Delta z}e^{Ktam(T - Ttam)} + \frac{\partial}{\partial z}(WS_s \cdot TAMp) + \frac{WTAM}{V} \qquad (4\text{-}76)$$

TAM   = total active metal concentration (mol m^{-3}) = TAMd + TAMp   (4-77)

TAMd = dissolved total active metal (mol m^{-3})

TAMp = particulate total active metal (mol m^{-3})

KHbmf   = dissolved oxygen concentration at which total active metal release is half the anoxic release
              rate (g O$_2$ m^{-3})

BFTAM   = anoxic release rate of total active metal (mol m^{-2} day^{-1}), applied to the bottom layer only

Ktam   = effect of temperature on sediment release of total active metal (°C^{-1})

Ttam   = reference temperature for sediment release of total active metal (°C)

WS$_s$ = settling velocity of particulate metal (m day^{-1})

WTAM   = external loads of total active metal (mol day^{-1}).

In estuaries, iron and manganese exist in particular and dissolved forms depending on dissolved oxygen concentration. In the oxygenated water, most of the iron and manganese exist as particulate while under anoxic conditions, large fractions are dissolved, although solid-phase sulfides and carbonates exist and may predominate. The partitioning between particulate and dissolved phases is expressed using a concept that total active metal concentration must achieve a minimum level, which is a function of dissolved oxygen, before precipitation occurs:

$$TAMd = minimum\{TAMdmx \cdot \exp(-Kdotam \cdot DO) , TAM\} \qquad (4\text{-}78)$$

$$TAMp = TAM - TAMd \qquad (4\text{-}79)$$

TAMdmx = solubility of total active metal under anoxic conditions (mol m^{-3})

Kdotam   = constant that relates total active metal solubility to dissolved oxygen (per g O$_2$ m^{-3}).

4.11   Fecal Coliform Bacteria

Fecal coliform bacteria are indicative of organisms from the intestinal tract of humans and other animals and can be used as an indicator bacteria as a measure of public health (Thomann and Mueller 1987). In

the present model, fecal coliform bacteria have no interaction with other state variables, and have only one sink term, die-off. The kinetic equation, including external loads, may be written as:

$$\frac{\partial FCB}{\partial t} = - KFCB \cdot TFCB^{T-20} \cdot FCB + \frac{WFCB}{V} \tag{4-80}$$

FCB = bacteria concentration (MPN per 100 ml)

KFCB = first order die-off rate at 20°C (day^{-1})

TFCB = effect of temperature on decay of bacteria (°C^{-1})

WFCB = external loads of fecal coliform bacteria (MPN per 100 ml m^3 day^{-1}).

4.12   Method of Solution

The kinetic equations for the 21 state variables in the EFDC water column water quality model can be expressed in a 21 × 21 matrix after linearizing some terms, mostly Monod type expressions:

$$\frac{\partial}{\partial t}[C] = [K] \cdot [C] + [R] \tag{4-81}$$

where [C] is in mass volume^{-1}, [K] is in time^{-1}, and [R] is in mass volume^{-1} time^{-1}. Since the settling of particulate matter from the overlying cell acts as an input for a given cell, when Eq. 4-81 is applied to a cell of finite volume, it may be expressed as:

$$\frac{\partial}{\partial t}[C]_k = [K1]_k \cdot [C]_k + \lambda \cdot [K2]_k \cdot [C]_{k+1} + [R]_k \tag{4-82}$$

where the four matrices [C], [K1], [K2], and [R] are defined in Appendix A of Park et al. (1995). The subscript k designates a cell at the kth vertical layer. The layer index k increases upward with KC vertical layers; k = 1 is the bottom layer and k = KC is the surface layer. Then $\lambda = 0$ for k = KC; otherwise, $\lambda = 1$. The matrix [K2] is a diagonal matrix, and the non-zero elements account for the settling of particulate matter from the overlying cell.

Equation 4-82 is solved using a second-order accurate trapezoidal scheme over a time step of θ, which may be expressed as:

$$[C]_k^N = \left([I] - \frac{\theta}{2}[K1]_k^O \right)^{-1} \cdot \left([C]_k^O + \frac{\theta}{2}\{[K1]_k^O \cdot [C]_k^O + \lambda[K2]_k^O \cdot [C]_{k+1}^A\} + \theta[R]_k^O \right) \tag{4-83}$$

where $\theta = 2 \cdot m \cdot \Delta t$ is the time step for the kinetic equations; [I] is a unit matrix; $[C]^A = [C]^N + [C]^O$; the superscripts O and N designate the variables before and after being adjusted for the relevant kinetic processes. Since Eq. 4-83 is solved from the surface layer downward, the term with $[C]_{k+1}{}^A$ is known for the kth layer and thus placed on the RHS. In Eq. 4-83, inversion of a matrix can be avoided if the 21 state

variables are solved in a proper order. The kinetic equations are solved in the order of the variables in the matrix [C] defined in Appendix A of Park et al. (1995).

4.13   Macroalgae (Periphyton) State Variable

The EFDC water quality model was augmented to represent benthic attached algae (often referred to as macroalgae in estuarine waters and periphyton in fresh waters) using the existing framework for phytoplankton growth kinetics. Mathematical relationships based on the impacts of temperature, available light, available nutrients, stream velocity, and density-dependent interactions were incorporated into the algae growth kinetics framework within EFDC. The major differences between modeling techniques for attached and free-floating algae are: (1) attached algae are expressed in terms of areal densities rather than volumetric concentrations; (2) attached algae growth can be limited by the availability of bottom substrate; (3) the availability of nutrients to the macroalgae matrix can be influenced by stream velocity; and (4) macroalgae are not subject to hydrodynamic transport. A good description of periphyton kinetics as it relates to water quality modeling can be found in Warwick et al. (1997) and has been used to develop this section of the report.

A mass-balance approach was used to model macroalgae growth, with carbon serving as the measure of standing crop size or biomass. For each model grid cell the equation for macroalgae growth is slightly different than the one for free-floating algae (Eq. 4-6):

$$P_m = PM_m \cdot f_1(N) \cdot f_2(I) \cdot f_3(T) \cdot f_4(V) \cdot f_5(D) \tag{4-84}$$

where

PM_m = maximum growth rate under optimal conditions for macroalgae

$f_1(N)$ = effect of suboptimal nutrient concentration ($0 \le f_1 \le 1$)

$f_2(I)$ = effect of suboptimal light intensity ($0 \le f_2 \le 1$)

$f_3(T)$ = effect of suboptimal temperature ($0 \le f_3 \le 1$)

$f_4(V)$ = velocity limitation factor ($0 \le f_4 \le 1$)

$f_5(D)$ = density-dependent growth rate reduction factor ($0 \le f_5 \le 1$).

The basic growth kinetics for macroalgae were developed from those supplied by EFDC and others developed by Runke (1985). The macroalgae population as a whole is characterized by the total biomass present without considering the different species and their associated environmental processes. The optimum growth for the given temperature is adjusted for light, nutrients, velocity, and density-dependent limitations. Each growth limitation factor can vary from 0 to 1. A value of 1 indicates the factor does not limit growth, and a value of 0 means the factor is so severely limiting that growth is stopped entirely (Bowie et al. 1985).

Stream velocity has a twofold effect on periphyton productivity in freshwater streams: velocity increases to a certain level to enhance biomass accrual, but further increases result in substantial scouring (Horner et al. 1990). A benthic algal population is typified as a plant community with an understory and an overstory. The entire community is called a matrix. As the matrix develops, the periphyton community is composed of an outer layer of photosynthetically active cells and inner layers of senescent and decomposing cells. Layering can also develop among different species of periphyton. Environmental conditions within the matrix are altered by the physical structure of the periphyton. This influences nutrient uptake and primary production rates of the algae (Sand-Jensen 1983). Above a certain level, current has a simulating effect on periphyton metabolism by mixing the overlying waters with nutrient-poor waters that develop around cells (Whitford and Schumacher 1964). The physical structure of the periphyton community and nutrient uptake by periphyton interfere with nutrient flux through the microbial matrix (Stevenson and Glover 1993).

Current is constantly scouring periphyton from its substrate. At high enough velocities, shear stress can result in substantial biomass reduction. Even at low velocities, sudden increases in velocity raise instantaneous loss rates substantially, but these high rates persist only briefly (Horner et al. 1990). An increase in velocity above that to which benthic algae are accustomed leads to increased loss rates and temporarily reduced biomass. However, recolonization and growth after biomass reduction are usually rapid. The effects of suboptimal velocity upon growth rate are represented in the model by a velocity limitation function.   Two options are available in the model for specifying the velocity limitation: (1) a Michaelis-Menton (or Monod) equation (4-85) and (2) a five-parameter logistic function (4-86). The Monod equation limits macroalgae growth due to low velocities, whereas the five-parameter logistic function can be configured to limit growth due to either low or high velocities (Figure 4-2).

Velocity limitation option 1, the Michaelis-Menton equation, is written as follows:
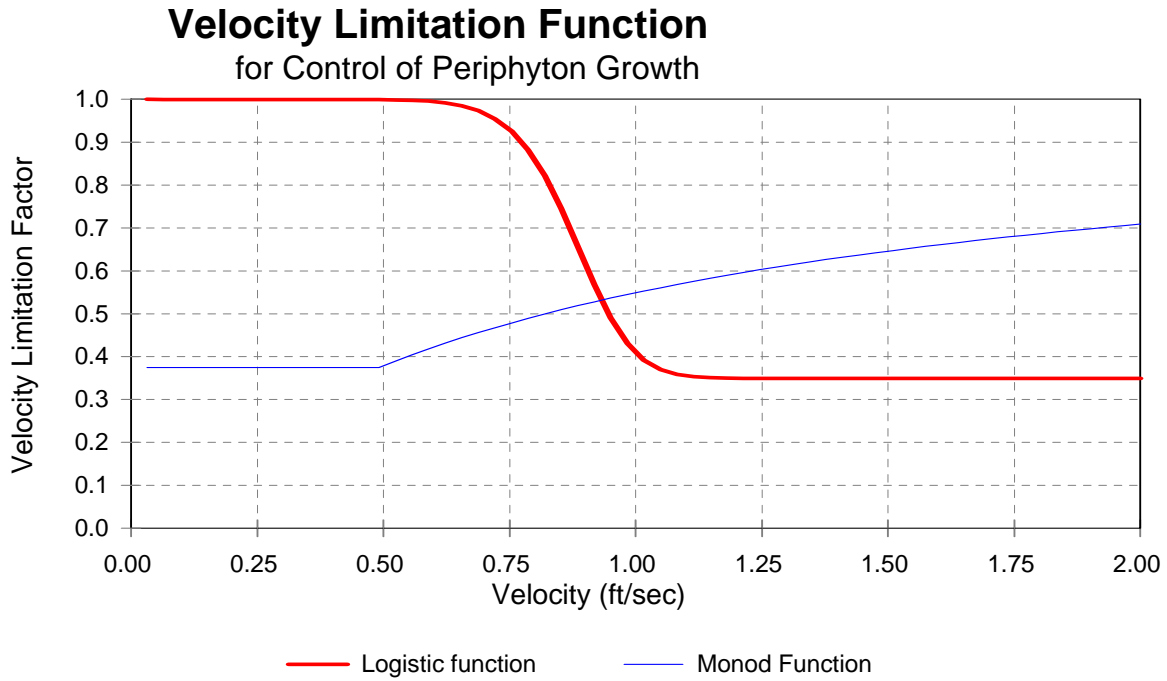
Velocity Limitation Function
for Control of Periphyton Growth

Figure 4-2. Velocity limitation function for (Option 1) the Monod equation where KMV = 0.25 m/sec and KMVmin=0.15 m/sec, and (Option 2) the five-parameter logistic function where *a*=1.0, b=12.0, *c*=0.3, *d*=0.35, and e=3.0 (high velocities are limiting)

$$f_4(V) \;=\; \frac{U}{KMV \;+\; U} \tag{4-85}$$

where

      U   = stream velocity (m/sec)
      KMV   = half-saturation velocity (m/sec)

Velocity limitation option 2, the five-parameter logistic function is as follows:

$$f_4(V) \;=\; d \;+\; \frac{a \;-\; d}{\left[\; 1 \;+\; \left(\dfrac{U}{c}\right)^{b} \;\right]^{e}} \tag{4-86}$$

where

      U = stream velocity (m/sec)
      a = asymptote at minimum x
      b = slope after asymptote a
      c = x-translation

> d = asymptote at maximum x
> e = slope before asymptote d

The half-saturation velocity in Eq. 4-85 is the velocity at which half the maximum growth rate occurs. This effect is analogous to the nutrient limitation because the effect of velocity at suboptimal levels on periphyton growth is due to increasing the exchange of nutrients between the algal matrix and the overlying water (Runke 1985). However, this formula can be too limiting at low velocities. This function does not allow periphyton growth in still waters, but periphyton does grow in still waters such as lakes. Therefore, the function is applied only at velocities above a minimum threshold level (KMVmin). When velocities are at or below this lower level, the limitation function is applied at the minimum level. Above this velocity, the current produces a steeper diffusion gradient around the periphyton (Whitford and Schumacher 1964). A minimum formulation is used to combine the limiting factors for nitrogen, phosphorus, and velocity. The most severely limiting factor alone limits periphyton growth. Note that Eq. 4-86 can be configured so that low velocities are limiting by setting parameter d greater than parameter a, and vice versa to limit growth due to high velocities. In waters that are rich in nutrients, low velocities will not limit growth. However, high velocities may cause scouring and detachment of the macroalgae, resulting in a reduction in biomass. The five-parameter logistic function can be configured to approximate this reduction by limiting growth at high velocities.

Macroalgae (periphyton) growth can also be limited by the availability of suitable substrate (Ross 1983). Macroalgae communities reach maximum rates of primary productivity at low levels of biomass (McIntire 1973; Pfeifer and McDiffett 1975). The relationship between standing crop and production employs the Michaelis-Menton kinetic equation:

$$f_5(D) = \frac{KBP}{KBP + P_m} \tag{4-87}$$

where
> KBP = half-saturation biomass level (g C/m^2)
> P_m = macroalgae biomass level (g C/m^2).

The half-saturation biomass level (KBP) is the biomass at which half the maximum growth rate occurs. Caupp et al. (1991) used a KBP value of 5.0 g C/m^2 (assuming 50% of ash free dry mass is carbon) for a region of the Truckee River system in California. The function in Eq. 4-87 allows maximum rates of primary productivity at low levels of biomass with decreasing rates of primary productivity as the community matrix expands.

5 - EFDC SEDIMENT PROCESS MODEL

A sediment process model developed by DiToro and Fitzpatrick (1993; hereinafter referred to as D&F) and was coupled with CE-QUAL-ICM for Chesapeake Bay water quality modeling (Cerco and Cole 1993). The sediment process model was slightly modified and incorporated into the EFDC water quality model to simulate the processes in the sediment and at the sediment-water interface. The description of the EFDC sediment process model in this section is from Park et al. (1995). The sediment process model has 27 water-quality related state variables and fluxes (Table 5-1).

Table 5-1. EFDC sediment process model state variables and flux terms

(1) particulate organic carbon G1 class in layer 2	(15) nitrate nitrogen in layer 1
(2) particulate organic carbon G2 class in layer 2	(16) nitrate nitrogen in layer 2
(3) particulate organic carbon G3 class in layer 2	(17) phosphate phosphorus in layer 1
(4) particulate organic nitrogen G1 class in layer 2	(18) phosphate phosphorus in layer 2
(5) particulate organic nitrogen G2 class in layer 2	(19) available silica in layer 1
(6) particulate organic nitrogen G3 class in layer 2	(20) available silica in layer 2
(7) particulate organic phosphorus G1 class in layer 2	(21) ammonia nitrogen flux
(8) particulate organic phosphorus G2 class in layer 2	(22) nitrate nitrogen flux
(9) particulate organic phosphorus G3 class in layer 2	(23) phosphate phosphorus flux
(10) particulate biogenic silica in layer 2	(24) silica flux
(11) sulfide/methane in layer 1	(25) sediment oxygen demand
(12) sulfide/methane in layer 2	(26) release of chemical oxygen demand
(13) ammonia nitrogen in layer 1	(27) sediment temperature
(14) ammonia nitrogen in layer 2	

The nitrate state variables, (15), (16), and (22), in the model represent the sum of nitrate and nitrite nitrogen. The three G classes for particulate organic matter (POM) in Layer 2 and the two layers for inorganic substances are described below.

In the sediment model, benthic sediments are represented as two layers (Fig. 5-1). The upper layer (Layer 1) is in contact with the water column and may be oxic or anoxic depending on dissolved oxygen concentration in the overlying water. The lower layer (Layer 2) is permanently anoxic. The upper layer depth, which is determined by the penetration of oxygen into the sediments, is at its maximum only a small fraction of the total depth. Because H_1 (~ 0.1 cm) « H_2,

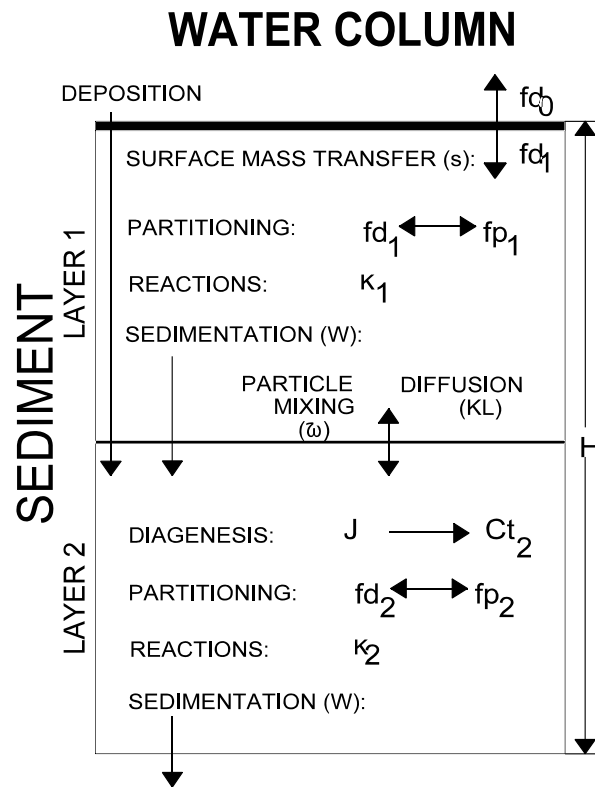$$H = H_1 + H_2 \approx H_2 \tag{5-1}$$

WATER COLUMN

Figure 5-1. Sediment layers and processes included in sediment process model.

where H is the total depth (approximately 10 cm), H_1 is the upper layer depth and H_2 is the lower layer depth.

The model incorporates three basic processes (Fig. 5-2): (1) depositional flux of POM, (2) the diagenesis of POM, and (3) the resulting sediment flux. The sediment model is driven by net settling of particulate organic carbon, nitrogen, phosphorus, and silica from the overlying water to the sediments (**depositional flux**). Because of the negligible thickness of the upper layer (Eq. 5-1), deposition is considered to proceed from the water column directly to the lower layer. Within the lower layer, the model simulates the diagenesis (mineralization or decay) of deposited POM, which produces oxygen demand and inorganic nutrients (**diagenesis flux**). The third basic process is the flux of substances produced by diagenesis (**sediment flux**). Oxygen demand, as sulfide (in salt water) or methane (in fresh water), takes three paths out of the sediments: (1) oxidation at the sediment-water interface as sediment oxygen demand, (2) export to the water column as chemical oxygen demand, or (3) burial to deep, inactive

sediments. Inorganic nutrients produced by diagenesis take two paths out of the sediments: (1) release to the water column or (2) burial to deep, inactive sediments (Fig. 5-2).
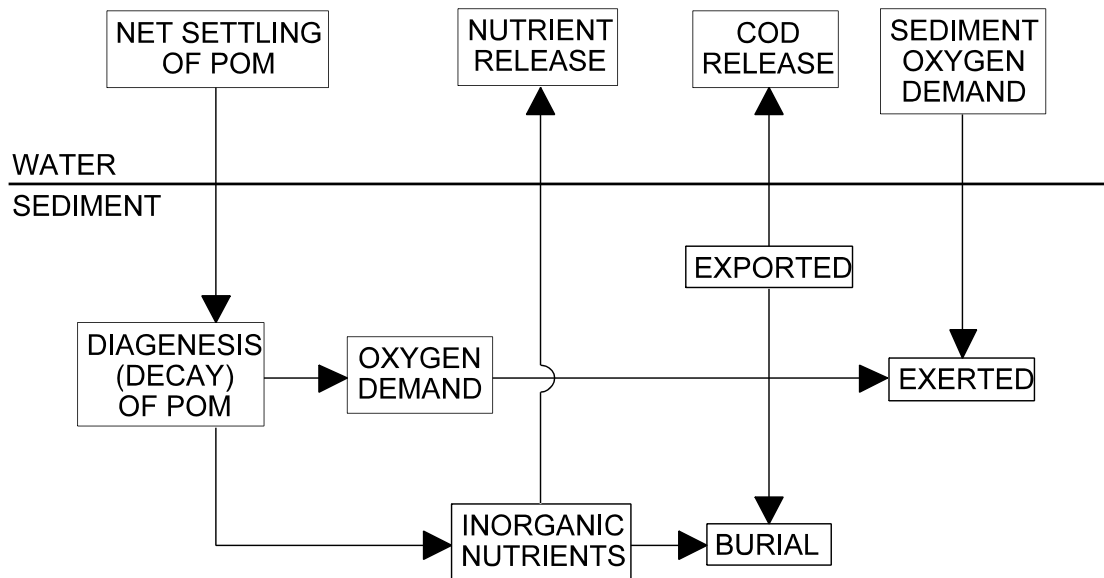

Figure 5-2. Schematic diagram for sediment process model

This section describes the three basic processes with reactions and sources/sinks for each state variable. The method of solution includes finite difference equations, solution scheme, boundary, and initial conditions. Complete model documentation can be found in D&F (1993).

5.1   Depositional Flux

Deposition is one process that couples the water column model with the sediment model. Consequently, deposition is represented in both the water column and sediment models. In the water column model, the governing mass-balance equations for the following state variables contain settling terms, which represent the depositional fluxes:

- three algal groups, cyanobacteria, diatoms and green algae (Eq. 4-5)
- refractory and labile particulate organic carbon (Equations 4-20 and 4-21)
- refractory and labile particulate organic phosphorus (Equations 4-35 and 4-36) and total phosphate (Eq. 4-38)
- refractory and labile particulate organic nitrogen (Equations 4-48 and 4-49)
- particulate biogenic silica (Eq. 4-61) and available silica (Eq. 4-62).

The sediment model receives these depositional fluxes of particulate organic carbon (POC), particulate organic nitrogen (PON), particulate organic phosphorus (POP), and particulate biogenic silica (PSi). Because of the negligible thickness of the upper layer (Eq. 5-1), deposition is considered to proceed from the water column directly to the lower layer. Since the sediment model has three G classes of POM, G_i (i = 1, 2, or 3), depending on the time scales of reactivity (Section 5.2), the POM fluxes from the water column should be mapped into three G classes based on their reactivity. Then the depositional fluxes for the ith G class (i = 1, 2, or 3) may be expressed as:

$$J_{POC,i} = FCLP_i \cdot WS_{LP} \cdot LPOC^N + FCRP_i \cdot WS_{RP} \cdot RPOC^N + \sum_{x=c,d,g} FCB_{x,i} \cdot WS_x \cdot B_x^N \tag{5-2}$$

$$J_{PON,i} = FNLP_i \cdot WS_{LP} \cdot LPON^N + FNRP_i \cdot WS_{RP} \cdot RPON^N + \sum_{x=c,d,g} FNB_{x,i} \cdot ANC_x \cdot WS_x \cdot B_x^N \tag{5-3}$$

$$J_{POP,i} = FPLP_i \cdot WS_{LP} \cdot LPOP^N + FPRP_i \cdot WS_{RP} \cdot RPOP^N + \sum_{x=c,d,g} FPB_{x,i} \cdot APC \cdot WS_x \cdot B_x^N$$

$$+ \ \gamma_i \cdot WS_{TSS} \cdot PO4p^N \tag{5-4}$$

$$J_{PSi} = WS_d \cdot SU^N + ASC_d \cdot WS_d \cdot B_d^N + WS_{TSS} \cdot SAp^N \tag{5-5}$$

$J_{POM,i}$ = depositional flux of POM (M = C, N or P) routed into the ith G class (g m^{-2} day^{-1})

J_{PSi} = depositional flux of PSi (g Si m[-2] day^{-1})

$FCLP_i$, $FNLP_i$, $FPLP_i$ =   fraction of water column labile POC, PON, and POP, respectively, routed into the ith G class in sediment

$FCRP_i$, $FNRP_i$, $FPRP_i$ =   fraction of water column refractory POC, PON, and POP, respectively, routed into the ith G class in sediment

$FCB_{x,i}$, $FNB_{x,i}$, $FPB_{x,i}$ =   fraction of POC, PON, and POP, respectively, in the algal group x routed into the ith G class in sediment

γ_i =   1   for i = 1

           0   for i = 2 or 3.

In the source code, the sediment process model is solved after the water column water quality model, and the calculated fluxes using the water column conditions at t = t_n are used for the computation of the water quality variables at t = t_n + θ. The superscript N indicates the variables after being updated for the kinetic processes, as defined in Eq. 4-82.

The settling of sorbed phosphate is considered to contribute to the labile G_1 pool in Eq. 5-4, and settling of sorbed silica contributes to J_{PSi} in Eq. 5-5 to avoid creation of additional depositional fluxes for

inorganic particulates. The sum of distribution coefficients should be unity: $\sum_i FCLP_i = \sum_i FNLP_i = \sum_i FPLP_i = \sum_i FCRP_i = \sum_i FNRP_i = \sum_i FPRP_i = \sum_i FCB_{x,i} = \sum_i FNB_{x,i} = \sum_i FPB_{x,i} = 1$. The settling velocities, WS_{LP}, WS_{RP}, WS_x, and WS_{TSS}, as defined in the EFDC water column model (Section 4), are net settling velocities. If total active metal is selected as a measure of sorption site, WS_{TSS} is replaced by WS_s in Equations 5-4 and 5-5 (see Sections 4.5 and 4.7).

5.2   Diagenesis Flux

Another coupling point of the sediment model to the water column model is the sediment flux, which is described in Section 5.3. The computation of sediment flux requires that the magnitude of the diagenesis flux be known. The diagenesis flux is explicitly computed using mass-balance equations for deposited POC, PON, and POP. (Dissolved silica is produced in the sediments as the result of the dissolution of PSi. Since the dissolution process is different from the bacterial-mediated diagenesis process, it is presented separately in Section 5.4.) In the mass-balance equations, the depositional fluxes of POM are the source terms and the decay of POM in the sediments produces the diagenesis fluxes. The integration of the mass-balance equations for POM provides the diagenesis fluxes that are the inputs for the mass-balance equations for ammonium, nitrate, phosphate, and sulfide/methane in the sediments (Section 5.3).

The difference in decay rates of POM is accounted for by assigning a fraction of POM to various decay classes (Westrisch and Berner 1984). POM in the sediments is divided into three G classes, or fractions, representing three scales of reactivity. The G_1 (labile) fraction has a half life of 20 days, and the G_2 (refractory) fraction has a half life of one year. The G_3 (inert) fraction is nonreactive, i.e., it undergoes no significant decay before burial into deep, inactive sediments. The varying reactivity of the G classes controls the time scale over which changes in depositional flux will be reflected in changes in diagenesis flux. If the G_1 class would dominate the POM input into the sediments, then there would be no significant time lag introduced by POM diagenesis and any changes in depositional flux would be readily reflected in diagenesis flux.

Because the upper layer thickness is negligible (Eq. 5-1) and thus depositional flux is considered to proceed directly to the lower layer (Equations 5-2 to 5-5), diagenesis is considered to occur in the lower layer only. The mass-balance equations are similar for POC, PON, and POP, and for different G classes. The mass-balance equation in the anoxic lower layer for the ith G class (i = 1, 2, or 3) may be expressed as:

$$H_2 \frac{\partial G_{POM,i}}{\partial t} = -K_{POM,i} \cdot \theta_{POM,i}^{T-20} \cdot G_{POM,i} \cdot H_2 - W \cdot G_{POM,i} + J_{POM,i} \qquad (5\text{-}6)$$

$G_{POM,i}$ = concentration of POM (M = C, N, or P) in the ith G class in Layer 2 (g m^{-3})

$K_{POM,i}$ = decay rate of the ith G class POM at 20°C in Layer 2 (day^{-1})

$\theta_{POM,i}$ = constant for temperature adjustment for $K_{POM,i}$

T = sediment temperature (°C)

W = burial rate (m day^{-1}).

Since the G_3 class is inert, $K_{POM,3} = 0$.

Once the mass-balance equations for $G_{POM,1}$ and $G_{POM,2}$ are solved, the diagenesis fluxes are computed from the rate of mineralization of the two reactive G classes:

$$ J_M = \sum_{i=1}^{2} K_{POM,i} \cdot \theta_{POM,i}^{T-20} \cdot G_{POM,i} \cdot H_2 \tag{5-7} $$

J_M = diagenesis flux (g^{-2} day^{-1}) of carbon (M = C), nitrogen (M = N), or phosphorus (M = P).

5.3   Sediment Flux

The mineralization of POM produces soluble intermediates, which are quantified as diagenesis fluxes in the previous section. The intermediates react in the oxic and anoxic layers, and portions are returned to the overlying water as sediment fluxes. Computation of sediment fluxes requires mass-balance equations for ammonium, nitrate, phosphate, sulfide/methane, and available silica. This section describes the flux portion for ammonium, nitrate, phosphate, and sulfide/methane of the model. Available silica is described in Section 5.4.

In the upper layer, the processes included in the flux portion are (Fig. 5-1)

- exchange of dissolved fraction between Layer 1 and the overlying water
- exchange of dissolved fraction between Layer 1 and 2 via diffusive transport
- exchange of particulate fraction between Layer 1 and 2 via particle mixing
- loss by burial to the lower layer (Layer 2)
- removal (sink) by reaction
- internal sources.

Since the upper layer is quite thin, $H_1 \sim 0.1$ cm (Eq. 5-1) and the surface mass transfer coefficient (*s*) is on the order of 0.1 m day^{-1}, then the residence time in the upper layer is $H_1/s \sim 10^{-2}$ days. Hence, a steady-state approximation is made in the upper layer. Then the mass-balance equation for ammonium, nitrate, phosphate, or sulfide/methane in the upper layer is:

$$ H_1 \frac{\partial Ct_1}{\partial t} = 0 = s(fd_0 \cdot Ct_0 - fd_1 \cdot Ct_1) + KL(fd_2 \cdot Ct_2 - fd_1 \cdot Ct_1) $$

$$+ \; \tilde{\omega}(fp_2 \cdot Ct_2 \; - \; fp_1 \cdot Ct_1) \; - \; W \cdot Ct_1 \; - \; \frac{\kappa_1^2}{s} Ct_1 \; + \; J_1 \qquad (5\text{-}8)$$

Ct_1 & Ct_2 = total concentrations in Layer 1 and 2, respectively (g m^{-3})

Ct_o = total concentration in the overlying water (g m^{-3})

s = surface mass transfer coefficient (m day^{-1})

KL   = diffusion velocity for dissolved fraction between Layer 1 and 2 (m day^{-1})

$\tilde{\omega}$ = particle mixing velocity between Layer 1 and 2 (m day^{-1})

fd_o = dissolved fraction of total substance in the overlying water ($0 \le fd_o \le 1$)

fd_1 = dissolved fraction of total substance in Layer 1 ($0 \le fd_1 \le 1$)

fp_1 = particulate fraction of total substance in Layer 1 ($= 1 - fd_1$)

fd_2 = dissolved fraction of total substance in Layer 2 ($0 \le fd_2 \le 1$)

fp_2 = particulate fraction of total substance in Layer 2 ($= 1 - fd_2$)

κ_1 = reaction velocity in Layer 1 (m day^{-1})

J_1 = sum of all internal sources in Layer 1 (g m^{-2} day^{-1}).

The first term on the RHS of Eq. 5-8 represents the exchange across sediment-water interface. Then the sediment flux from Layer 1 to the overlying water, which couples the sediment model to the water column model, may be expressed as:

$$J_{aq} \; = \; s(fd_1 \cdot Ct_1 \; - \; fd_o \cdot Ct_o) \qquad (5\text{-}9)$$

J_{aq} = sediment flux of ammonium, nitrate, phosphate, or sulfide/methane to the overlying water (g m^{-2} day^{-1}).

The convention used in Eq. 5-9 is that positive flux is from the sediment to the overlying water.

In the lower layer, the processes included in the flux portion are (Fig. 5-1)

- exchange of dissolved fraction between Layer 1 and 2 via diffusive transport
- exchange of particulate fraction between Layer 1 and 2 via particle mixing
- deposition from Layer 1 and burial to the deep inactive sediments
- removal (sink) by reaction
- internal sources including diagenetic source.

The mass-balance equation for ammonium, nitrate, phosphate or sulfide/methane in the lower layer is:

$$H_2 \frac{\partial Ct_2}{\partial t} \; = \; - \; KL(fd_2 \cdot Ct_2 \; - \; fd_1 \cdot Ct_1) \; - \; \tilde{\omega}(fp_2 \cdot Ct_2 \; - \; fp_1 \cdot Ct_1)$$

$$+ \; W(Ct_1 \; - \; Ct_2) \; - \; \kappa_2 \cdot Ct_2 \; + \; J_2 \qquad (5\text{-}10)$$

κ_2 = reaction velocity in Layer 2 (m day^{-1})

J_2 = sum of all internal sources including diagenesis in Layer 2 (g m^{-2} day^{-1}).

The substances produced by mineralization of POM in sediments may be present in both dissolved and particulate phases. This distribution directly affects the magnitude of the substance that is returned to the overlying water. In Equations 5-8 to 5-10, the distribution of a substance between the dissolved and particulate phases in a sediment is parameterized using a linear partitioning coefficient. The dissolved and particulate fractions are computed from the partitioning equations:

$$fd_1 = \frac{1}{1 + m_1 \cdot \pi_1} \qquad\qquad\qquad fp_1 = 1 - fd_1 \qquad\qquad\qquad (5\text{-}11)$$

$$fd_2 = \frac{1}{1 + m_2 \cdot \pi_2} \qquad\qquad\qquad fp_2 = 1 - fd_2 \qquad\qquad\qquad (5\text{-}12)$$

m_1, m_2 = solid concentrations in Layer 1 and 2, respectively (kg L^{-1})

π_1, π_2 = partition coefficients in Layer 1 and 2, respectively (per kg L^{-1}).

The partition coefficient is the ratio of particulate to dissolved fraction per unit solid concentration (i.e., per unit sorption site available).

All terms, except the last two terms, in Equations 5-8 and 5-10 are common to all state variables and are described in Section 5.3.1. The last two terms represent the reaction and source/sink terms, respectively. These terms, which take different mathematical formulations for different state variables, are described in Sections 5.3.2 to 5.3.5 for ammonium, nitrate, phosphate, and sulfide/methane, respectively.

5.3.1   Common Parameters for Sediment Flux

Parameters that are needed for the sediment fluxes are s, $\tilde{\omega}$, KL, W, H_2, m_1, m_2, π_1, π_2, κ_1, κ_2, J_1, and J_2 in Equations 5-8 to 5-12. Of these, κ_1, κ_2, J_1, and J_2 are variable-specific. Among the other common parameters, W, H_2, m_1, and m_2, are specified as input. The modeling of the remaining three parameters, s, $\tilde{\omega}$, and KL, is described in this section.

5.3.1.1 Surface mass transfer coefficient. Owing to the observation that the surface mass transfer coefficient, s, can be related to the sediment oxygen demand, SOD (DiToro et al. 1990), s can be estimated from the ratio of SOD and overlying water oxygen concentration:

$$s = \frac{D_1}{H_1} = \frac{SOD}{DO_0} \qquad\qquad\qquad\qquad\qquad\qquad (5\text{-}13)$$

D_1 = diffusion coefficient in Layer 1 (m^2 day^{-1}).

Knowing *s*, it is possible to estimate the other model parameters.

5.3.1.2 Particulate phase mixing coefficient. The particle mixing velocity between Layer 1 and 2 is parameterized as:

$$\widetilde{\omega} = \frac{D_p \cdot \theta_{Dp}^{T-20}}{H_2} \frac{G_{POC,1}}{G_{POC,R}} \frac{DO_0}{KM_{Dp} + DO_0}$$

(5-14)

D_p = apparent diffusion coefficient for particle mixing (m^2 day^{-1})

θ_{Dp} = constant for temperature adjustment for D_p

$G_{POC,R}$ = reference concentration for $G_{POC,1}$ (g C m^{-3})

KM_{Dp} = particle mixing half-saturation constant for oxygen (g O_2 m^{-3}).

The enhanced mixing of sediment particles by macrobenthos (bioturbation) is quantified by estimating D_p. The particle mixing appears to be proportional to the benthic biomass (Matisoff 1982), which is correlated to the carbon input to the sediment (Robbins et al. 1989). This is parameterized by assuming that benthic biomass is proportional to the available labile carbon, $G_{POC,1}$, and $G_{POC,R}$ is the reference concentration at which the particle mixing velocity is at its nominal value. The Monod-type oxygen dependency accounts for the oxygen dependency of benthic biomass.

It has been observed that a hysteresis exists in the relationship between the bottom water oxygen and benthic biomass. Benthic biomass increases as the summer progresses. However, the occurrence of anoxia/hypoxia reduces the biomass drastically and also imposes stress on benthic activities. After full overturn, the bottom water oxygen increases, but the population does not recover immediately. Hence, the particle mixing velocity, which is proportional to the benthic biomass, does not increase in response to the increased bottom water oxygen. Recovery of benthic biomass following hypoxic events depends on many factors including severity and longevity of hypoxia, constituent species, and salinity (Diaz and Rosenberg 1995).

This phenomenon of reduced benthic activities and hysteresis is parameterized based on the idea of stress that low oxygen imposes on the benthic population. It is analogous to the modeling of the toxic effect of chemicals on organisms (Mancini 1983). A first order differential equation is employed, in which the benthic stress (1) accumulates only when overlying oxygen is below KM_{Dp} and (2) is dissipated at a first order rate (Fig. 5-3a):

$$\frac{\partial ST}{\partial t} = -K_{ST} \cdot ST + \left(1 - \frac{DO_0}{KM_{Dp}}\right) \qquad\qquad if \quad DO_0 < KM_{Dp}$$

(5-15)

$$\frac{\partial ST}{\partial t} = -K_{ST} \cdot ST \qquad\qquad\qquad if \quad DO_0 > KM_{Dp}$$

ST   = accumulated benthic stress (day)

K_{ST} = first order decay rate for ST (day^{-1}).

The behavior of this formulation can be understood by evaluating the steady-state stresses at two extreme conditions of overlying water oxygen, DO_0:

       as $DO_0 = 0$ $K_{ST} \cdot ST = 1$ $f(ST) = (1 - K_{ST} \cdot ST) = 0$

       as $DO_0 \geq KM_{Dp}$ $K_{ST} \cdot ST = 0$ $f(ST) = (1 - K_{ST} \cdot ST) = 1$

The dimensionless expression, $f(ST) = 1 - K_{ST} \cdot ST$, appears to be the proper variable to quantify the effect of benthic stress on benthic biomass and thus particle mixing (Fig. 5-3b).

The final formulation for the particle mixing velocity, including the benthic stress, is:

$$\omega = \frac{D_p \cdot \theta_{Dp}^{T-20}}{H_2} \frac{G_{POC,1}}{G_{POC,R}} \frac{DO_0}{KM_{Dp} + DO_0} f(ST) + \frac{Dp_{min}}{H_2}$$

(5-16)

Dp_{min} = minimum diffusion coefficient for particle mixing (m^2 day^{-1}).

The reduction in particle mixing due to the benthic stress, f(ST), is estimated by employing the following procedure. The stress, ST, is normally calculated with Eq. 5-15. Once DO_0 drops below a critical concentration, $DO_{ST,c}$, for $NC_{hypoxia}$ consecutive days or more, the calculated stress is not allowed to decrease until t_{MBS} days of $DO_0 > DO_{ST,c}$. That is, only when hypoxic days are longer than critical hypoxia days ($NC_{hypoxia}$), the maximum stress, or minimum (1 - $K_{ST} \cdot ST$), is retained for a specified period (t_{MBS} days) after DO_0 recovery (Fig. 5-3). No hysteresis occurs if DO_0 does not drop below $DO_{ST,c}$ or if hypoxia lasts less than $NC_{hypoxia}$ days. When applying maximum stress for t_{MBS} days, the subsequent hypoxic days are not included in t_{MBS}. This parameterization of hysteresis essentially assumes seasonal hypoxia, i.e., one or two major hypoxic events during summer, and might be unsuitable for systems with multiple hypoxic events throughout a year.
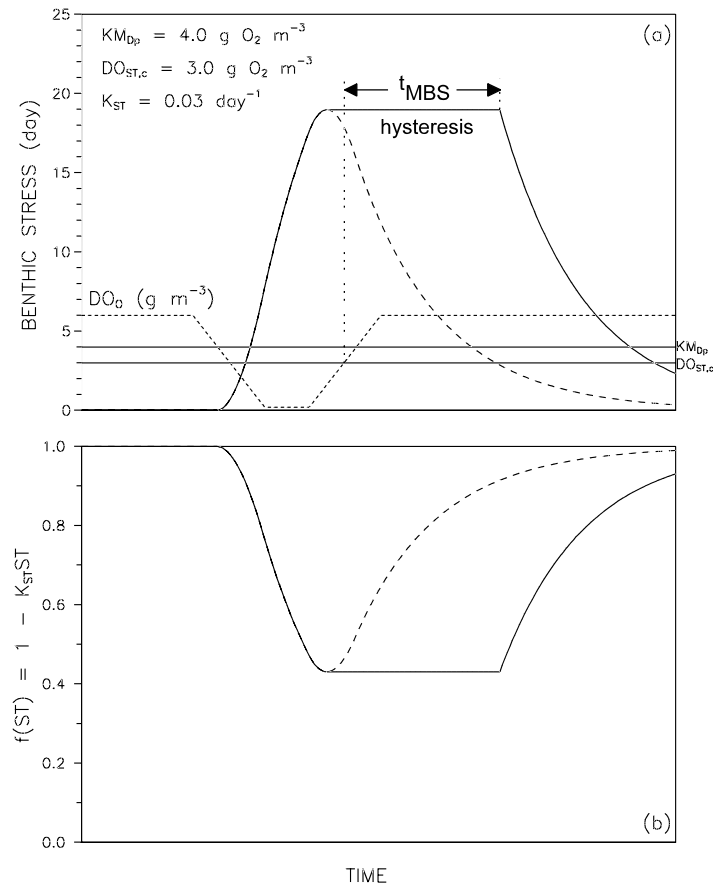
Figure 5-3.   Benthic stress (a) and its effect on particle mixing (b) as a function of overlying water column dissolved oxygen concentration

Three parameters relating to hysteresis, $DO_{ST,c}$, $NC_{hypoxia}$, and t_{MBS}, are functions of many factors including severity and longevity of hypoxia, constituent species, and salinity, and thus have site-specific variabilities (Diaz and Rosenberg 1995). The critical overlying oxygen concentration, $DO_{ST,c}$, also depends on the distance from the bottom of the location of DO_0. The critical hypoxia days, $NC_{hypoxia}$, depend on tolerance of benthic organisms to hypoxia and thus on benthic community structure (Diaz and Rosenberg 1995). The time lag for the recovery of benthic biomass following hypoxic events, t_{MBS}, tends to be longer for higher salinity. The above three parameters are considered to be spatially constant input parameters.

5.3.1.3 Dissolved phase mixing coefficient. Dissolved phase mixing between Layer 1 and 2 is via passive molecular diffusion, which is enhanced by the mixing activities of the benthic organisms (bio-irrigation). This is modeled by increasing the diffusion coefficient relative to the molecular diffusion coefficient:

$$KL = \frac{D_d \cdot \theta_{Dd}^{T-20}}{H_2} + R_{BI,BT} \cdot \omega \qquad (5\text{-}17)$$

D_d = diffusion coefficient in pore water (m^2 day^{-1})

θ_{Dd} = constant for temperature adjustment for D_d

$R_{BI,BT}$ = ratio of bio-irrigation to bioturbation.

The last term in Eq. 5-17 accounts for the enhanced mixing by organism activities.

5.3.2   Ammonia Nitrogen

Diagenesis is assumed not to occur in the upper layer because of its shallow depth, and ammonium is produced by diagenesis in the lower layer:

$$J_{1,NH4} = 0 \qquad\qquad J_{2,NH4} = J_N \;\; (from\; Eq.\; 5\text{-}7) \qquad (5\text{-}18)$$

Ammonium is nitrified to nitrate in the presence of oxygen. A Monod-type expression is used for the ammonium and oxygen dependency of the nitrification rate. Then the oxic layer reaction velocity in Eq. 5-8 for ammonium may be expressed as:

$$\kappa_{1,NH4}^2 = \frac{DO_0}{2 \cdot KM_{NH4,O2} + DO_0} \frac{KM_{NH4}}{KM_{NH4} + NH4_1} \kappa_{NH4}^2 \cdot \theta_{NH4}^{T-20} \qquad (5\text{-}19)$$

and then the nitrification flux becomes:

$$J_{Nit} = \frac{\kappa_{1,NH4}^2}{s} \cdot NH4_1 \qquad (5\text{-}20)$$

$KM_{NH4,O2}$ = nitrification half-saturation constant for dissolved oxygen (g O_2 m^{-3})

$NH4_1$ = total ammonium nitrogen concentration in Layer 1 (g N m^{-3})

KM_{NH4} = nitrification half-saturation constant for ammonium (g N m^{-3})

κ_{NH4} = optimal reaction velocity for nitrification at 20°C (m day^{-1})

θ_{NH4} = constant for temperature adjustment for κ_{NH4}

J_{Nit} = nitrification flux (g N m^{-2} day^{-1}).

Nitrification does not occur in the anoxic lower layer:

$$\kappa_{2,NH4} = 0 \qquad (5\text{-}21)$$

Once Equations 5-8 and 5-10 are solved for NH4$_1$ and NH4$_2$, the sediment flux of ammonium to the overlying water, J$_{aq,NH4}$, can be calculated using Eq. 5-9. Note that it is not NH4$_1$ and NH4$_2$ that determine the magnitude of J$_{aq,NH4}$ (Section X-B-2 in D&F 1993). The magnitude is determined by (1) the

diagenesis flux, (2) the fraction that is nitrified, and (3) the surface mass transfer coefficient (*s*) that mixes the remaining portion.

5.3.3   Nitrate Nitrogen

Nitrification flux is the only source of nitrate in the upper layer, and there is no diagenetic source for nitrate in both layers:

$$J_{1,NO3} = J_{Nit} \quad (from \ Eq. \ 5-19) \qquad\qquad\qquad J_{2,NO3} = 0 \tag{5-22}$$

Nitrate is present in sediments as dissolved substance, i.e., $\pi_{1,NO3} = \pi_{2,NO3} = 0$, making $fd_{1,NO3} = fd_{2,NO3} = 1$ (Equations 5-11 and 5-12): it also makes $\tilde{\omega}$ meaningless, hence $\tilde{\omega} = 0$. Nitrate is removed by denitrification in both oxic and anoxic layers with the carbon required for denitrification supplied by carbon diagenesis. The reaction velocities in Equations 5-8 and 5-10 for nitrate may be expressed as:

$$\kappa_{1,NO3}^2 = \kappa_{NO3,1}^2 \cdot \theta_{NO3}^{T-20} \tag{5-23}$$

$$\kappa_{2,NO3} = \kappa_{NO3,2} \cdot \theta_{NO3}^{T-20} \tag{5-24}$$

and the denitrification flux out of sediments as a nitrogen gas becomes:

$$J_{N2(g)} = \frac{\kappa_{1,NO3}^2}{s} NO3_1 + \kappa_{2,NO3} \cdot NO3_2 \tag{5-25}$$

$\kappa_{NO3,1}$ = reaction velocity for denitrification in Layer 1 at 20°C (m day^{-1})

$\kappa_{NO3,2}$ = reaction velocity for denitrification in Layer 2 at 20°C (m day^{-1})

θ_{NO3} = constant for temperature adjustment for $\kappa_{NO3,1}$ and $\kappa_{NO3,2}$

$J_{N2(g)}$ = denitrification flux (g N m^{-2} day^{-1})

$NO3_1$ = total nitrate nitrogen concentration in Layer 1 (g N m^{-3})

$NO3_2$ = total nitrate nitrogen concentration in Layer 2 (g N m^{-3}).

Once Equations 5-8 and 5-10 are solved for $NO3_1$ and $NO3_2$, the sediment flux of nitrate to the overlying water, $J_{aq,NO3}$, can be calculated using Eq. 5-9. The steady-state solution for nitrate showed that the nitrate flux is a linear function of $NO3_0$ (Eq. III-15 in D&F 1993): the intercept quantifies the amount of ammonium in the sediment that is nitrified but not denitrified (thus releases as $J_{aq,NO3}$), and the slope quantifies the extent to which overlying water nitrate is denitrified in the sediment. It also revealed that if the internal production of nitrate is small relative to the flux of nitrate from the overlying water, the normalized nitrate flux to the sediment, $- J_{aq,NO3}/NO3_0$, is linear in *s* for small *s* and constant for large *s*

(Section III-C in D&F 1993). For small s (~ 0.01 m day^{-1}), H_1 is large (Eq. 5-13) so that oxic layer denitrification predominates and $J_{aq,NO3}$ is essentially zero independent of $NO3_0$ (Fig. III-4 in D&F 1993).

5.3.4   Phosphate Phosphorus

Phosphate is produced by the diagenetic breakdown of POP in the lower layer:

$$J_{1,PO4} \;=\; 0 \qquad\qquad\qquad J_{2,PO4} \;=\; J_P \;\; (from\ Eq.\ 5\text{-}7) \qquad\qquad (5\text{-}26)$$

A portion of the liberated phosphate remains in the dissolved form and a portion becomes particulate phosphate, either via precipitation of phosphate-containing minerals (Troup 1974), e.g., vivianite, $Fe_3(PO_4)_2(s)$, or by partitioning to phosphate sorption sites (Lijklema 1980; Barrow 1983; Giordani and Astorri 1986). The extent of particulate formation is determined by the magnitude of the partition coefficients, $\pi_{1,PO4}$ and $\pi_{2,PO4}$, in Equations 5-11 and 5-12. Phosphate flux is strongly affected by DO_0, the overlying water oxygen concentration. As DO_0 approaches zero, the phosphate flux from the sediments increases. This mechanism is incorporated by making $\pi_{1,PO4}$ larger, under oxic conditions, than $\pi_{2,PO4}$. In the model, when DO_0 exceeds a critical concentration, $(DO_0)_{crit,PO4}$, sorption in the upper layer is enhanced by an amount $\Delta\pi_{PO4,1}$:

$$\pi_{1,PO4} \;=\; \pi_{2,PO4}\cdot(\Delta\pi_{PO4,1}) \qquad\qquad\qquad DO_0 \;>\; (DO_0)_{crit,PO4} \qquad\qquad (5\text{-}27)$$

When oxygen falls below $(DO_0)_{crit,PO4}$, then:

$$\pi_{1,PO4} \;=\; \pi_{2,PO4}\cdot(\Delta\pi_{PO4,1})^{DO_0/(DO_0)_{crit,PO4}} \qquad\qquad DO_0 \;\le\; (DO_0)_{crit,PO4} \qquad\qquad (5\text{-}28)$$

which smoothly reduces $\pi_{1,PO4}$ to $\pi_{2,PO4}$ as DO_0 goes to zero. There is no removal reaction for phosphate in both layers:

$$\kappa_{1,PO4} \;=\; \kappa_{2,PO4} \;=\; 0 \qquad\qquad\qquad\qquad (5\text{-}29)$$

Once Equations 5-8 and 5-10 are solved for $PO4_1$ and $PO4_2$, the sediment flux of phosphate to the overlying water, $J_{aq,PO4}$, can be calculated using Eq. 5-9.

5.3.5   Sulfide/Methane and Oxygen Demand

5.3.5.1 Sulfide. No diagenetic production of sulfide occurs in the upper layer. In the lower layer, sulfide is produced by carbon diagenesis (Eq. 5-7) decremented by the organic carbon consumed by denitrification (Eq. 5-25). Then:

$$J_{1,H2S} \;=\; 0 \qquad\qquad\qquad J_{2,H2S} \;=\; a_{O2,C}\cdot J_C \;-\; a_{O2,NO3}\cdot J_{N2(g)} \qquad\qquad (5\text{-}30)$$

$a_{O2,C}$ =   stoichiometric coefficient for carbon diagenesis consumed by sulfide oxidation (2.6667 g O_2-equivalents per g C)

$a_{O2,NO3}$ = stoichiometric coefficient for carbon diagenesis consumed by denitrification (2.8571 g O_2-equivalents per g N).

A portion of the dissolved sulfide that is produced in the anoxic layer reacts with the iron to form particulate iron monosulfide, FeS(s) (Morse et al. 1987). The particulate fraction is mixed into the oxic layer where it can be oxidized to ferric oxyhydroxide, Fe_2O_3(s). The remaining dissolved fraction also diffuses into the oxic layer where it is oxidized to sulfate. Partitioning between dissolved and particulate sulfide in the model represents the formation of FeS(s), which is parameterized using partition coefficients, $\pi_{1,H2S}$ and $\pi_{2,H2S}$, in Equations 5-11 and 5-12.

The present sediment model has three pathways for sulfide, the reduced end product of carbon diagenesis: (1) sulfide oxidation, (2) aqueous sulfide flux, and (3) burial. The distribution of sulfide among the three pathways is controlled by the partitioning coefficients and the oxidation reaction velocities (Section V-E in D&F 1993). Both dissolved and particulate sulfide are oxidized in the oxic layer, consuming oxygen in the process. In the oxic upper layer, the oxidation rate that is linear in oxygen concentration is used (Cline and Richards 1969; Millero 1986; Boudreau 1991). In the anoxic lower layer, no oxidation can occur. Then the reaction velocities in Equations 5-8 and 5-10 may be expressed as:

$$\kappa^2_{1,H2S} = (\kappa^2_{H2S,d1} \cdot fd_{1,H2S} + \kappa^2_{H2S,p1} \cdot fp_{1,H2S}) \theta^{T-20}_{H2S} \frac{DO_0}{2 \cdot KM_{H2S,O2}} \tag{5-31}$$

$$\kappa_{2,H2S} = 0 \tag{5-32}$$

$\kappa_{H2S,d1}$ = reaction velocity for dissolved sulfide oxidation in Layer 1 at 20°C (m day^{-1})

$\kappa_{H2S,p1}$ = reaction velocity for particulate sulfide oxidation in Layer 1 at 20°C (m day^{-1})

θ_{H2S} = constant for temperature adjustment for $\kappa_{H2S,d1}$ and $\kappa_{H2S,p1}$

$KM_{H2S,O2}$ = constant to normalize the sulfide oxidation rate for oxygen (g O_2 m^{-3}).

The constant, $KM_{H2S,O2}$, which is included for convenience only, is used to scale the oxygen concentration in the overlying water. At $DO_0 = KM_{H2S,O2}$, the reaction velocity for sulfide oxidation rate is at its nominal value.

The oxidation reactions in the oxic upper layer cause oxygen flux to the sediment, which exerts SOD. By convention, SOD is positive: SOD = -$J_{aq,O2}$. The SOD in the model consists of two components, carbonaceous sediment oxygen demand (CSOD) due to sulfide oxidation and nitrogenous sediment oxygen demand (NSOD) due to nitrification:

$$SOD = CSOD + NSOD = \frac{\kappa_{1,H2S}^2}{s} H2S_1 + a_{O2,NH4} \cdot J_{Nit} \tag{5-33}$$

$H2S_1$ = total sulfide concentration in Layer 1 (g O_2-equivalents m^{-3})

$a_{O2,NH4}$ = stoichiometric coefficient for oxygen consumed by nitrification (4.33 g O_2 per g N).

Equation 4-29 is nonlinear for SOD because the RHS contains s (= SOD/DO$_0$) so that SOD appears on both sides of the equation: note that J_{Nit} (Eq. 5-20) is also a function of s. A simple back substitution method is used, as explained in Section 5.6.1.

If the overlying water oxygen is low, then the sulfide that is not completely oxidized in the upper layer can diffuse into the overlying water. This aqueous sulfide flux out of the sediments, which contributes to the chemical oxygen demand in the water column model, is modeled using

$$J_{aq,H2S} = s(fd_{1,H2S} \cdot H2S_1 - COD) \tag{5-34}$$

The sulfide released from the sediment reacts very quickly in the water column when oxygen is available, but can accumulate in the water column under anoxic conditions. The COD, quantified as oxygen equivalents, is entirely supplied by benthic release in the water column model (Eq. 3-16). Since sulfide also is quantified as oxygen equivalents, COD is used as a measure of sulfide in the water column in Eq. 5-34.

5.3.5.2 Methane. When sulfate is used up, methane can be produced by carbon diagenesis and methane oxidation consumes oxygen (DiToro et al. 1990). Owing to the abundant sulfate in the saltwater, only the aforementioned sulfide production and oxidation are considered to occur in the saltwater. Since the sulfate concentration in fresh water is generally insignificant, methane production is considered to replace sulfide production in fresh water. In fresh water, methane is produced by carbon diagenesis in the lower layer decremented by the organic carbon consumed by denitrification, and no diagenetic production of methane occurs in the upper layer (Eq. 5-30):

$$J_{1,CH4} = 0 \qquad\qquad J_{2,CH4} = a_{O2,C} \cdot J_C - a_{O2,NO3} \cdot J_{N2(g)} \tag{5-35}$$

The dissolved methane produced takes two pathways: (1) oxidation in the oxic upper layer causing CSOD or (2) escape from the sediment as aqueous flux or as gas flux:

$$J_{2,CH4} = CSOD + J_{aq,CH4} + J_{CH4(g)} \tag{5-36}$$

$J_{aq,CH4}$ = aqueous methane flux (g O_2-equivalents m^{-2} day^{-1})

$J_{CH4(g)}$ = gaseous methane flux (g O_2-equivalents m^{-2} day^{-1}).

A portion of dissolved methane that is produced in the anoxic layer diffuses into the oxic layer where it is oxidized. This methane oxidation causes CSOD in the freshwater sediment (DiToro et al. 1990):

$$CSOD = CSOD_{max} \cdot \left(1 - sech[\frac{\kappa_{CH4} \cdot \theta_{CH4}^{T-20}}{s}] \right) \tag{5-37}$$

$$CSOD_{max} = minimum \{\sqrt{2 \cdot KL \cdot CH4_{sat} \cdot J_{2,CH4}}, J_{2,CH4}\} \tag{5-38}$$

$$CH4_{sat} = 100\left(1 + \frac{h + H_2}{10} \right) 1.024^{20-T} \tag{5-39}$$

$CSOD_{max}$ = maximum CSOD occurring when all the dissolved methane transported to the oxic layer is oxidized

κ_{CH4} = reaction velocity for dissolved methane oxidation in Layer 1 at 20°C (m day^{-1})

θ_{CH4} = constant for temperature adjustment for κ_{CH4}

$CH4_{sat}$ = saturation concentration of methane in the pore water (g O_2-equivalents m^{-3}).

The term, $(h + H_2)/10$ where h and H_2 are in meters, in Eq. 5-39 is the depth from the water surface that corrects for the in situ pressure. Equation 5-39 is accurate to within 3% of the reported methane solubility between 5 and 20°C (Yamamoto et al. 1976).

If the overlying water oxygen is low, the methane that is not completely oxidized can escape the sediment into the overlying water either as aqueous flux or as gas flux. The aqueous methane flux, which contributes to the chemical oxygen demand in the water column model, is modeled using (DiToro et al. 1990):

$$J_{aq,CH4} = CSOD_{max} \cdot sech[\frac{\kappa_{CH4} \cdot \theta_{CH4}^{T-20}}{s}] = CSOD_{max} - CSOD \tag{5-40}$$

Methane is only slightly soluble in water. If its solubility, $CH4_{sat}$ given by Eq. 5-39, is exceeded in the pore water, it forms a gas phase that escapes as bubbles. The loss of methane as bubbles, i.e., the gaseous methane flux, is modeled using Eq. 5-36 with $J_{2,CH4}$ from Eq. 5-35, CSOD from Eq. 5-37, and $J_{aq,CH4}$ from Eq. 5-40 (DiToro et al. 1990).

5.4 Silica

The production of ammonium, nitrate, and phosphate in sediments is the result of the mineralization of POM by bacteria. The production of dissolved silica in sediments is the result of the dissolution of particulate biogenic or opaline silica, which is thought to be independent of bacterial processes.

The depositional flux of particulate biogenic silica from the overlying water to the sediments is modeled using Eq. 5-5. With this source, the mass-balance equation for particulate biogenic silica may be written as:

$$H_2 \frac{\partial PSi}{\partial t} \ = \ - \ S_{Si} \cdot H_2 \ - \ W \cdot PSi \ + \ J_{PSi} \ + \ J_{DSi} \tag{5-41}$$

PSi = concentration of particulate biogenic silica in the sediment (g Si m^{-3})

S_{Si} = dissolution rate of PSi in Layer 2 (g Si m^{-3} day^{-1})

J_{PSi} = depositional flux of PSi (g Si m^{-2} day^{-1}) given by Eq. 5-5

J_{DSi} = detrital flux of PSi (g Si m^{-2} day^{-1}) to account for PSi settling to the sediment that is not associated with the algal flux of biogenic silica.

The processes included in Eq. 5-41 are dissolution (i.e., production of dissolved silica), burial, and depositional and detrital fluxes from the overlying water. Equation 5-41 can be viewed as the analog of the diagenesis equations for POM (Eq. 5-6). The dissolution rate is formulated using a reversible reaction that is first order in silica solubility deficit and follows a Monod-type relationship in particulate silica:

$$S_{Si} \ = \ K_{Si} \cdot \theta_{Si}^{T \, - \, 20} \frac{PSi}{PSi \ + \ KM_{PSi}} (Si_{sat} \ - \ fd_{2,Si} \cdot Si_2) \tag{5-42}$$

K_{Si} = first order dissolution rate for PSi at 20°C in Layer 2 (day^{-1})

θ_{Si} = constant for temperature adjustment for K_{Si}

KM_{PSi} = silica dissolution half-saturation constant for PSi (g Si m^{-3})

Si_{sat} = saturation concentration of silica in the pore water (g Si m^{-3}).

The mass-balance equations for mineralized silica can be formulated using the general forms, Equations 5-8 and 5-10. There is no source/sink term and no reaction in the upper layer:

$$J_{1,Si} \ = \ \kappa_{1,Si} \ = \ 0 \tag{5-43}$$

In the lower layer, silica is produced by the dissolution of particulate biogenic silica, which is modeled using Eq. 5-42. The two terms in Eq. 5-42 correspond to the source term and reaction term in Eq. 5-10:

$$J_{2,Si} \ = \ K_{Si} \cdot \theta_{Si}^{T \, - \, 20} \frac{PSi}{PSi \ + \ KM_{PSi}} Si_{sat} \cdot H_2 \tag{5-44}$$

$$\kappa_{2,Si} \ = \ K_{Si} \cdot \theta_{Si}^{T \, - \, 20} \frac{PSi}{PSi \ + \ KM_{PSi}} f_{d2,Si} \cdot H_2 \tag{5-45}$$

A portion of silica dissolved from particulate silica sorbs to solids and a portion remains in the dissolved form. Partitioning using the partition coefficients, $\pi_{1,Si}$ and $\pi_{2,Si}$, in Equations 5-11 and 5-12 controls the

extent to which dissolved silica sorbs to solids. Since silica shows similar behavior as phosphate in the adsorption-desorption process, the same partitioning method as applied to phosphate (Section 5.3.4) is used for silica. That is, when DO_0 exceeds a critical concentration, $(DO_0)_{crit,Si}$, sorption in the upper layer is enhanced by an amount $\Delta\pi_{Si,1}$:

$$\pi_{1,Si} = \pi_{2,Si} \cdot (\Delta\pi_{Si,1}) \qquad\qquad DO_0 > (DO_0)_{crit,Si} \qquad\qquad (5\text{-}46)$$

When oxygen falls below $(DO_0)_{crit,Si}$, then:

$$\pi_{1,Si} = \pi_{2,Si} \cdot (\Delta\pi_{Si,1})^{DO_0/(DO_0)_{crit,Si}} \qquad\qquad DO_0 \leq (DO_0)_{crit,Si} \qquad\qquad (5\text{-}47)$$

which smoothly reduces $\pi_{1,Si}$ to $\pi_{2,Si}$ as DO_0 goes to zero.

Once Equations 5-8 and 5-10 are solved for Si_1 and Si_2, the sediment flux of silica to the overlying water, $J_{aq,Si}$, can be calculated using Eq. 5-9.

5.5 Sediment Temperature

All rate coefficients in the aforementioned mass-balance equations are expressed as a function of sediment temperature, T. The sediment temperature is modeled based on the diffusion of heat between the water column and sediment:

$$\frac{\partial T}{\partial t} = \frac{D_T}{H^2}(T_W - T) \qquad\qquad (5\text{-}48)$$

D_T = heat diffusion coefficient between the water column and sediment (m^2 sec^{-1})

T_W = temperature in the overlying water column (°C) calculated by Eq. 4-82.

The model application in D&F and Cerco and Cole (1993) used $D_T = 1.8 \times 10^{-7}$ m^2 sec^{-1}.

5.6 Method of Solution

5.6.1 Finite-Difference Equations and Solution Scheme

An implicit integration scheme is used to solve the governing mass-balance equations. The finite difference form of Eq. 5-8 may be expressed as:

$$0 = s(fd_0 \cdot Ct_0' - fd_1 \cdot Ct_1') + KL(fd_2 \cdot Ct_2' - fd_1 \cdot Ct_1') + \omega(fp_2 \cdot Ct_2' - fp_1 \cdot Ct_1')$$

$$- W \cdot Ct_1' - \frac{\kappa_1^2}{s}Ct_1' + J_1' \qquad\qquad (5\text{-}49)$$

where the primed variables designate the values evaluated at $t+\theta$ and the unprimed variables are those at t, where θ is defined in Eq. 4-82. The finite difference form of Eq. 5-10 may be expressed as:

$$0 = -KL(fd_2 \cdot Ct_2' - fd_1 \cdot Ct_1') - \bar{\omega}(fp_2 \cdot Ct_2' - fp_1 \cdot Ct_1') + W(Ct_1' - Ct_2')$$

$$- (\kappa_2 + \frac{H_2}{\theta})Ct_2' + \left(J_2' + \frac{H_2}{\theta}Ct_2\right) \tag{5-50}$$

The two terms, $-(H_2/\theta)Ct_2'$ and $(H_2/\theta)Ct_2$, are from the derivative term, $H_2(\partial Ct_2/\partial t)$ in Eq. 5-10, each of which simply adds to the Layer 2 removal rate and the forcing function, respectively. Setting these two terms equal to zero results in the steady-state model. The two unknowns, Ct_1' and Ct_2', can be calculated at every time step using:

$$\begin{pmatrix} s \cdot fd_1 + a_1 + \dfrac{\kappa_1^2}{s} & -a_2 \\ -a_1 & a_2 + W + \kappa_2 + \dfrac{H_2}{\theta} \end{pmatrix} \begin{pmatrix} Ct_1' \\ Ct_2' \end{pmatrix} = \begin{pmatrix} J_1' + s \cdot fd_0 \cdot Ct_0' \\ J_2' + \dfrac{H_2}{\theta}Ct_2 \end{pmatrix} \tag{5-51}$$

$$a_1 = KL \cdot fd_1 + \bar{\omega} \cdot fp_1 + W \qquad\qquad a_2 = KL \cdot fd_2 + \bar{\omega} \cdot fp_2 \tag{5-52}$$

The solution of Eq. 5-51 requires an iterative method since the surface mass transfer coefficient, s, is a function of the SOD (Eq. 5-13), which is also a function of s (Eq. 5-33). A simple back substitution method is used:

(1) Start with an initial estimate of SOD: for example, SOD = $a_{O2,C} \cdot J_C$ or the previous time step SOD.

(2) Solve Eq. 5-51 for ammonium, nitrate, and sulfide/methane.

(3) Compute the SOD using Eq. 5-33.

(4) Refine the estimate of SOD: a root finding method (Brent's method in Press et al. 1986) is used to make the new estimate.

(5) Go to (2) if no convergence.

(6) Solve Eq. 5-51 for phosphate and silica.

For the sake of symmetry, the equations for diagenesis, particulate biogenic silica and sediment temperature are also solved in implicit form. The finite difference form of the diagenesis equation (Eq. 5-6) may be expressed as:

$$G_{POM,i}' = \left(G_{POM,i} + \frac{\theta}{H_2}J_{POM,I}\right)\left(1 + \theta \cdot K_{POM,i} \cdot \theta_{POM,i}^{T-20} + \frac{\theta}{H_2}W\right)^{-1} \tag{5-53}$$

The finite difference form of the PSi equation (Eq. 5-41) may be expressed as:

$$PSi' = \left(PSi + \frac{\theta}{H_2}(J_{PSi} + J_{DSi}) \right)\left(1 + \theta \cdot K_{Si} \cdot \theta_{Si}^{T-20} \frac{Si_{sat} - f_{d2,Si} \cdot Si_2}{PSi + KM_{PSi}} + \frac{\theta}{H_2} W \right)^{-1} \tag{5-54}$$

using Eq. 5-36 for the dissolution term, in which PSi in the Monod-type term has been kept at time level t to simplify the solution. The finite difference form of the sediment temperature equation (Eq. 5-48) may be expressed as:

$$T' = \left(T + \frac{\theta}{H^2} D_T \cdot T_W \right)\left(1 + \frac{\theta}{H^2} D_T \right)^{-1} \tag{5-55}$$

5.6.2 Boundary and Initial Conditions

The above finite difference equations constitute an initial boundary-value problem. The boundary conditions are the depositional fluxes ($J_{POM,i}$ and J_{PSi}) and the overlying water conditions (Ct_0 and T_W) as a function of time, which are provided from the water column water quality model. The initial conditions are the concentrations at $t = 0$, $G_{POM,i}(0)$, $PSi(0)$, $Ct_1(0)$, $Ct_2(0)$, and $T(0)$, to start the computations. Strictly speaking, these initial conditions should reflect the past history of the overlying water conditions and depositional fluxes, which is often impractical because of lack of field data for these earlier years.

6 - EFDC WATER QUALITY MODEL CALIBRATION

The EFDC hydrodynamic and water quality model was used to determine the receiving water quality conditions in the tidal and non-tidal streams in the Christina River Basin. Nutrient loads were input to the EFDC model by means of linkage to the HSPF watershed loading models and the XP-SWMM CSO simulation flow model. Flows and loads from over 100 NPDES facilities were also included in the EFDC model.

6.1   Modeling Assumptions

The main objective of applying the EFDC model was to develop hydrodynamic and water quality information for the primary stream channels throughout Christina River Basin. Specifically, it was necessary to accurately understand the variability of flow throughout the stream network under variable flow conditions. Major assumptions that contributed to the final approach taken included:

- The waterbody was well mixed laterally and vertically, therefore a longitudinal one-dimensional configuration was appropriate for the freshwater stream channels.
- Thermal stratification was not likely due to the shallow and narrow characteristics of the creek, thus temperature is not an important driving force for flow and transport.
- Wind effects on flow and transport were not a critical factor due to the one-dimensional flow pattern.
- The impact of groundwater interaction on flow and transport was minimal during low flow conditions, thus flow distribution can be obtained through directly balancing upstream and downstream flow rates.

6.2   Model Configuration

The general procedure for application of the EFDC model to the Christina River Basin followed a sequence of steps beginning with model configuration and continued through model execution of the calibration time period. Model configuration involved the construction of the horizontal grid for the waterbodies in the basin, interpolation of bathymetric data to the grid, construction of EFDC input files, and compilation of the Fortran source code with appropriate parameter specification of array dimensions. The model included 120 NPDES point-source discharges and 28 consumptive use water withdrawals. The locations of the NPDES discharges are shown in Figure 6-1. Schematic drawings of the EFDC grid configuration are presented in Appendix C. The locations of the NPDES discharges relative to EFDC grid cells are shown in Figure C-1. The locations of the water withdrawals are shown in Figure C-2. The EFDC model also included flows and loads from 38 CSO discharges and was linked to the HSPF watershed loading models to incorporate nonpoint source flows and loads.
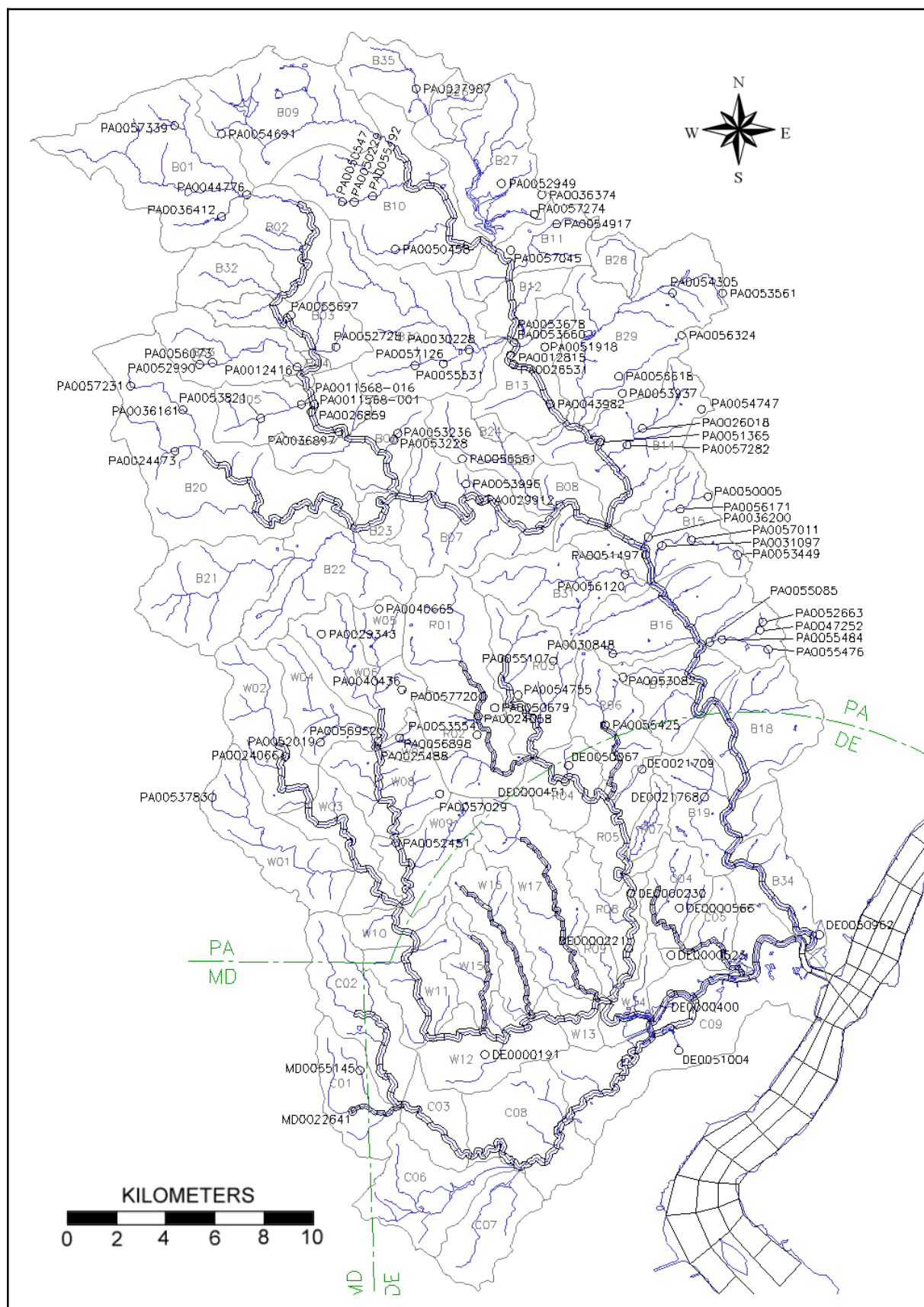
Figure 6-1. Locations of NPDES discharges in Christina River Basin.

6.2.1   Segmentation

The numerical model domain includes the tidal Delaware River from Reedy Point on the south to Chester on the north. Both the tidal and nontidal Christina River reaches are included in the model. The lower Christina River is directly connected to the Delaware River. The nontidal Christina River is connected to the tidal portion by a dam control structure at Smalleys Pond. The tidal Brandywine Creek is connected to the tidal Christina River by means of a tidal inlet control structure. The tidal White Clay Creek is also connected to the tidal Christina River via a tidal inlet control structure.

The basic equations in EFDC were solved using the finite-difference method. The grid was designed to resolve velocity shears both axially and laterally, and at the same time allow a time step suitable for efficient computation. Solutions to the hydrodynamics were obtained using a 60-second time step. The spatial domain of the study area was divided into a grid of discrete cells. To achieve close conformance of the grid to the estuary geometry, the cells in the Delaware River were represented using curvilinear horizontal grid cells constructed using an orthogonal mapping procedure (Ryskin and Leal 1983) to form a 2-D grid domain. The cells in the narrow tidal and nontidal streams were represented by a 1-D Cartesian coordinate system (see Figure C-1). To obtain adequate resolution in the streams, longitudinal cells were configured according to lengths ranging from 500 to approximately 1,000 meters. Cell widths were adjusted according to estimated wetted stream channel widths under low-flow conditions. Velocities were computed on the boundaries between cells, and temperature, salinity, and density were computed at the center of each cell. The numerical grid consisted of 406 cells in the horizontal plane and a single vertical layer. A single layer was chosen because the estuary and streams are well mixed, thereby implying that stratification would not be an issue. In addition, field data available from STORET and from Davis (1998) did not distinguish vertical sample depths.

6.2.2   Streamflow Estimation

Variable streamflow discharge was estimated using flows from the HSPF model for the calibration period 1994-1998. The streamflow was validated using observed daily average flows at several USGS stream gages throughout the Christina River Basin (Senior and Koerkle, (2003a, 2003b, 2003c, and 2003d).

6.2.3   Atmospheric and Tidal Boundary Conditions

Atmospheric nutrient loads are typically divided into wet and dry deposition. Wet deposition is associated with dissolved substances in rainfall. The settling of particulate matter during non-rainfall events contributes to dry deposition. Observations of concentrations in rainwater are frequently available, and dry deposition is usually estimated as a fraction of the wet deposition. The atmospheric deposition rates reported in the Long Island Sound Study (HydroQual, 1991) and the Chesapeake Bay Model Study (Cerco and Cole, 1993) as well as information provided by DNREC for Lewes, Delaware, were used to

develop both dry and wet deposition loads for the EFDC model of the Christina River Basin (see Tables 6-1 and 6-2). Meteorological information (i.e., atmospheric pressure, temperature, relative humidity, wind speed and direction, rainfall, cloud cover, and solar radiation) was obtained from the NOAA National Climatic Data Center weather station (WBAN 13781) at the New Castle County Airport near Wilmington, Delaware.

Table 6-1. Atmospheric dry deposition rates used in Christina River Basin EFDC model.

Parameter	Deposition Rate $(g/m^2/day)$	Parameter	Deposition Rate $(g/m^2/day)$
Refractory Part. Organic Carbon	0.000387	Refractory Part. Organic Nitrogen	0.000530
Labile Part. Organic Carbon	0.000387	Labile Part. Organic Nitrogen	0.000530
Dissolved Organic Carbon	0.000773	Dissolved Organic Nitrogen	0.000771
Dissolved Organic Phosphorus	0.000054	Ammonia Nitrogen	0.000214
Orthophosphate	0.000019	Nitrate+Nitrite Nitrogen	0.000393
Available Silica	0.000247		

Table 6.2. Atmospheric wet deposition concentrations used in Christina River Basin EFDC model.

Parameter	Concentration (mg/L)	Parameter	Concentration (mg/L)
Refractory Part. Organic Carbon	0.325	Refractory Part. Organic Nitrogen	0.0
Labile Part. Organic Carbon	0.325	Labile Part. Organic Nitrogen	0.0
Dissolved Organic Carbon	0.650	Dissolved Organic Nitrogen	0.140
Dissolved Organic Phosphorus	0.045	Ammonia Nitrogen	0.222
Orthophosphate	0.016	Nitrate+Nitrite Nitrogen	0.332
Available Silica	0.0		

Tides were specified at the north and south boundaries in the Delaware River based on the astronomical harmonic constants for the NOAA subordinate tide stations at Reedy Point, Delaware (south boundary) and Chester, Pennsylvania (north boundary). The predicted tides from the harmonic constants do not include any low-frequency influences due to storms or regional low-pressure conditions (NOAA, 1998)..

The specification of boundary conditions was required at the model north and south interface with the Delaware River. The EFDC water quality model accommodates 21 boundary variables, each specified in an individual time-series data file of concentrations. Advective boundary conditions in the Christina River model were of the "upwind" type. Evaluation of the boundary concentration depended on the direction of flow at the boundary. When flow was out of the model, the boundary concentration was assigned the concentration in the model cell immediately upstream of the boundary. When the tidal flow was into the model, the boundary concentration was assigned a specified, time-varying value

representative of conditions outside the model domain. To estimate recirculation at the boundary near the time of flow reversal from outgoing to incoming tide, the last outgoing concentration at the boundary is used as the incoming concentration for a certain amount of time specified by the user. This concentration linearly approaches the specified outside boundary concentration over that time period. For the Christina River model, the recirculation time interval was specified as 60 minutes based on experience gained from previous water quality model applications of the EFDC model.

Delaware River boundary conditions for salinity, temperature, total suspended sediment, algae, organic carbon, dissolved oxygen, nitrogen, phosphorus, silica, and fecal coliform bacteria were specified based on available STORET data at stations in the Delaware River. The boundary time-series were created using observations that were averaged by month over the simulation period. If data for a parameter were not available for any given month, then the long-term average (over the period 1988-1998) for that month was used instead.

6.2.4   Initial Conditions

Initial conditions for freshwater streams in the EFDC model at the starting time of October 1, 1994, were estimated using the simulated flows and nutrient concentrations calculated by the HSPF model. Initial water quality concentration conditions in the tidal Delaware River and tidal Christina River were estimated using the ending conditions from the 1995 low-flow validation run (September 30, 1995). These initial conditions allow the model to begin its simulation at a stable numeric state. The impacts of initial conditions diminish quickly with time.

6.2.5   Point and Nonpoint Source Representation

External flows and loads of nutrients and oxygen demand were divided into four categories: (1) nonpoint source loads (i.e., diffuse sources) including tributary sources and groundwater sources, (2) point-source, (3) water withdrawals, and (4) atmospheric deposition. Nonpoint source loads were carried by freshwater flows and groundwater entering the main stream reaches. Point-source loads were discharges from the NPDES facilities and CSOs in the study area. Consumptive use water withdrawals were removed from the model system at the appropriate grid cell. Atmospheric loads were transfers from the atmosphere to the water surface via rainfall (wet deposition) and other processes (dry deposition). Atmospheric deposition is not a significant source in the narrow stream channels, but may be more important in the open estuary waterbodies in the lower Christina River and Delaware River because of the larger water surface area in those regions.

Nonpoint sources were estimated by the delineation of subbasins and land use categories in the HSPF watershed loading models.   The nonpoint source loads generated by the watershed models provided

predictive nutrient loads to the receiving waters reflective of variable meteorological (rainfall-runoff) characteristics.

Discharge Monitoring Records (DMRs) for various NPDES point sources in the Brandywine Creek watershed were provided in hard copy form by the Brandywine Valley Association. Other DMRs were provided in electronic format by PADEP and DNREC. The hard-copy data were keypunched and the electronic data were reformatted into a database file for use in developing point source loads for the water quality model. A list of all 120 NPDES discharges included in the model is given in Appendix C (Table C-1). The August 1997 field monitoring study (Davis 1998) included seven NPDES discharges that were monitored for flow and water quality parameters (see Appendix C, Figure C-3). Loading values for the various water quality constituents were computed based on the flow rates and concentrations provided on the DMRs or measured during the August 1997 study.

The NPDES discharges included single residence discharges (SRD) that are not required to submit DMR data. For purposes of model calibration, it was assumed that these SRD discharges operated at their permit discharge limits. Characteristic concentrations for the various water quality parameters were assigned to the NPDES source based on the type of discharge, and the loading in kg/day for each constituent was computed for input to the EFDC model. The characteristic effluent concentrations used for this study are listed in Appendix C, Table C-2, and the characteristic effluent parameter ratios are listed in Table C-3. The characteristic effluent concentrations and parameter ratios were derived from effluent monitoring data collected by Davis (1998) in August 1998 and from literature values reported in the *Technical Guidance Manual for Developing TMDLs* (USEPA, 1995).

For model calibration, a time-series of monthly average loads for the 1994-1998 simulation period was developed for nutrients, dissolved oxygen, CBOD, and total suspended solids for each NPDES point source based on available discharge monitoring records (DMRs). The methodology for estimating the various species of nitrogen and phosphorus is outlined in Table 6-3 and was described in the low-flow modeling report (USEPA, 2000). The ratios for converting CBOD5 to organic carbon for the model were determined based on data collected during a special study conducted in August-September 1999 from several of the larger WWTPs in the basin (USEPA, 2000).

Table 6-3. Methodology for developing EFDC point source loads from DMR data.

Water Quality Parameter	EFDC Code	Calculation
CBOD-5-day		CBOD5 = BOD5 * (CBOD5:BOD5 ratio)
CBOD-ultimate		CBODu = CBOD5 * (CBODu:CBOD5 ratio)
Total organic carbon	TOC	TOC = CBODu * (TOC:CBODu ratio)
Dissolved organic carbon	DOC	DOC = TOC * (DOC:TOC ratio)
Refractory particulate organic carbon	RPOC	0.5 * (TOC - DOC)
Labile particulate organic carbon	LPOC	0.5 * (TOC - DOC)
Total phosphorus Total organic phosphorus		If TP not reported on DMR, use default TP from Table C-2 TOP = TP - (TP * (OPO4:TP ratio))
Refractory particulate organic phosphorus	RPOP	0.25 TOP
Labile particulate organic phosphorus	LPOP	0.25 TOP
Dissolved organic phosphorus	DOP	0.50 TOP
Total orthophosphate	PO4T	TP * (OPO4:TP ratio)
Total nitrogen Nitrite nitrogen Total organic nitrogen		TN = NH3-N * (TN:NH3 ratio) NO2-N = NH3-n * (NO2:NO3 ratio) TON = TN - NO2-N - NO3-N - NH3-N
Refractory particulate organic nitrogen	RPON	0.25 TON
Labile particulate organic nitrogen	LPON	0.25 TON
Dissolved organic nitrogen	DON	0.50 TON
Ammonia nitrogen	NH3	reported on DMR (or use default NH3-N from Table C-2)
Nitrate nitrogen	NO3	NO3-N = NH3 * (NO3:NH3 ratio)
Unavailable biogenic silica	SUU	0.10 mg/L (default value)
Dissolved available silica	SAA	1.00 mg/L (default value)
Chemical oxygen demand	COD	9.6 * CBOD5
Dissolved oxygen	DOO	reported on DMR (or use default value from Table C-2)
Total active metal	TAM	0.0 (not simulated)
Fecal coliform bacteria	FCB	reported on DMR (or use default value from Table C-2)

CSO flows were estimated using XP-SWMM and were provided by the City of Wilmington. Nutrient loads from CSO outfalls were estimated using the XP-SWMM flow rates and event mean concentrations based on storm event monitoring conducted by the City of Wilmington and Delaware DNREC (see Tables 2-1a, b, and c).

6.2.6   Time Step and Simulation Duration

The EFDC model was executed at a time step of 60 seconds and the calibration simulated four consecutive water years covering the period from October 1, 1994 to October 1, 1998. A listing of the key EFDC input data files is presented in Appendix D.

6.3   Model Calibration Results

Model calibration involves the adjustment of certain model input quantities in an attempt to achieve a specified level of model performance. An extensive set of field data were gathered, processed, and displayed for modeling hydrodynamics and water quality transport in the Christina River Basin. The data set included database files containing more than 40,000 records at about 200 stations scattered throughout the interior of the basin as well as in the Delaware River itself. This section presents the results of the calibration of the EFDC hydrodynamic and water quality model. Parameters considered for calibration include flow rate and a suite of water quality parameters including nitrogen, phosphorus, carbon, and dissolved oxygen.

6.3.1   Tide Elevation and Phase

Calibration of the model with respect to water surface elevation was accomplished by analysis of observed and model predicted time-series data at two interior tide stations. For tidal waters, least squares harmonic analysis is the most commonly utilized procedure (Oey, Mellor, and Hires, 1985; Cheng et al., 1993; Shen et al., 1999). Tide elevation data were obtained from the USGS tide stations on the Christina River at the Port of Wilmington near the mouth and at Newport about 7.0 miles upstream of the mouth. These data were compared with surface elevations computed by the model at cell 56,13 (Port of Wilmington) and 45,13 (Newport). The time-series of tide elevations for the month of August 1997 for both the field data and model results were subjected to a harmonic analysis. The five most important astronomical harmonic constituents (M2, S2, N2, K1, and O1) were computed for both the field data and model simulation results. The harmonic analysis results, shown in Table 6-4, indicate the model is in good agreement with the measured tide data for both amplitude and phase. The model-data amplitudes for the M2 harmonic constituent agree within 5 cm (6%) and the phases agree to within 4 degrees (3%). Time-series graphs (Appendix C, Figure C-4) of the observed and model tide elevations at both the Port of Wilmington and Newport covering a 15-day period (August 1 - 15, 1997) provide a visual means of assessing the skill of the model in simulating tidal elevations. The model tides are forced at the north and south boundaries in the Delaware River based on the NOAA predictions at the Reedy Point, DE, and Chester, PA, subordinate stations (NOAA, 1998).

Table 6-4. Harmonic analysis of tides at Port of Wilmington and Newport

Harmonic Constant	Port of Wilmington		Newport	
	Amplitude (m)	Phase (degrees)	Amplitude (m)	Phase (degrees)
M2 - observed M2 - model Difference	0.7594 0.7135 0.0459	130.382 134.180 -3.798	0.6901 0.6768 0.0133	153.634 155.560 -1.926
S2 - observed S2 - model Difference	0.0894 0.1001 -0.0107	20.621 30.806 -10.185	0.0900 0.0890 0.0010	36.374 59.180 -22.806
N2 - observed N2 - model Difference	0.1271 0.1383 -0.0112	323.153 336.181 -13.028	0.1275 0.1240 0.0035	345.054 3.603 -18.549
K1 - observed K1 - model Difference	0.0802 0.0633 0.0169	174.059 178.335 -4.276	0.0615 0.0606 0.0009	184.740 190.948 -6.208
O1 - observed O1 - model Difference	0.0626 0.0546 0.0080	316.879 326.765 -9.886	0.0546 0.0514 0.0032	332.386 337.937 -5.551

6.3.2   Water Depth and Stream Velocity

Measurements of flow, water depth, and stream velocity were made at eight locations during the August 1997 field survey (Davis, 1998). The field measurements were made on the following dates: East Branch Brandywine Creek (08/12 - 08/14/1997), West Branch Brandywine Creek (08/19 - 08/20/1997), West Branch Red Clay Creek (08/05 - 08/07/1997 and 08/12 - 08/14/1997), and East Branch White Clay Creek (08/26 - 08/28/1997). A comparison of these measurements with the model results at the appropriate grid cell (I,J) location is given in Table 6-5.

Table 6-5. Model-data comparison of velocity, flow, and geometry (August 1997 data).

Stream Reach	EFDC Cell	Velocity (fps)		Depth (ft)		Flow (cfs)		Channel Width (ft)	
		Field	EFDC	Field	EFDC	Field	EFDC	Field	EFDC
East Branch Brandywine Creek	54,61	0.33	0.48	0.82	0.87	14.5	25.6	53.6	52.5
East Branch Brandywine Creek	54,56	0.85	0.56	1.02	1.11	34.3	34.5	39.6	52.5
West Branch Brandywine Creek	19,79	0.40	0.41	1.09	0.94	9.5	14.9	45.0	42.6
West Branch Brandywine Creek	26,79	0.41	0.36	0.70	0.82	32.0	32.9	111.5	111.5
East Branch White Clay Creek	19,31	0.44	0.40	0.93	0.96	5.30	5.33	13.0	12.8
East Branch White Clay Creek	19,29	0.42	0.41	0.85	0.86	7.35	7.34	20.6	20.3
West Branch Red Clay Creek	29,43	0.35	0.44	0.75	0.78	3.55	3.35	13.5	13.5
West Branch Red Clay Creek	33,43	0.49	0.52	0.90	0.94	5.45	4.92	12.4	12.4

6.3.3   Sediment Oxygen Demand and Benthic Nutrient Flux Rates

The need for a predictive benthic sediment processes model for water quality modeling projects has been apparent for some time. When using a water quality model for management scenario analysis, one of the biggest sources of uncertainty involves what to use for the future sediment flux rates after a proposed management control has been implemented. The predictive sediment submodel in EFDC helps address this uncertainty with two fundamental capabilities: (1) the ability to predict effects of management alternatives on sediment-water exchange processes and (2) the ability to predict the time scale for alterations in the sediment-water exchange processes. To meet these requirements, a predictive sediment process model was incorporated into the EFDC model framework and was based on DiToro and Fitzpatrick (1993). The sediment submodel is driven by net settling of organic matter from the water column to the sediments. In the benthos, the sediment submodel simulates the decay (diagenesis) of organic matter, which produces oxygen demand and inorganic nutrients. Oxygen demand takes three paths out of the sediments: (1) export to the water column as chemical oxygen demand, (2) oxidation at the sediment-water interface as sediment oxygen demand, or (3) burial to a deep, inactive sediment layer. The inorganic nutrients produced by diagenesis can take two pathways out of the bottom sediment: (1) release back to the overlying water column or (2) burial to the deep, inactive sediment layer.

In the predictive sediment submodel, benthic sediments are represented as two layers with a total depth of 10 cm. The upper benthic layer is in contact with the water column and may be oxic or anoxic depending on the dissolved oxygen concentration in the water. The lower benthic layer is permanently anoxic. The thickness of the upper benthic layer is determined by the penetration of oxygen into the sediments, and at its maximum thickness, the oxic layer depth is a small fraction of the total thickness. The sediment submodel consists of three basic processes:

- Particulate organic matter settles from the water column to the sediments. Because of the negligible thickness of the upper benthic layer, deposition proceeds from the water column directly to the lower anoxic layer.

- Within the lower layer, organic matter is subject to decay (diagenesis).

- The flux of substances produced by diagenesis moves to the upper benthic layer, to the water column, and to the deep, inactive benthic layer (burial). The flux portion of the sediment submodel is the most complex. The computation of flux requires consideration of (1) reactions in both benthic layers, (2) sedimentation from the upper to lower benthic layer as well as from the lower benthic layer to the deep inactive sediments, (3) particle mixing between layers, (4) diffusion between layers, and (5) mass transfer between the upper layer and the water column.

Very limited field data were available during the calibration period to verify the flux rates computed by the predictive sediment submodel. SOD rates were measured in July and August 1996, at three locations

in the tidal Christina River and Brandywine Creek. An SOD rate of 0.5 g/m^2/day was used in the tidal Delaware River in another model study commissioned by the Delaware River Basin Commission (DRBC) and was used as the basis for comparison to predicted SOD rates from this study. The simulated SOD rates were converted to rates at 20°C and are compared with the measured data in Table 6-6. The relative errors were less than 13% at all locations, which is considered to be a very good model-data skill assessment.

Table 6-6. Model-data comparison of sediment oxygen demand rates (g/m^2/day)

Location	Sampling Date	Monitored SOD at 20°C	EFDC Model SOD at 20°C	Relative Error
Christina River at I-495 bridge	Aug 12, 1996	0.81	0.91	12.9%
Christina River at Newport, Rt. 141 bridge	Jul 10, 1996	1.67	1.56	6.5%
Brandywine Creek, 0.6 mi. from mouth	Aug 12, 1996	1.23	1.19	3.4%
Delaware River (from HydroQual study)	-	0.50	0.46	8.8%

6.3.4   Water Quality Results

Each field observation was collected at an instant in time and at a single point in space. Time scales realistically represented in the EFDC model were determined by time scales of primary forcing functions: 60-second tidal hydrodynamics time-step, hourly meteorological inputs, monthly ocean boundary conditions, daily nonpoint source loads, monthly point source loads, daily CSO loads, constant atmospheric dry deposition, and hourly atmospheric wet deposition during rain events. The minimum model spatial scales were determined by the size of the grid cells, ranging from 500 to about 1,000 meters in the longitudinal direction along the streams. The disparity in the temporal and spatial scales between the model and prototype, especially for the nonpoint and point source loads, meant that individual observations may not be directly comparable with model prediction at a specific time in a given model grid cell.

Model-data comparisons were be made qualitatively (time-series graphics) and quantitatively (model-data statistics).   The time-series graphics are provided in Appendix A and cover the entire 4-year calibration period beginning Oct 1, 1994 and continuing to Oct 1, 1998. The model-data time-series comparison graphics were made at 27 monitoring locations on various streams in the study area (see the map in Appendix A, Figure A-0).

The graphical model-data time-series comparisons in Appendix A provide a qualitative evaluation of model performance. A seasoned modeler can examine the plots and form an experience-based judgment on the status of model calibration and verification. The model-data statistical analysis provides a different

perspective on model-data comparison that numerically quantifies the state of model calibration/verification (sometimes referred to as model "skill assessment").

Although numerous methods exist for analyzing and summarizing model performance, there is no consensus in the modeling community on a standard analytical suite. A set of basic statistical methods were used to compare model predictions and sampling observations which included the mean error statistic, the absolute mean error, the root-mean-square error, and the relative error. Statistics for the observations and model predictions were calculated over the period Oct 1, 1994 to Oct 1, 1998 at 24 monitoring locations in the Christina River Basin (see Table 6-7 and the map in Appendix A, Figure A-0).

Table 6-7. Monitoring stations used for time-series model-data statistical analysis

Station	EFDC grid cell (I,J)	Stream and Location
104011	54,20	Brandywine Creek at Brandywine Park
104021	54,23	Brandywine Creek at Road 279
104051	54,32	Brandywine Creek at Smith Bridge
WQN0105	54,36	Brandywine Creek
103041	43,38	Red Clay Creek at Ashland, DE
103061	48,52	Burroughs Run at Rt. 241
103031	43,30	Red Clay Creek at Woodale, DE
103011	43,24	Red Clay Creek at Stanton, DE
WQN0149	19,18	White Clay Creek
105031	21,18	White Clay Creek at Road 329 near Thompson
105011	41,18	White Clay Creek at Rt. 7 in Stanton
105131	31,34	Muddy Run at Road 303
105071	31,40	Mill Creek at Road 282
106191	14,13	Christina River above Newark at Rt. 273
106141	22,13	Christina River at Road 26
106031	32,13	Christina River at Smalleys Pond
106021	47,13	Christina River at Rt. 141 in Newport
106011	53,13	Christina River at US Rt. 13
106291	55,13	Christina River at RR Bridge near Port of Wilmington
106281	43,55	Little Mill Creek at Atlantic Avenue
BCWB05	27,79	Brandywine Creek West Branch at Modena, PA
BCWB04	21,79	Brandywine Creek West Branch at Coatesville, PA
BCEB02	54,55	Brandywine Creek East Branch below Downingtown, PA
RCWB02	29,43	Red Clay Creek West Branch near Kennett Square, PA

6.3.4.1 Mean Error Statistic. The mean error between model predictions and observations is defined in Eq. 6-1. A mean error of zero is ideal. A non-zero value is an indication that the model may be biased toward either over- or underprediction. A positive mean error indicates that on average the model predictions are less than the observations. A negative mean error indicates that on average the model

predictions are greater than the observed data. The mean error statistic may give a false ideal value of zero (or near zero) if the average of the positive deviations between predictions and observations is about equal to the average of the negative deviations in a data set. Because of that possibility, it is never a good idea to rely solely on this statistic as a measure of performance. Instead, it should be used in tandem with the other statistical measures that are described in this section.

$$E = \frac{\Sigma (O - P)}{n} \tag{6-1}$$

where:

E = mean error
O = observation, aggregated by month and over the water column
P = model prediction, aggregated by month and over vertical layers
n = number of observed-predicted pairs

6.3.4.2 Absolute Mean Error Statistic. The absolute mean error between model predictions and observations is defined in Eq. 6-2. An absolute mean error of zero is ideal. The magnitude of the absolute mean error indicates the average deviation between model predictions and observed data. Unlike the mean error, the absolute mean error cannot give a false zero.

$$E_{abs} = \frac{\Sigma |O - P|}{n} \tag{6-2}$$

where:

E_{abs} = absolute mean error.

6.3.4.3 Root-Mean-Square Error Statistic. The root-mean-square error (E_{rms}) is defined in Eq. 6-3. A root-mean-square error of zero is ideal. The root-mean-square error is an indicator of the deviation between model predictions and observations. The E_{rms} statistic is an alternative to (and is usually larger than) the absolute mean error.

$$E_{rms} = \sqrt{\frac{\Sigma (O - P)^2}{n}} \tag{11-3}$$

where:

E_{rms} = root-mean-square error

6.3.4.4 Relative Error Statistic. The relative error between model predictions and observations is defined in Eq. 6-4. A relative error of zero is ideal. The relative error is the ratio of the absolute mean error to the mean of the observations and is expressed as a percent.

$$E_{rel} = \frac{\Sigma \, |O \, - \, P|}{\Sigma \, O}$$

(6-4)

where:

E_{rel} = relative error.

6.3.4.5 Statistics Results. A summary of the error statistics for eight key water quality parameters of the Christina River Basin model calibration simulation is given in Table 6-8. The relative error statistic permits comparisons between the various water quality substances. Temperature and dissolved oxygen were the parameters with the smallest relative error. The results for temperature indicate a relative error of about 5.5%, and the relative error for dissolved oxygen was less than 8.3%. The relative error for total nitrogen was about 15%, ammonia nitrogen was 41%, total phosphorus was about 29%, total organic carbon was less than 18%, and dissolved organic carbon was about 30%.

Table 6-8. Statistical summary of EFDC water quality model 1994-1998 calibration results

Parameter	Mean Error	Absolute Mean Error	RMS Error	Relative Error	Number of Samples
Dissolved Oxygen (mg/L)	-0.2777	0.7587	1.1401	8.21%	859
Total Organic Carbon (mg/L)	0.5409	1.1434	2.0986	17.70%	820
Diss. Organic Carbon (mg/L)	1.2370	1.6205	2.3721	30.11%	818
Total Nitrogen (mg/L)	0.1979	0.4579	0.7880	15.20%	778
Ammonia Nitrogen (mg/L)	0.0107	0.0284	0.0545	40.96%	774
Nitrate Nitrogen (mg/L)	0.0373	0.3285	0.5041	13.94%	812
Total Phosphorus (mg/L)	0.0178	0.0345	0.0752	29.03%	785
Temperature (degC)	-0.2671	0.7253	1.2604	5.54%	862

According to the *Technical Guidance Manual for Performing Waste Load Allocations* (USEPA 1990), acceptable relative error statistic criteria are 15% for dissolved oxygen and 45% for nutrient parameters (nitrogen, phosphorus, and carbon). The overall relative error statistics for the Christina River model were 8.2% for dissolved oxygen, 15.2% for total nitrogen, 29.0% for total phosphorus, and 17.7% for total organic carbon. Since the relative error statistics for the Christina River EFDC water quality model meet the general guidance criteria published in USEPA (1990), and the model is considered acceptable for conducting TMDL allocation analyses.

7 - REFERENCES

Ambrose, R.B., T.A. Wool, and J.L. Martin. 1993. The water quality analysis and simulation program, WASP5: Part A, model documentation version 5.1. U.S. Environmental Protection Agency, Environmental Research Laboratory, Athens, GA, 210 pp.

Andrews, D.G., and M.E. McIntyre. 1978. An exact theory for of nonlinear waves on a Lagrangian flow. *J. Fluid Mech.* 89:609-646.

Banks, R.B. and F.F. Herrera. 1977. Effect of wind and rain on surface reaeration. *ASCE J. of the Environ. Engr. Div.* 103(EE3):489-504.

Bennett, A.F. 1976. Open boundary conditions for dispersive waves. J. Atmos. Sci. 32:176-182.

Bennett, A.F., and P.C. McIntosh. 1982. Open ocean modeling as an inverse problem: tidal theory. *J. Phys. Ocean.* 12:1004-1018.

Bennett, J.R., and A.H. Clites. 1987. Accuracy of trajectory calculation in a finite-difference circulation model. *J. Comp. Phys.* 68:272-282.

Blumberg, A.F., and L.H. Kantha. 1985. Open boundary condition for circulation models. *J. Hydr. Engr.* 111:237-255.

Blumberg, A.F., and G.L. Mellor. 1987. A description of a three-dimensional coastal ocean circulation model. *Three-Dimensional Coastal Ocean Models, Coastal and Estuarine Science, Vol. 4,* ed. N.S. Heaps, pp. 1-19. American Geophysical Union.

Boni, L., E. Carpené, D. Wynne, and M. Reti. 1989. Alkaline phosphatase activity in *Protogonyaulax tamarensis*. *J. of Plankton Research* 11(5):879-885.

Boudreau, B.P. 1991. Modelling the sulfide-oxygen reaction and associated pH gradients in porewaters. *Geochimica et Cosmochimica Acta*, 55:145-159.

Bowie, G.L., W.B. Mills, D.B. Porcella, C.L. Campbell, J.R. Pagenkopf, G.L. Rupp, K.M. Johnson, P.W.H.Chan, S.A. Gherini, and C.E. Chamberlin. 1985. Rates, constants and kinetics formulations in surface water quality modeling (2nd edition). EPA/600/3-85/040, U.S. Environmental Protection Agency, Environmental Research Lab., Athens, GA, 455 pp.

Burban, P.Y., W. Lick, and J. Lick. 1989. The flocculation of fine-grained sediments in estuarine waters. *J. Geophys. Res.* 94:8323-8330.

Burban, P.Y., Y.J. Xu, J. McNeil, and W. Lick. 1990. Settling speeds of flocs in fresh and seawater. *J. Geophys. Res.* 95:18,213-18,220.

Carritt, D.E. and S. Goodgal. 1954. Sorption reactions and some ecological implications. *Deep-Sea Research* 1:224-243.

Caupp, C.L., Brock, J.T., and Runke, H.M. 1991. Application of the dynamic stream simulation and assessment model (DSSAM III) to the Truckee River below Reno, Nevada: Model formulation and program description. Report prepared by Rapid Creek Water Works for Nevada Division of Environmental Protection, Carson City and Washoe County Dept. Of Comprehensive Planning, Reno, NV.

Cerco, C.F., and T. Cole. 1993. Three-dimensional eutrophication model of Chesapeake Bay. *J. Environ. Engnr.* 119:1006-1025.

Cheng, R.T., V. Casulli, and J.W. Gartner. 1993. Tidal, residual, intertidal mudflat (TRIM) model and its applications to San Francisco Bay, California. *Estuarine, Coastal, and Shelf Science* 36: 235-280.

Chróst, R.J. and J. Overbek. 1987. Kinetics of alkaline phosphatase activity and phosphorus availability for phytoplankton and bacterioplankton in Lake Plußsee (North German eutrophic lake). *Microbial Ecology* 13:229-248.

Cline, J.D. and F.A. Richards. 1969. Oxygenation of hydrogen sulfide in seawater at constant salinity, temperature and pH. *Environmental Science & Technology*, 3(9):838-843.

Cole, T.M., and E.M. Buchak. 1994. CE-QUAL-W2: A two-dimensional laterally averaged, hydrodynamic and water quality model, Version 2.0, Report ITL-93-7. U. S. Army Corps of Engineers, Waterway Experiment Station, Vicksburg, MS.

Davis, J. 1998. Measurement of community photosynthesis and respiration rates for selected reaches of the Christina Watershed. Prepared for Pennsylvania Department of Environmental Protection and Delaware Department of Natural Resources and Environmental Control, March 1998.

Diaz, R.J. and R. Rosenberg. 1995. Marine benthic hypoxia: a review of its ecological effects and the behavioural responses of benthic macrofauna. *Oceanography and Marine Biology: an Annual Review* 33:245-303.

DiToro, D.M. 1980. Applicability of cellular equilibrium and Monod theory to phytoplankton growth kinetics. *Ecological Modelling* 8:201-218.

DiToro, D.M., P.R. Paquin, K. Subburamu, and D.A. Gruber. 1990. Sediment oxygen demand model: methane and ammonia oxidation. *ASCE J. Environ. Engr.* 116(5):945-986.

DiToro, D.M., and J.F. Fitzpatrick. 1993. Chesapeake Bay sediment flux model. Contract Report EL-93-2. Prepared by HydroQual, Inc. for U. S. EPA Chesapeake Bay Program, U. S. Army Engineer District, Baltimore, MD, and U.S. Army Engineer Waterways Exp. Station.

Frick, W.E. 1984. Non-empirical closure of the plume equations, *Atmos. Environ.* 18:653-662.

Froelich, P.N. 1988. Kinetic control of dissolved phosphate in natural rivers and estuaries: a primer on the phosphate buffer mechanism. *Limnol. and Oceanogr.* 33(4, part 2):649-668.

Galperin, B., L.H. Kantha, S. Hassid, and A. Rosati. 1988. A quasi-equilibrium turbulent energy model for geophysical flows. *J. Atmos. Sci.* 45:55-62.

Genet, L.A., D.J. Smith, and M.B. Sonnen, M.B. 1974. Computer program documentation for the dynamic estuary model. Prepared for U.S. Environmental Protection Agency, Systems Development Branch, Washington, D.C.

Grant, W.D., and O.S. Madsen. 1986. The continental-shelf bottom boundary layer. *Annual Review of Fluid Mechanics*, ed. M. Van Dyke et al., pp. 365-306, Annual Review, Inc.

Giordani, P. and M. Astorri. 1986. Phosphate analysis of marine sediments. *Chemistry in Ecology* 2:103-112.

Hamrick, J.M. 1992a. A Three-Dimensional Environmental Fluid Dynamics Computer Code: Theoretical and Computational Aspects, Special Report 317. The College of William and Mary, Virginia Institute of Marine Science. 63 pp.

Hamrick, J.M. 1992b. Estuarine environmental impact assessment using a three-dimensional circulation and transport model. Estuarine and Coastal Modeling, Proceedings of the 2nd International Conference, M. L. Spaulding et al, Eds., American Society of Civil Engineers, New York, 292-303.

Hamrick, J. M. 1994: Linking hydrodynamic and biogeochemcial transport models for estuarine and coastal waters. *Estuarine and Coastal Modeling, Proceedings of the 3rd International Conference,* ed. M.L. Spaulding et al., pp. 591-608. American Society of Civil Engineers, New York.

Hamrick, J.M. 1996. A User's Manual for the Environmental Fluid Dynamics Computer Code (EFDC), Special Report 331. The College of William and Mary, Virginia Institute of Marine Science. 234 pp.

Hamrick, J.M., and T.S. Wu. 1996. Computational design and optimization of the EFDC/HEM3D surface water hydrodynamic and eutrophication models. *Computational Methods for Next Generation Environmental Models*, ed. G. Delich. Society of Industrial and Applied Mathematics, Philadelphia.

Horner, R.R., E.B. Welch, M.R. Seeley, and J.M. Jacoby. 1990. Responses of periphyton to changes in current velocity, suspended sediment, and phosphorus concentration. *Freshwater Biol.* 24(2):215-232.

HydroQual. 1991. Draft Water Quality Modeling Analysis of Hypoxia in Long Island Sound. Prepared for Management Committee Long Island Sound Estuary Study and New England Interstate Water Pollution Control Commission. Prepared by HydroQual, Inc., Mahwah, NJ. Job Number: NENG0012. July 1991.

Jirka, G. H., and R.L. Doneker. 1991. Hydrodynamic classification of submerged single-port discharges, *J. of Hydr. Engr.* 117:1095-1112.

Jirka, G.H., and P.J. Akar. 1991. Hydrodynamic classification of submerged multiport-diffuser discharges, *J. of Hydr. Engr.* 117:1113-1128.

Kang, I.S., and L.G. Leal. 1992. Orthogonal grid generation in a 2D domain via the boundary integral technique. *J. Comp. Phys.* 102:78-87.

Kremer, J.N. and S.W. Nixon. 1978. A coastal marine ecosystem: simulation and analysis. *Ecological Studies 24*, Springer-Verlag, New York. 217 pp.

Lebo, M.E. 1991. Particle-bound phosphorus along an urbanized coastal plain estuary. *Marine Chemistry* 34:225-246.

Lee, J.H.W., and V. Cheung. 1990. Generalized Lagrangian model for buoyant jets in a current. *J. Environ. Engrg.* 116:653-662.

Lijklema, L. 1980. Interaction of ortho-phosphate with iron (III) and aluminum hydroxides. *Environmental Science & Technology*, 14(5):537-541.

Madsen, P.A., and J. Larsen. 1987. An efficient finite-difference approach to the mild-slope equation. *Coastal Engr.* 11:329-351.

Mancini, J.L. 1983. A method for calculating effects, on aquatic organisms, of time varying concentrations. *Water Research* 17(10):1355-1362.

Matisoff, G. 1982. Mathematical models of bioturbation, ed. P.L. McCall and M.J.S. Tevesz, pp. 289-330. *Animal-Sediment Relations: The Biogenic Alteration of Sediments*, Plenum Press, NY.

Mellor, G.L., and T. Yamada. 1982. Development of a turbulence closure model for geophysical fluid problems. *Rev. Geophys. Space Phys.*, 20:851-875.

Millero, F.J. 1986. The thermodynamics and kinetics of the hydrogen sulfide system in natural waters. *Marine Chemistry* 18:121-147.

Mobley, C.D., and R.J. Stewart. 1980. On the numerical generation of boundary-fitted orthogonal Curvilinear coordinate systems. *J. Comp. Phys.* 34:124-135.

Morel, F. 1983. *Principles of Aquatic Chemistry.* John Wiley & Sons, New York, NY. 446 pp.

Morse, J.W., F.J. Millero, J.C. Cornwell, and D. Rickard, D. 1987. The chemistry of the hydrogen sulfide and iron sulfide systems in natural waters. *Earth-Science Reviews* 24:1-42.

Moustafa, M.Z., and J.M. Hamrick. 1994. Modeling circulation and salinity transport in the Indian River Lagoon. *Estuarine and Coastal Modeling, Proceedings of the 3rd International Conference*, ed. M. L. Spaulding et al., pp. 381-395. American Society of Civil Engineers, New York.

McIntire, C.C. 1973. Periphyton dynamics in laboratory streams: a simulation model and its implications. *Ecological Monographs.* 43:399-420.

Nixon, S. 1981. Remineralization and nutrient cycling in coastal marine ecosystems. *Estuaries and Nutrients*, ed. Neilson and Cronin. pp.111-138. Humana Press, Clifton, NJ.

NOAA. 1998. Tide Tables 1998. National Oceanographic and Atmospheric Administration, National Ocean Service, Silver Spring, MD.

O'Connor, D.J. and W.E. Dobbins. 1958. Mechanism of reaeration in natural streams. *Transactions of the American Society of Civil Engineers*, 123(2934):641-684.

Odum, E.P. 1971. *Fundamentals of ecology (3rd edition).* W.B. Saunders Co., Philadelphia, PA. 574pp.

Oey, L.-Y., G.L. Mellor, and R.I. Hires. 1985. A three-dimensional simulation of the Hudson Raritan estuary. *J. Phys. Oceanogr.* 15:1676-1720.

Park, K., A.Y. Kuo, J. Shen, and J.M. Hamrick. 1995. A three-dimensional hydrodynamic-eutrophication model (HEM3D): description of water quality and sediment processes submodels, Special Report 327. The College of William and Mary, Virginia Institute of Marine Science. 113 pp.

Parsons, T.R., M. Takahashi, and B. Hargrave. 1984. *Biological oceanographic processes (3rd edition).* Pergamon Press. 330 pp.

Pfeifer, R.F., and McDiffett, W. 1975. Some factors affecting primary production of stream communities. *Archives of Hydrobiol.* 75:306-317.

Redfield, A.C., B.H. Ketchum, and F.A. Richards. 1963. The influence of organisms on the composition of sea-water, ed. M.N. Hill, Chapter 2, pp 26-77. *The Sea - Ideas and Observations on Progress in the Study of the Seas: Vol. 2, Composition of Sea Water, Comparative and Descriptive Oceanography*, Interscience Publishers.

Rennie, S., and J.M. Hamrick. 1992. Techniques for visualization of estuarine and coastal flow fields. *Estuarine and Coastal Modeling, Proceedings of the 2nd International Conference*, ed. M. L. Spaulding et al., pp. 48-55. American Society of Civil Engineers, New York.

Robbins, J.A., T. Keilty, D.S. White, and D.N. Edgington. 1989. Relationships among tubificid abundances, sediment composition and accumulation rates in Lake Erie. *Canadian J. of Fisheries & Aquatic Sciences*, 46(2):223-231.

Rosati, A.K., and K. Miyakoda. 1988. A general circulation model for upper ocean simulation. *J. Phys. Ocean*, 18:1601-1626.

Ross, P.J. 1983. Dynamics of periphyton communities. *Periphyton in Freshwater Ecosystems*, ed. R.G. Wetzel, pp. 5-10. Junk, Boston, MA, 5-10.

Runke, H.M. 1985. Simulation of the lotic periphyton community of a small mountain stream by digital computer. PhD thesis, Utah State University, Logan, Utah.

Ryskin, G. and L.G. Leal. 1983. Orthogonal mapping. *J. Comp. Phys.* 50:71-100.

Sand-Jensen, K. 1983. Physical and chemical parameters regulating the growth of periphyton communities. *Periphyton in Freshwater Ecosystems*, ed. R.G. Wetzel, pp. 63-71. Junk, Boston, MA.

Senior and Koerkle. 2003a. Simulation of streamflow and water quality in the Brandywine Creek subbasin of the Christina River Basin, Pennsylvania and Delaware, 1994-98. U.S. Geological Survey Water-Resources Investigations Report 02-4279, 207pp.

Senior and Koerkle. 2003b. Simulation of streamflow and water quality in the White Clay Creek subbasin of the Christina River Basin, Pennsylvania and Delaware, 1994-98. U.S. Geological Survey Water-Resources Investigations Report 03-4031, 242pp.

Senior and Koerkle. 2003c. Simulation of streamflow and water quality in the Red Clay Creek subbasin of the Christina River Basin, Pennsylvania and Delaware, 1994-98. U.S. Geological Survey Water-Resources Investigations Report 03-4138, 119pp.

Senior and Koerkle. 2003d. Simulation of streamflow and water quality in the Christina River subbasin and overview of simulations in other subbasins of the Christina River Basin, Pennsylvania and Delaware, 1994-98. U.S. Geological Survey Water-Resources Investigations Report 03-4193, 144pp.

Shen, J., J. Boon, and A.Y. Kuo. 1999. A numerical study of a tidal intrusion front and its impact on larval dispersion in the James River estuary, Virginia. *Estuary* 22(3A):681-692.

Smolarkiewicz, P.K., and T.L. Clark. 1986. The multidimensional positive definite advection transport algorithm: further development and applications. *J. Comp. Phys.* 67:396-438.

Smolarkiewicz, P.K., and W.W. Grabowski. 1990. The multidimensional positive definite advection transport algorithm: nonoscillatory option. *J. Comp. Phys.* 86:355-375.

Smolarkiewicz, P.K., and L.G. Margolin. 1993. On forward-in-time differencing for fluids: extension to a curvilinear framework. *Mon. Weather Rev.* 121:1847-1859.

Steele, J.H. 1962. Environmental control of photosynthesis in the sea. *Limnol. and Oceanogr.* 7(2):137-150.

Stevenson, R.J., and Glover, R. 1993. Effects of algal density and current on ion transport through periphyton communities. *Limnol. and Oceanogr.*, 38(6):1276-1281.

Stumm, W. and J.J. Morgan. 1981. *Aquatic chemistry, an introduction emphasizing chemical equilibria in natural waters (2nd edition).* John Wiley & Sons, Inc. 780 pp.

Thomann, R.V., N.J. Jaworski, S.W. Nixon, H.W. Paerl, and J. Taft. 1985. The 1983 algal bloom in the Potomac Estuary. The Algal Bloom Expert Panel, pepared for the Potomac Strategy State/EPA Management Committee, US Environmental Protection Agency, Region III, Philadelphia, PA.

Thomann, R.V. and J.A. Mueller. 1987. *Principles of surface water quality modeling and control.* Harper & Row, Publishers, Inc. 644 pp.

Troup, R. 1974. The interaction of iron with phosphate, carbonate and sulfide in Chesapeake Bay interstitial waters: a thermodynamic interpretation. Ph.D. Dissertation, Johns Hopkins University, MD. 114 p.

USEPA. 1990. *Technical Guidance Manual for Performing Waste Load Allocations, Book III Estuaries, Part 2, Application of Estuarine Waste Load Allocation Models.* EPA823-R-92-003. U.S. Environmental Protection Agency, Office of Water. May 1990.

USEPA. 1995. *Technical Guidance Manual for Developing Total Maximum Daily Loads, Book II: Streams and Rivers, Part 1: Biochemical Oxygen Demand/Dissolved Oxygen and Nutrients/Eutrophication.* EPA 823-B-95-007. U.S. Environmental Protection Agency, Office of Water. September 1995.

USEPA. 2000. Hydrodynamic and water quality model of Christina River Basin. U.S. Environmental Protection Agency, Region III, Philadelphia, PA. December 2000.

USEPA. 2004. Christina River Basin High-Flow TMDLs for Nutrients, Low Dissolved Oxygen, and Bacteria: Data Report (Draft). U.S. Environmental Protection Agency, Region III, Philadelphia, PA. April 30, 2004.

USEPA. 2005. Total Maximum Daily Loads for Nutrients and Low Dissolved Oxygen in the Christina River Basin, Pennsylvania, Delaware, and Maryland. USEPA Region III, Philadelphia, PA. April 8, 2005.

Warwick, J.J., D. Cockrum, and M. Horvath. 1997. Estimating non-point source loads and associated water quality impacts. *ASCE J. Water Res. Plan. and Manage.* 123(5):302-310.

Westrich, J.T. and B.A. Berner. 1984. The role of sedimentary organic matter in bacterial sulfate reduction: the G model tested. *Limnol. and Oceanogr.* 29(2):236-249.

Wezernak, C.T. and J.J. Gannon. 1968. Evaluation of nitrification in streams. *ASCE J. Sanitary Engr. Div.* 94(5):883-895.

Whitford, L.A. and G.J. Schumacher. 1964. Effect of current on respiration and mineral uptake of Spirogyra and Oedogonium. *Ecology* 45:168-170.

Wu, T.S., J.M. Hamrick, S.C. McCutechon, and R.B. Ambrose. 1996. *Benchmarking the EFDC/HEM3D surface water hydrodynamic and eutrophication models. Computational Methods for Next Generation Environmental Models*, ed. G. Delich. Society of Industrial and Applied Mathematics, Philadelphia.

Yamamoto, S., J.B. Alcauskas, and T.E. Crozler. 1976. Solubility of methane in distilled water and seawater. *J. of Chemical and Engineering Data* 21(1):78-80.